TRANSFORM TECHNIQUES IN ELECTROCHEMISTRY

A Thesis Submitted to the Committee on Graduate Studies
in Partial Fulfilment of the Requirements for the
Degree of Master of Science
in the Faculty of Arts and Science

TRENT UNIVERSITY

by

Michael Roy Hempstead

Department of Chemistry

May, 1983

Acknowledgements

I wish to express my gratitude to all those who made this project possible. I am indebted to Professor Keith Oldham for the derivation of the basis for this research and for his guidance with the concepts behind its implementation. Special thanks are extended to Jan Myland for her assistance with the experimental aspects of this research and for the comradery that she provided which made my time in the lab more light-hearted.

I am also grateful for the moral support of my family and friends who kept my spirits high whenever frustrations beset me. A simple smile often meant so much.

I also wish to thank the Natural Sciences and Engineering Research Council of Canada for their generous financial support.

TABLE OF CONTENTS

Chapter		Page
1	INTRODUCTION	1
2	TRANSFORM ANALYSIS	3
	What is a transform?	3
	Why use a transform?	4
	What distinguishes an Integral Transform?	5
	Examples of Integral Transforms	6
	(i) Fourier Transformation	6
	(ii) Laplace Transformation	8
	(iii) Hilbert Transformation	10
	Implementation of Integral Transforms	11
	(i) Curve Fitting	12
3	ELECTROCHEMICAL CONCEPTS	21
	Heterogeneous Reaction Kinetics	21
	Mass Transport	22
	(i) Convection	22
	(ii) Migration	22
	(iii) Diffusion	23
	Fick's Laws of Diffusion	23
	The Nernst Equation	25
	Faradaic and Nonfaradaic Processes	25
	Polarization	27

Chapter		Page
4	PREVIOUS APPLICATIONS OF TRANSFORMS IN ELECTROCHEMISTRY	29
	Fick's Second Law and the Laplace Transform	29
	Analysis in the Laplace Plane	33
	Faradaic Admittance	35
	Spectroelectrochemistry	40
	Riemann-Liouville Transformation	44
	(i) Riemann-Liouville Transform Polarography	45
	(ii) Cottrell Filtering	47
5	REVERSAL TECHNIQUES IN ELECTROCHEMISTRY	49
	Double Step Chronoamperometry	50
	Double Step Chronocoulometry	52
	Collection Experiments	54
	Current Reversal Potentiometry	55
	Cyclic Voltammetry	58
	Stripping Analysis	63
6	GENERATION/RECAPTURE ANALYSIS	66
	Interrelationship of the Currents	69
	Hilbert Transform Analysis	74
	(i) Cottrellian Generation/Recapture Relationship	74
	(ii) Galvanostatic Generation/Recapture Relationship	76

Chapter		Page
7	CONSTRUCTION OF $i_r(t)$ FROM $i_g(t)$	78
	Numerical Hilbert Transformation	78
	Experimental Analysis	83
	Reagents and Solutions	83
	Apparatus	84
	Experimental	87
	Error Analysis	108
	Discussion	115
	Comments	117
8	RECONSTRUCTION OF $i_g(t)$ FROM $i_r(t)$	118
	I) Curve Fitting	118
	(i) Power Series	121
	(ii) Orthogonal Polynomials	126
	Summary of Curve Fitting	134
	II) Iterative Hilbert Transformation	134
	Summary of Iterative Hilbert Transformation . .	142
9	AN APPLICATION OF GENERATION/RECAPTURE ANALYSIS . .	143
	LCEC versus GC/MS	143
	Elimination of Dissolved Oxygen Interference . . .	145
10	SUMMARY	147

Appendix Page

A Proof of the generation/recapture relationship by Laplace transformation 148

B Proof of the generation/recapture relationship by Riemann-Liouville transformation 155

C Listings of some essential programs 158

D Instrumental Calibration 175

E Evaluation of fitting functions 177

Part I: Functions for power series fit 177

Part II: Functions for orthogonal polynomials fit 181

F Listings of some fits 184

Table

I Properties and examples of Hilbert Transforms . . 193

II Summarized knowledge of the generation and recapture functions 195

LIST OF SYMBOLS 196

REFERENCES 206

CHAPTER 1

INTRODUCTION

Transform techniques offer many advantages to chemists because they can provide a variety of simple procedures for manipulating digitized data. The Fourier transform has gained distinction in chemical analysis particularly in spectroscopic applications. The advantages of this transform were first exploited in the 1950's by astronomers to improve the otherwise poor signal-to-noise ratio of their infrared spectra.[1] The computations required for data reduction, however, were extremely slow and required a large computer. In 1965, Cooley and Tukey[2] published a fast Fourier transform (FFT) algorithm that significantly shortened computation time. A calculation that took six hours on a large computer using a conventional algorithm could now be performed in ten seconds on a mini-computer using the FFT algorithm.[1] Analog-to-digital converters with suitable speed and accuracy were already available at this time and commercial stand-alone Fourier transform infrared (FT-IR) and Fourier transform nuclear magnetic resonance (FT-NMR) spectrometers were available within three years.

The application of transform methods to other spectroscopic techniques required additional theoretical and/or technical developments. As an example, the first commercially available

Fourier transform mass spectrometer was not marketed until 1981[1] because of demands on the analog-to-digital converter. Other transforms have also found applications in spectroscopy. Hadamard transform methods for IR[3] and Hilbert transform methods for NMR[4] were both introduced in 1968.

Although transform methods have been exploited chiefly for spectroscopy, they also have applications in other analytical techniques. For instance, many transform techniques have been applied to electrochemistry. Some of these applications will be discussed more thoroughly in a later chapter. In addition, an application of the Hilbert transform will be developed for a specific type of electrochemical analysis. After this transform technique is validated theoretically, some investigations of its implementation with digitized data will be reported and conclusions concerning its success will be drawn.

CHAPTER 2

TRANSFORM ANALYSIS

What is a Transform?

Many simple mathematical operations may be classified as transformations.[1] The multiplication of a function F(t) by a constant or by a second function is a transformation of F(t). The operation of differentiation transforms F(t) into its image, or transform, F'(t). If this mathematical operator is represented by the letter D then the transform can be written

$$D\{F(t)\} = F'(t) \tag{2.1}$$

Similarly, the operation of integration, represented by the letter I, transforms F(t) into a function f(x) where

$$I\{F(t)\} = \int_0^x F(t)dt = f(x) \tag{2.2}$$

If a transform, T, of a function F gives the image G, then an inverse transform, T^{-1}, exists such that

$$T^{-1}\{G\} = F \tag{2.3}$$

Table 2.1 summarizes the transforms that have been discussed thus far along with their corresponding inverse transforms.

T	T^{-1}
multiplication differentiation integration	division integration differentiation

Table 2.1 Some transforms and their inverses.

Why use a Transform?

There is a wide variety of transforms that have been studied extensively and whose properties are well established. The analysis of a problem can often be simplified by employing one of these transforms. A comparison between transform analysis and conventional analysis is presented in Figure 2.1. It can be seen from this flowchart that although the route to the solution can involve more operations, the overall analysis can be simplified significantly with the aid of a transform.

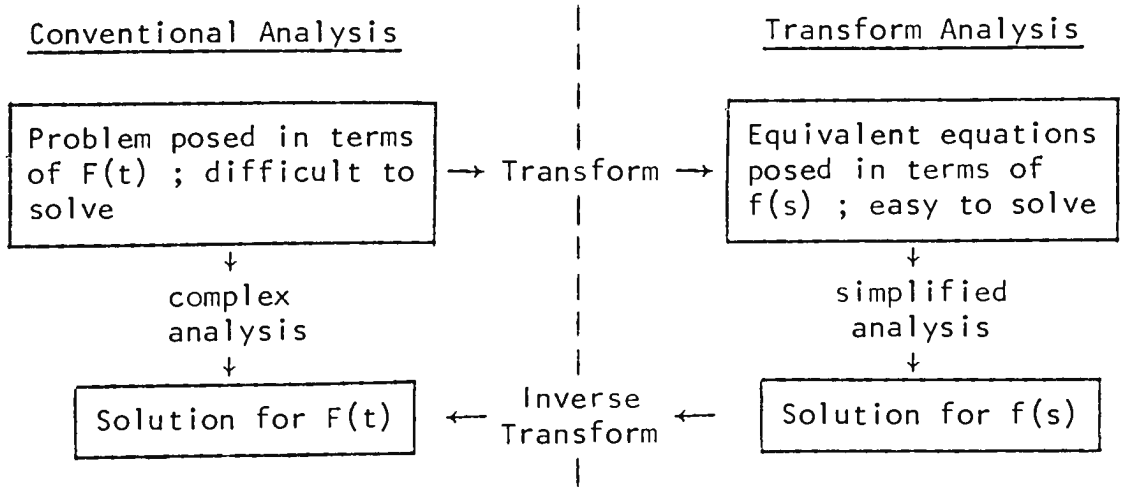

Figure 2.1 Flowchart for both conventional and transform analysis.

The analysis can only be simplified, however, if the appropriate transform is chosen. As an analogy, assume that two numbers are to be divided but a calculator is not available. The conventional analysis would be to perform long division, which can be tedious. Another approach would be to subtract the logarithm of the denominator from that of the numerator, and then take the antilogarithm of this difference. The logarithm transforms multiplications and divisions into additions and subtractions. This is an operation specific to the logarithm which simplifies the analysis for this particular type of problem. The transform is easy to implement since tables of logarithms and antilogarithms may be easily looked up and hence an awkward division may be evaluated without the aid of a calculator.

What distinguishes an Integral Transform?

Integral transforms are simply transforms that require the evaluation of an integral. Equation (2.2) illustrates the simplest integral transform. These transforms are commonly encountered in calculus, but usually they incorporate the following conditions. Often the function $F(t)$ is limited to an interval $a \leq t \leq b$ and hence the integration is performed between these limits. Usually $F(t)$ is also multiplied by a second function $K(t,x)$ known as the kernel. The integral transformation of $F(t)$ with respect to the kernel $K(t,x)$ may be represented by

the equation

$$\mathcal{T}\{F(t)\} = \int_a^b K(t,x)F(t)dt \qquad (2.4)$$

which will yield a function f(x). Any integral transform can be described in the form of equation (2.4) given the appropriate limits and kernel.

Examples of Integral Transforms

(i) Fourier Transformation

The use of integral transforms dates back to the middle of the nineteenth century when the interference of light was first used to obtain spectra. Lord Rayleigh demonstrated that a unique spectral distribution could not be obtained from the visibility curve itself and that it was necessary to perform a Fourier transformation.[2] The calculation of a digital Fourier transform was beyond the technology of that age, but Michelson did manage to build a harmonic synthesizer which was capable of outputting the Fourier transform of a synthetic input signal.[3] This was the first Fourier transform computer and it was a remarkable achievement. It would be forty years before the same operation would be performed on a digital computer.[4]

The processing of data with a Fourier transform was used extensively in the past by electrical engineers for circuit analysis[5] and only recently have chemists begun to incorporate this procedure to compliment classical analytical techniques. The

development of the on-line fast Fourier transform (FFT) has lead to a rapid growth in Fourier transform methods since 1973.[6] This FFT algorithm allows a computer to resolve the response obtained from an experiment in which several excitation frequencies are applied simultaneously. This capacity for simultaneous measurement is sometimes called the multiplex advantage of transform methods.[7]

In spectroscopic analysis, one is concerned with the frequency or spectral response of a system to a pulse or complex distribution of amplitudes with time. The Fourier transform relates the distribution of the signal expressed in terms of time with its distribution in terms of frequency. It is defined by

$$H(f) = \int_{-\infty}^{\infty} h(t)\exp(-j2\pi ft)dt \qquad (2.5)$$

with its inverse given by

$$h(t) = \int_{-\infty}^{\infty} H(f)\exp(j2\pi ft)df \qquad (2.6)$$

where $j=(-1)^{\frac{1}{2}}$, $H(f)$ is the frequency-domain function, and $h(t)$ is the time-domain function.

The Fourier transform possesses properties that are extremely useful for signal processing. A common application is for noise reduction. If a signal is monitored in which there is information at a few low frequencies, but noise at higher frequencies, the transformation of the signal will yield a frequency spectrum in

which the amplitudes of high-frequency components may be set to zero. Inverse transformation will then yield smoothed time-domain data. Other operations permit integration and differentiation, correlations between two signals, or correlation of a signal with itself.[8]

The application of the Fourier transform has become a routine procedure to obtain high-resolution IR and NMR spectra. Similar analytical methods are presently being developed for mass spectrometry and microwave spectroscopy. A number of Fourier transform techniques have also been successfully applied in several areas of electrochemistry.[9]

(ii) Laplace Transformation

The Laplace transform is a valuable mathematical tool for solving linear differential equations. It was developed over 150 years ago by P.S. de Laplace but it has only recently achieved widespread use.[10]

The application of this transform was pioneered by Heaviside in the 1890's. His early work revolved around ordinary linear differential equations that were applicable to electric circuit theory. He later studied partial differential equations that were characteristic of diffusion systems. The validity of Heaviside's solutions was doubted by pure mathematicians since much of his work was based on empirical concepts. In 1916, however, Browich

proved the necessary mathematics to validate Heaviside's methods.[11] This is a rare example of the application of a mathematical procedure preceding the development of a sound theoretical base.

The Laplace transform is defined as

$$L\{F(t)\} = f(s) = \int_0^\infty F(t)\exp(-st)dt \qquad (2.7)$$

in which the independent variable, often being time, is replaced with the "dummy" variable s. This transformation converts differential equations in t into algebraic equations in s. The initial conditions and boundary values of the differential equation may also be transformed and then incorporated into the algebraic equations so that a solution may be obtained that satisfies these conditions.

The solution to the algebraic equations is then inverse transformed to give a solution in t for the original differential equation. The inverse transform is given by

$$L^{-1}\{f(s)\} = F(t) = \frac{1}{2\pi j}\int_{a-j\infty}^{a+j\infty} f(s)\exp(st)ds \qquad (2.8)$$

where "a" is chosen to the right of any singularity of f(s). Extensive tables of Laplace transforms are available[12-15] and these usually permit one to avoid the arduous task of evaluating these integral transforms. Sometimes, however, the inversion may only be accomplished by transforming a product of two functions of s for which the individual inverse transforms are known. If

$L^{-1}\{f(s)\} = F(t)$ and $L^{-1}\{g(s)\} = G(t)$, then the inverse transformation of the product $f(s)g(s)$ is given by the convolution theorem,[16]

$$L^{-1}\{f(s)g(s)\} = \int_0^t G(\tau)F(t-\tau)d\tau \qquad (2.9)$$

where τ is a dummy variable of integration. The form of this equation does not demand an analytical solution since, if necessary, the integral may be evaluated numerically. This procedure is particularly useful in the treatment of transient techniques that involve continuously varying perturbations (e.g. cyclic voltammetry).

(iii) Hilbert Transformation

This transform was developed from a study of the Fourier transform.[17] The transform is given by

$$g(y) = \frac{1}{\pi} \int_{-\infty}^{\infty} \frac{f(x)}{x-y}\, dx \qquad (2.10)$$

with its inverse given by

$$f(x) = -\frac{1}{\pi} \int_{-\infty}^{\infty} \frac{g(y)}{y-x}\, dy \qquad (2.11)$$

where $\int$ denotes the Cauchy Principal Value of the integral. This relationship is skew reciprocal because, apart from sign, the same rules that govern transformation also govern the inversion of the transform. It is necessary to calculate the Cauchy Principal

Value of these integrals because the integrands have singularities when x and y are equal. In general, if the integrand has a singularity at c, a<c<b, then the Cauchy Principal Value of

$$\int_a^b F(x)dx \tag{2.12}$$

is[18]

$$\oint_a^b F(x)dx = \lim \left[\int_a^{c-\varepsilon} F(x)dx + \int_{c+\varepsilon}^b F(x)dx \right] \tag{2.13}$$

where ε is positive and approaches zero.

The Hilbert transform has rarely been applied to aid in the analysis of physical systems. It has been used, however, to reduce distortion in optical systems[19] and to calculate potential functions for circuit analysis.[20] It also has important applications in aerodynamics.[21] This transform has also been used for the automatic phase correction of magnetic resonance spectra.[22]

Implementation of Integral Transforms

The evaluation of an integral transform requires that the function within the integral be analytic between the limits of integration. This would enable the function to be calculated at any point between these limits. Data obtained experimentally, however, is often digital and hence the function within the integrand are defined only at specific locations. Approximations, therefore, must be made to evaluate the transform.

Experimental data are often obtained at regularly spaced intervals. This permits the integral transform to be approximated by a summation. If data described by a function F(t) are known at intervals of Δt, then

$$\int_a^b F(t) \simeq \Delta t \sum_{j=0}^{J-1} F(a+j\Delta t) \quad , J = \frac{b-a}{\Delta t} \tag{2.14}$$

This method does not require that an analytical expression be known; only that the value of F(t) be known at intervals of Δt starting at the initial value a.

An alternative method is to fit the experimental data to an analytical expression and then calculate the transform by integration. A combination of several analytical functions may be required to fit the data accurately. Each of these functions would be transformed individually and then the overall transform would be obtained from their sum.

(i) Curve Fitting

If data are to be fitted to an analytical function, the first step is to select an appropriate function or set of functions. Although this may at first appear to be a simple task, the number of analytical functions at hand is virtually endless and often several functions must be tested before a suitable fit will be obtained for the experimental response.

The selection of appropriate fitting functions may be simplified if an expression is known that describes the experimental response under ideal conditions. Additional functions are then added to deal with the non-ideal contributions to the response. These additional functions are usually selected so as to form a power series; that is, if the ideal response is dependent upon x^p, where p need not be an integer, then the equation used for the fit is often of the form

$$F(x) \approx a_0 + a_1 x^p + a_2 x^{2p} + \cdots + a_n x^{np} \qquad (2.15)$$

in which there are n+1 terms. The precision of the fit can be improved by selecting n to be large, but this can introduce terms of questionable significance as well as complicating the calculation of coefficients for the fit.

If an expression is not known for the ideal response, the curve may still be approximated by a power series like equation (2.15). If p is chosen to be unity, then the power series becomes a polynomial in x; that is,

$$F(x) \approx a_0 + a_1 x + a_2 x^2 + \cdots + a_n x^n \qquad (2.16)$$

where n is the degree of the polynomial.

In general, a polynomial fitting routine will yield values for the coefficients that are dependent upon the degree of the polynomial to which the fit is made. Consider, for instance, the

calculation of a_0, the intercept of the curve with the ordinal axis. The coefficient a_1 represents the slope of the curve at a_0, and the other coefficients represent higher order derivatives at the same intercept point. If the data are not clustered about this intercept point, its location could be highly dependent upon the degree of the polynomial used to fit the data.

It might be possible to extract more meaningful information from the data by determining the average value, the average slope, the average curvature, etc., of the data. Such coefficients would represent physical characteristics of the data.

Any polynomial, such as equation (2.16) may be reformulated as a sum of orthogonal polynomials

$$F(x) \simeq b_0 + \sum_{k=1}^{n} \left[b_k G_k(x) \right] \tag{2.17}$$

with the orthogonal property

$$\sum \left[G_k(x) G_m(x) \right] = 0 \tag{2.18}$$

for $k \neq m$. This reformulation will permit coefficients to be calculated that are independent of the degree of the polynomial.[23]

One set of orthogonal polynomials that often arise in descriptions of physical systems are the Legendre polynomials. These polynomials are solutions of the differential equation

$$(1-x^2)y'' - 2xy' + n(n+1)y = 0 \tag{2.19}$$

which is Legendre's differential equation of degree n. This equation occurs, for example, in the process of obtaining solutions to Laplace's equation in spherical coordinates. The Laplace equation is perhaps the most important partial differential equation in applied mathematics. It can be used to describe physical systems such as:[24]

(i) the gravitational potential in regions not occupied by attracting matter
(ii) the electrostatic potential in a uniform dielectric
(iii) the magnetic potential in free space
(iv) the temperature, in the theory of thermal equilibrium of solids.

The first few Legendre polynomials are

$$\begin{aligned} P_0(x) &= 1 & P_2(x) &= \tfrac{1}{2}(3x^2-1) \\ P_1(x) &= x & P_3(x) &= \tfrac{1}{2}(5x^3-3x) \end{aligned} \qquad (2.20)$$

where the subscript on P is the value of n used in equation (2.19). Higher-order polynomials may be obtained from the iteration formula[25]

$$P_n(x) = \frac{1}{n}\left[(2n-1)xP_{n-1}(x) - (n-1)P_{n-2}(x)\right] \qquad (2.21)$$

These polynomials are restricted to values of x that lie within $-1 \leq x \leq 1$. The general solution of Legendre's equation, however, may be written as

$$y = AP_n(x) + BQ_n(x) \tag{2.22}$$

where A and B are arbitrary constants and $Q_n(x)$ is Legendre's function of the second kind. This function is not a polynomial and it has different definitions in the regions $|x|>1$ and $|x|<1$, as can be readily seen from $Q_0(x)$:[26]

$$Q_0(x) = \frac{1}{2}\,\ell n\left(\frac{x+1}{x-1}\right) = \coth^{-1}(x) \quad , \; |x|>1 \tag{2.23a}$$

$$Q_0(x) = \frac{1}{2}\,\ell n\left(\frac{1+x}{1-x}\right) = \tanh^{-1}(x) \quad , \; |x|<1 \tag{2.23b}$$

Higher-order functions may be calculated from the equation[27]

$$Q_n(x) = P_n(x)Q_0(x) - \sum_{n=1}^{m} \frac{1}{m} P_{m-1}(x)P_{n-m}(x) \tag{2.24}$$

which is valid for all values of x.

The Legendre polynomial and the Legendre function of the second kind may alternatively be expressed as[28]

$$P_n(x) = {}_2F_1\left(-n,n+1;1;\frac{1-x}{2}\right) \quad , \quad |x|<1 \tag{2.25}$$

and

$$Q_n(x) = \frac{2^n(n!)^2}{(2n+1)!\,(x-1)^{n+1}}\,{}_2F_1\left(n+1,n+1;2n+2;\frac{2}{1-x}\right) \quad , \quad |x|>1 \tag{2.26}$$

These equations establish a link to another useful fitting function, Gauss' hypergeometric function. This function is

defined by[29]

$$ {}_2F_1(a,b;c;x) = \sum_{n=0}^{\infty} \frac{(a)_n (b)_n}{(c)_n (1)_n} x^n \tag{2.27} $$

where

$$ (a)_n = a(a+1)(a+2) \cdots (a+n-1) \tag{2.28} $$

This is a very versatile function that can be used to describe many other analytical functions.

Consider the differential equation

$$ (1-x^2)y'' + [\beta-\alpha-(\alpha+\beta+2)x]y' + n(n+\alpha+\beta+1)y = 0 \tag{2.29} $$

which is very similar to the differential equation (2.19). The general solution to this differential equation may be written as

$$ y = AP_n^{(\alpha,\beta)}(x) + BQ_n^{(\alpha,\beta)}(x) \tag{2.30} $$

where $P_n^{(\alpha,\beta)}(x)$ are the Jacobi polynomials and $Q_n^{(\alpha,\beta)}(x)$ are the Jacobi functions of the second kind. The Jacobi polynomials may be calculated from the recurrence formula[30]

$$ \begin{aligned} &2n(n+\alpha+\beta)(2n+\alpha+\beta-2)P_n^{(\alpha,\beta)}(x) \\ &= (2n+\alpha+\beta-1)\{(2n+\alpha+\beta)(2n+\alpha+\beta-2)x+\alpha^2-\beta^2)\}P_{n-1}^{(\alpha,\beta)}(x) \\ &\quad -2(n+\alpha-1)(n+\beta-1)(2n+\alpha+\beta)P_{n-2}^{(\alpha,\beta)}(x) \quad , \quad n = 2,3,4,\cdots \end{aligned} \tag{2.31} $$

given

$$P_0^{(\alpha,\beta)}(x) = 1$$
$$P_1^{(\alpha,\beta)}(x) = \tfrac{1}{2}(\alpha+\beta+2)x + \tfrac{1}{2}(\alpha-\beta) \tag{2.32}$$

Another method would be to evaluate these polynomials from[31,32]

$$P_n^{(\alpha,\beta)}(x) = \frac{\Gamma(n+\alpha+1)}{\Gamma(n+1)\Gamma(\alpha+1)}\, {}_2F_1\left(-n, n+\alpha+\beta+1; \alpha+1; \frac{1-x}{2}\right) \tag{2.33}$$

where $\Gamma(n)$ is the gamma function for which[33]

$$\Gamma(n+1) = n\Gamma(n) = n! \tag{2.34}$$

and

$$\Gamma(\tfrac{1}{2}) = \pi^{\frac{1}{2}} \tag{2.35}$$

are just a few of its properties. The Jacobi function of the second kind may be expressed similarly as

$$Q_n^{(\alpha,\beta)}(x) = \frac{2^{n+\alpha+\beta}}{(x-1)^{n+\alpha+1}(x+1)^{\beta}} \frac{\Gamma(n+\alpha+1)\Gamma(n+\beta+1)}{(2n+\alpha+\beta+2)}$$
$$\times\ {}_2F_1\left(n+1, n+\alpha+1; 2n+\alpha+\beta+2; \frac{2}{1-x}\right) \tag{2.36}$$

Both equations (2.33) and (2.36) simplify to the analogous expressions for their Legendre counterparts when both α and β are zero. This shows that any property derived for the Jacobi functions may be applied to the Legendre functions by setting α and β to zero.

The functions $Q_n^{(\alpha,\beta)}(x)$ satisfy the same recurrence formula as the functions $P_n^{(\alpha,\beta)}(x)$[i.e. equation (2.31)]. The functions for n=0 and n=1 are required as seeds for this recurrence formula. Both of these functions could be determined from equation 2.36, or $Q_0^{(\alpha,\beta)}(x)$ could be determined from this equation and $Q_1^{(\alpha,\beta)}(x)$ could be evaluated from

$$Q_1^{(\alpha,\beta)}(x) = P_1^{(\alpha,\beta)}(x)Q_0^{(\alpha,\beta)}(x) - 2^{\alpha+\beta-1}(\alpha+\beta+2)\frac{\Gamma(\alpha+1)\Gamma(\beta+1)}{\Gamma(\alpha+\beta+2)}(x-1)^{-\alpha}(x+1)^{-\beta} \quad (2.37)$$

which requires less manipulation. The calculation of higher order Jacobi functions of the second kind may be simplified with the aid of the expression[34]

$$\begin{aligned} &Q_n^{(\alpha,\beta)}(x) \\ &= P_n^{(\alpha,\beta)}(x)Q_0^{(\alpha,\beta)}(x) \\ &\quad - \frac{1}{2}(x-1)^{-\alpha}(x+1)^{-\beta}\int_{-1}^{1}(1-t)^{\alpha}(1+t)^{\beta}\frac{P_n^{(\alpha,\beta)}(x) - P_n^{(\alpha,\beta)}(t)}{x-t}\,dt \\ &= P_n^{(\alpha,\beta)}(x)Q_0^{(\alpha,\beta)}(x) - q_n^{(\alpha,\beta)}(x) \end{aligned} \quad (2.38)$$

where $q_n^{(\alpha,\beta)}(x)$ incorporates a finite Hilbert transform. Since the recurrence formula is applicable to both $Q_n^{(\alpha,\beta)}(x)$ and $P_n^{(\alpha,\beta)}(x)$, it must also be applicable to $q_n^{(\alpha,\beta)}(x)$. This function can be expressed in simpler terms than the $Q_n^{(\alpha,\beta)}(x)$ function and thus it is easier to manipulate within the recurrence

formula. The calculation of $Q_n^{(\alpha,\beta)}(x)$ may be simplified, therefore, by evaluating $Q_0^{(\alpha,\beta)}(x)$, $P_n^{(\alpha,\beta)}(x)$, and $q_n^{(\alpha,\beta)}(x)$.

The functions that have been described here are but a few of the countless analytical expressions that can be used to fit experimental data. They have illustrated the fitting expressions may be as simple as a power series, or as complex as a family of elaborate transcendental functions. It would clearly be best to use analytical expressions upon which the ideal response is dependent, but for many experiments, such expressions are not known. Sometimes this problem can be sidestepped by selecting functions that have the same general shape as the response. Usually if a family of these functions is used, the response can be described very accurately. If, however, a fitting routine is desired which will describe a response of any shape, a power series that converges rapidly, or a Fourier series, would be a good choice. Clearly the selection of fitting functions is largely intuitive, but knowledge of the physical nature of the response carries much of the weight in this decision.

CHAPTER 3

ELECTROCHEMICAL CONCEPTS

It may be beneficial to discuss briefly some electrochemical concepts before considering how transforms may be used to aid in the analysis of electrochemical experiments.

Heterogeneous Reaction Kinetics[1,2]

Electrochemical reactions that involve the transfer of an electron at an electrode/solution interface are examples of a class of reactions known as heterogeneous reactions. The kinetics of heterogeneous reactions are normally part of a sequence of steps involving both transport through the solution and transfer of charge at the interface.

Consider an electrode reaction

$$O + ne \rightleftarrows R \tag{3.1}$$

in which a dissolved oxidized species, O, is converted to a soluble reduced form, R, by the transfer of n electrons. At least five separate steps are required for the conversion of O to R:

(1) transport of O from the bulk solution to the interface
(2) adsorption of O onto the surface
(3) charge transfer at the electrode to form R
(4) desorption of R from the surface
(5) transport of R from the interface into the bulk solution.

Steps (2) through (4) are commonly referred to as the activation

process, whereas steps (1) and (5) are known as mass transport processes. For the simplest electrochemical reactions, the effect of adsorption/desorption is negligible and the rate of the activation process is dependent upon the standard heterogeneous charge-transfer rate constant k_s and the transfer coefficient α. As k_s becomes larger, the overall rate becomes progressively more dependent upon the mass transport processes. If k_s is very large, then the charge-transfer occurs very quickly and the reaction is said to be reversible or nernstian.

Mass Transport

There are three mechanisms for mass transport in solution. These are convection, migration, and diffusion.

i) Convection

This is a very efficient means of mass transport in which the solute is moved by moving the whole solution. This, however, is not a very reproducible process and hence it is usually avoided for quantitative analysis. The exceptions to this are studies with a rotating disc electrode in which the convection is reproducible. Convection may be inhibited by not stirring the solution and also by performing rapid experiments so that natural convection does not have sufficient time to become established.

ii) Migration

This process arises from the interaction of ions with an

electric field within the solution. This is a relatively slow process for the fields commonly encountered in electrochemical experiments. This mechanism is also undesirable for quantitative analysis. The contribution from migration may be rendered insignificant by using relatively large concentrations of a supporting electrolyte that serves to decrease the cell resistance.

iii) Diffusion

Diffusion occurs in a fluid whenever there is a concentration gradient. It is a slow process that attempts to equalize the concentration throughout the solution. The mathematics of diffusion has been studied in a number of physical systems and it is well established. Thus, for many electrochemical experiments, the idealized reaction is often considered under diffusion control since other mass transport mechanisms may be successfully inhibited.

Fick's Laws of Diffusion

Fick's laws are partial differential equations that describe the flux of a substance and its concentration as functions of time and position. Consider the case of linear diffusion in which species O diffuses along an axis normal to the electrode surface. The flux of species O at a given location x at a time t may be written as $J_o(x,t)$ with units of mol $s^{-1}m^{-2}$. Thus $J_o(x,t)$ represents the number of moles of species O that passes a given

location per second per m^2 of area normal to the axis of diffusion. Fick's first law states that this flux is proportional to the concentration gradient, $\partial C_o/\partial x$:

$$-J_o(x,t) = D_o \frac{\partial C_o(x,t)}{\partial x} \tag{3.2}$$

where D_o is the diffusion coefficient of species O with units of $m^2 s^{-1}$ and the direction of positive flux is taken to be away from the electrode. The current that flows across the electrode interface is given by

$$-J_o(0,t) = \frac{i(t)}{nAF} = D_o \left[\frac{\partial C_o(x,t)}{\partial x}\right]_{x=0} \tag{3.3}$$

since the total number of electrons transferred at the electrode in a unit time must be proportional to the quantity of O that reaches the electrode in that time period.

Fick's second law, an extension of the first law, states

$$\frac{\partial C_o(x,t)}{\partial t} = D_o \frac{\partial^2 C_o(x,t)}{\partial x^2} \tag{3.4}$$

which relates the change in the concentration with distance to the change in concentration with time.

Partial differential equations, such as Fick's laws, can be very difficult to solve; but solutions are given in the next chapter by simplifying the mathematics with the Laplace transform.

The Nernst Equation

The potential of an electrode is given by the Nernst equation[1] as

$$E = E^\circ - \frac{RT}{nF} \ln\left(a_R/a_O\right) \tag{3.5}$$

where E° is the standard potential of the half-reaction

$$O + ne \rightleftarrows R \tag{3.6}$$

and 'a' denotes the activity of species O or R at the electrode surface. The calculation of the electrode potential would not normally be possible with equation (3.5) because the activities of O and R are rarely known. However, this equation may be rewritten as

$$E = E^{\circ\prime} - \frac{RT}{nF} \ln\left(C_R^S / C_O^S\right) \tag{3.7}$$

where $E^{\circ\prime}$ is the formal potential of the half-reaction and C_j^s represents the surface concentration of species j. The formal potential is given[1] by

$$E^{\circ\prime} = E^\circ - \frac{RT}{nF} \ln\left(\gamma_R/\gamma_O\right) \tag{3.8}$$

where γ denotes an activity coefficient. Therefore the electrode potential may be calculated with equation (3.7) if the formal potential and the concentrations of O and R are known.

Faradaic and Nonfaradaic Processes

There are two types of processes that can occur at an

electrode. One kind obeys Faraday's law which states that the amount of chemical reaction caused by the flow of current is proportional to the amount of electricity passed. These are known as faradaic processes. An example of such a process is the transfer of an electron across a metal-solution interface which causes an oxidation or reduction to occur. Under some conditions, the potential across an electrode-solution interface may be varied over a range without permitting charge transfer processes to occur. These reactions may not occur because they are either thermodynamically or kinetically unfavorable. However, processes such as adsorption and desorption can occur and the structure of the electrode-solution interface can change significantly with potential or solution composition. These processes are examples of nonfaradaic processes. Although a charge does not cross the interface for any of these processes, external currents can flow, if only transiently.

Both faradaic and nonfaradaic processes occur during an electrode reaction. Usually the information of primary interest is contained within the faradaic current which must be separated from the nonfaradaic current. One of the major contributions to the nonfaradaic current is a charging current associated with the electrode double layer. This double layer forms because the charge that is distributed on the electrode surface will be

counterbalanced by ions within the solution. This gives the electrode-solution interface the properties of a capacitor and hence when the potential is changed, a current will flow. Two techniques, both of which rely on Riemann-Liouville transforms, will be presented in the next chapter to illustrate methods by which the currents from faradaic and nonfaradaic processes may be separated.

Polarization[3,4]

When a current is passed across on electrode-solution interface, the potential of the electrode is shifted from the equilibrium value before current flowed. This phenomenon is known as polarization and it arises from the slow rate of some of the partial processes that are required to convert O to R. If this rate-determining process is mass transport, then the electrode is concentration polarized. Similarly, if the rate-determining process is the charge-transfer reaction, the electrode is activation polarized. Still another form of polarization can arise, namely ohmic polarization, when resistance within the cell is a limiting factor.

The effect of ohmic polarization is usually minimized by using a supporting electrolyte. Since activation polarization is dependent upon the value of the rate constant k_s, it is not easily adjustable. Concentration polarization can be easily obtained by

applying a potential at which all of species O that is in contact with the electrode will be immediately reduced to species R. This will limit the current to the rate at which O can be transported to the electrode surface.

If an electrode is very polarized, then the current resulting from the electrode reaction will change only slightly as the potential of the electrode undergoes a relatively large variation. Thus a small variation in potential within the range of concentration polarization will have a negligible effect on the current response. This property can often be exploited to relax restrictions placed upon a potential waveform within the region of polarization.

CHAPTER 4

PREVIOUS APPLICATIONS OF TRANSFORMS IN ELECTROCHEMISTRY

The nature of electrochemistry makes it a prime candidate for analysis by a wide variety of mathematical techniques. The interrelationships between current, potential, and time seem endless since each parameter can be varied in a number of ways to affect the other two. Some of these relationships can become rather complicated and they can only be deciphered with the aid of higher order mathematics. Many of these mathematical techniques have been applied in other chemical disciplines, especially in the realm of spectroscopy, but the variety and versatility of these techniques will be illustrated by considering only electrochemical applications.

Fick's Second Law and the Laplace Transform

Many physical systems may be described by equations that require the evaluation of derivatives or integrals. The method by which a solution to these equations is found can often be simplified with the aid of the Laplace transform. The Laplace transform of a derivative, is given in the equation

$$L\left[\frac{d}{dt} F(t)\right] = sf(s) - F(0) \qquad (4.1)$$

This transforms the complicated operation of differentiation in

the time domain into the simpler operations of multiplication and subtraction in the s-domain. Similarly, the Laplace transform of an integral,

$$L\left[\int_0^t F(t)dt \right] = \frac{f(s)}{s} \tag{4.2}$$

simplifies the operation of integration in the time domain into division.[1]

Although equations comprised of derivatives can be difficult to solve, partial differential equations present even greater difficulties. The Laplace transform may be applied here to transform these partial differential equations into ordinary differential equations. As an example, consider Fick's second law [i.e. equation (3.4)]. This equation relates the first derivative of concentration with respect to time to the second derivative of concentration with respect to distance. The Laplace transform of Fick's second law with respect to time is[2]

$$s\overline{C}_o(x,s) - C_o(x,0) = D_o \frac{d^2\overline{C}_o(x,s)}{dx^2} \tag{4.3}$$

in which the bar over the C denotes that it is a transformed function. If the system starts at equilibrium, the initial condition is

$$C_o(x,0) = C_o^* \tag{4.4}$$

where C_o^* is the bulk concentration of species O. Equation (4.3) now becomes

$$s\bar{C}_o(x,s) - C_o^* = D_o \frac{d^2C_o(x,s)}{dx^2} \qquad (4.5)$$

which is a second order ordinary differential equation in distance. This equation may then be solved to yield

$$\bar{C}_o(x,s) = C_o^*/s + A(s)\exp[-(s/D)^{\frac{1}{2}}x] + B(s)\exp[(s/D)^{\frac{1}{2}}x] \qquad (4.6)$$

where A(s) and B(s) are independent of x. The evaluation of A(s) and B(s) requires two boundary conditions; that is, $\bar{C}_o(x,s)$ must be known at two values of x. A common boundary condition is that the concentration of species O at an infinite distance from the electrode remains at the bulk concentration. This forces B(s) to be zero and hence equation (4.6) becomes

$$\bar{C}_o(x,s) = C_o^*/s + A(s)\exp[-(s/D)^{\frac{1}{2}}x] \qquad (4.7)$$

The second boundary condition usually pertains to behaviour at the electrode surface which will then complete the solution to equation (4.5).

The solution to Fick's second law will describe the concentration as a function of distance and time. It is generally more useful, however, to determine the current that flows across the electrode-solution interface. The relationship between

current and the flux of species 0 was given in equation (3.3). Its Laplace transform is

$$\frac{\bar{i}(s)}{nAF} = D_o\left[\frac{d\bar{C}_o(x,s)}{dx}\right]_{x=0} \tag{4.8}$$

in which $\bar{i}(s)$ is the Laplace transform of the current from the time domain.

An experiment that is often performed is one in which the electrode is concentration polarized. This condition may be established by applying a potential at which any of species 0 that is in contact with the electrode will immediately be reduced to species R. Equation (4.7) now becomes

$$\bar{C}_o(x,s) = C_o^*/s - (C_o^*/s)\exp[-(s/D)^{\frac{1}{2}}x] \tag{4.9}$$

upon application of this second boundary condition. Equation (4.8) may be evaluated by substitution of the x-derivation of equation (4.9) to yield

$$\bar{i}(s) = nAFD_o^{\frac{1}{2}}C_o^*/s^{\frac{1}{2}} \tag{4.10}$$

for which inversion yields the current-time response

$$i(t) = nAFC_o^*\left(\frac{D_o}{\pi t}\right)^{\frac{1}{2}} \tag{4.11}$$

which is known as the Cottrell equation. Note that the effect of depleting the electroactive species near the electrode surface is

characterized by a $t^{-\frac{1}{2}}$ function. This form of time dependence is frequently encountered in other experiments that are controlled by diffusion.

The same technique that was outlined above can often be used for the analysis of systems in which the electron transfer reaction is perturbed by homogeneous chemical reactions that involve O or R.[3]

Analysis in the Laplace Plane[4,5]

The Laplace transform of the current, $\bar{i}(s)$, is often a much simpler function than the time domain current, $i(t)$. Therefore, for cases in which the functionality of the time domain current cannot be determined, or when it can only be approximated, it may be advantageous to analyze the experimental data in the Laplace plane. This technique, in which the data must be Laplace transformed, has not been used extensively even though its utility has been demonstrated.[6]

The most convenient method of performing the Laplace transform of the data is to multiply each data point $i(t)$ by $\exp(-st)$ and then to perform a numerical integration of the resulting curve. This process is repeated for a number of desired values of s until a new collection of data points describing $\bar{i}(s)$ is obtained.

As an illustration of the application of this method, consider the response to a potential step perturbation of the irreversible

reaction

$$O + ne \xrightarrow{k} R \tag{4.12}$$

where k is the rate constant corresponding to the final potential. The Laplace transform of the current response for this reaction is found by methods similar to those discussed in the previous section to be

$$\bar{i}(s) = \frac{nAFkC_o^* D_o^{\frac{1}{2}}}{s^{\frac{1}{2}}(k+s^{\frac{1}{2}}D_o^{\frac{1}{2}})} \tag{4.13}$$

which upon rearrangement yields

$$\frac{1}{\bar{i}(s)s^{\frac{1}{2}}} = \frac{1}{nAFC_o^* D_o^{\frac{1}{2}}} + \frac{s^{\frac{1}{2}}}{nAFkC_o^*} \tag{4.14}$$

Thus, a plot of $1/\bar{i}(s)s^{\frac{1}{2}}$ against $s^{\frac{1}{2}}$ will yield a straight line with a slope of $1/nAFkC_o^*$ from which k may be determined.

The current response in the time domain for the reaction is

$$i(t) = nAFkC_o^* \exp[k^2/D_o t]\operatorname{erfc}[k/(D_o t)^{\frac{1}{2}}] \tag{4.15}$$

where erfc is the complement of the error function. This expression can be used for quantitative kinetic analysis only by expanding the product of the exponential and error function complement in terms for either small or large values of t. This approximation, therefore, neglects data from intermediate times. Analysis in the Laplace plane, however, does not suffer from this

limitation since all of the data are used in the calculation of the Laplace transform.

Analysis in the Laplace plane would be particularly valuable for systems in which the electrochemical reaction is coupled to chemical processes. In these systems, the inverse transformation of $\bar{i}(s)$ is often difficult, whereas the function $\bar{i}(s)$ itself is commonly a simple algebraic function of s.

Faradaic Admittance [7-9]

In many electrochemical experiments, the system is subjected to a large perturbation which drives the electrode to a condition far from equilibrium. A response is then observed, usually in the form of a transient signal. A useful alternative is to perturb the cell with a small alternating signal and then to observe the way in which the system follows the perturbation. This technique permits measurements of high precision to be made since the response may be periodic indefinitely and therefore may be averaged over a long time. Also, since the experiment is performed close to equilibrium, important simplifications can be made in the treatment of kinetics and diffusion. This technique has been applied chiefly to quasi-reversible systems in which the response is dependent upon both diffusion and heterogeneous charge-transfer kinetics. For such reactions, as k_s becomes larger, the reaction rate becomes progressively more diffusion controlled.

In such experiments, a dc mean potential value, E_{dc}, is imposed on the working electrode. This dc potential is then scanned slowly with time. A sinusoidal component, E_{ac}, of perhaps 5 mV peak-to-peak amplitude is superimposed upon the dc potential. The responses that are measured are I_{ac}, the magnitude of the ac component of the current at the frequency of E_{ac}, and ϕ, the phase angle of the ac current with respect to E_{ac}. The role of the dc potential is to set the mean surface concentrations of O and R. This potential usually differs from the equilibrium value and hence a thin layer next to the electrode will be established through which O and R must diffuse. This layer grows with time and it soon exceeds the zone affected by the rapid sinusoidal perturbations. Therefore, the mean surface concentrations of O and R resemble bulk concentrations to the ac part of the experiment. Hence the ac current response has the same period as E_{ac} but it will lag by the phase angle ϕ which is dependent upon the rate of the electrode reactions.

This method of analysis is referred to as either a faradaic admittance or faradaic impedance technique. Impedance is the total "effective resistance" to an ac current and admittance is the reciprocal of this quantity. However, neither of these quantities need be determined since the parameters of interest may be obtained from the expression[10]

$$\cot(\phi) - 1 = (\tfrac{1}{2}D\omega)^{\frac{1}{2}}/k_s \qquad (4.16)$$

where ω is the frequency of the ac modulation and D is a diffusion coefficient given by

$$D = D_O^{\alpha} D_R^{1-\alpha} \qquad (4.17)$$

in which α is the charge transfer coefficient representing the fraction of the potential that favors the reduction reaction. Hence a plot of $\cot(\phi)$ against $\omega^{\frac{1}{2}}$ should be linear with an intercept of unity and a slope from which k_s can be calculated for a known D.

Faradaic admittance measurements depend on the linearity of current-overpotential relations at low overpotentials. This linear behaviour is established when the electrochemical response is diffusion controlled. In a linear system, excitation at a frequency ω provides a current that is also of frequency ω. The current-overpotential function for an electrode reaction may be nonlinear, however, over moderate ranges of overpotential producing a distorted response that is not purely sinusoidal. Even so, the response will be periodic and can be represented by a Fourier synthesis of signals at frequencies ω, 2ω, 3ω,..., etc. The Fourier synthesis is performed with a Fourier series such as

$$E(t) = \frac{a_0}{2} + \sum_{n=1}^{\infty} [a_n \cos(n\omega t) + b_n \sin(n\omega t)] \qquad (4.18)$$

or, alternatively

$$E(t) = K_0 + \sum_{n=1}^{\infty} K_n \sin(n\omega t + \phi_n) \qquad (4.19)$$

where K_0 is the dc level and K_n is the amplitude of the component with frequency $n\omega$ and phase angle ϕ_n.

Although the advantage of ac measurements were recognized in the late 1940's and early 1950's, ac techniques have made their most significant advances since the introduction of the Fast Fourier Transform in the past decade which revolutionized instrumentation for faradaic admittance measurements. The use of the FFT in faradaic admittance studies is particularly useful when the electrochemical response is not diffusion controlled or the current-overpotential function is nonlinear.

The complete characterization of an electrochemical process by admittance methods is a tedious operation because information is required at a set of frequencies ranging over 2 to 3 decades and at a set of potentials ranging over $E^{\circ\prime} \pm 100$ mV. The time required for this analysis may be reduced by applying an excitation signal comprised of a Fourier synthesis of all of the desired frequencies. This excitation signal is often a noise waveform rather than a pure sinusoid. The best choice for this signal is an odd-harmonic, phase-varying pseudorandom white noise.[11] This noise is produced by the superposition of several

frequencies, all of which have equal amplitude so that they carry the same weight. The phase angles are randomized so that there will not be large swings in the amplitude of the total excitation signal. The frequencies selected for the excitation signal are all odd harmonics of the lowest frequency. This choice ensures that second-harmonic components will not appear in the currents measured for the fundamental frequencies.

The application of this excitation signal will induce a current that will show related "noisy" variations. The response is monitored with the aid of computer interfaced instrumentation and then Fourier transformation yields the distribution of harmonics embodied within the response. The faradaic admittance may then be calculated at the frequency of each Fourier component for a potential E_{dc}. Changing E_{dc} after each complete set of measurements will then permit the faradaic admittance to be determined as a function of both E_{dc} and ω.

The efficiency of this technique has been enhanced by the ability of the Fourier transform to resolve a complex waveform into its components. This has made it possible to apply as many as 15 frequencies at once[11] instead of only one as was the conventional method. This capacity for simultaneous measurement illustrates the multiplex advantage that was mentioned in a previous chapter.

Spectroelectrochemistry [12-14]

In recent years there has been much interest in studying electrode processes by experiments that involve more than the usual electrochemical variables of current and potential. Part of the motivation for this work has been to provide ways to obtain information about electrochemical systems that could not be obtained from purely electrochemical experiments.

In the 1960's, experiments were developed that combined ultraviolet-visible spectroscopy with conventional electrochemical techniques. These methods have proved to be very valuable for the characterization and monitoring of electrogenerated species.

Electrochemistry has long served as a means of generating and monitoring reactive species in solution, usually on a time scale of a few seconds down to the submillisecond range. In most electrochemical experiments, the potential is controlled and a current is monitored to obtain mechanistic and thermodynamic information. Methods based on the measurement of current have been used with significant success but they often lack selectivity since the observed current may reflect reactions from several species in solution.

The information gained from an electrochemical experiment can often be enhanced by the addition of an optical probe to gather spectral information about the material generated at the

electrode. This modification also increases the selectivity of the experiment.

Several spectroelectrochemical methods have been developed which combine a variety of spectroscopic and electrochemical techniques. Some of the configurations that have been used for absorption spectroelectrochemistry include passing light through an optically transparent electrode,[15] reflecting light off an electrode,[16] and passing light parallel to a planar electrode.[17] These techniques have been employed successfully for a number of systems and have increased the utility of spectroelectrochemistry for studies of fast reactions.

There are some limitations, however, when these techniques are applied to systems with short-lived or weakly absorbing electrogenerated species. In all electrochemical experiments, the events of interest occur within a thin layer of solution close to the electrode surface. If the dominant mode of mass transport is diffusion, then this region is referred to as the diffusion layer. This region is very thin [$\sim(Dt)^{\frac{1}{2}}$ or ~100 μm at 10s] which places restrictions on the optical methods that can be applied. One restriction is that the effective path length for a beam passing through a transparent electrode is determined by the thickness of the diffusion layer. This technique, therefore, would only be sensitive to strong absorbers with relatively long lifetimes.

Absorption spectroelectrochemistry is generally limited to concentrations above 10^{-4} M whereas the detection limit should be in the order of 10^{-6} M or 10^{-8} M to make it a more generally useful analytical tool.

One technique that has displayed many advantages over previous methods is diffractive spectroelectrochemistry. This method analyses the diffraction of UV-visible light by an electrode. Consider a beam of light impinging on an electrode as shown in Figure 4.1.

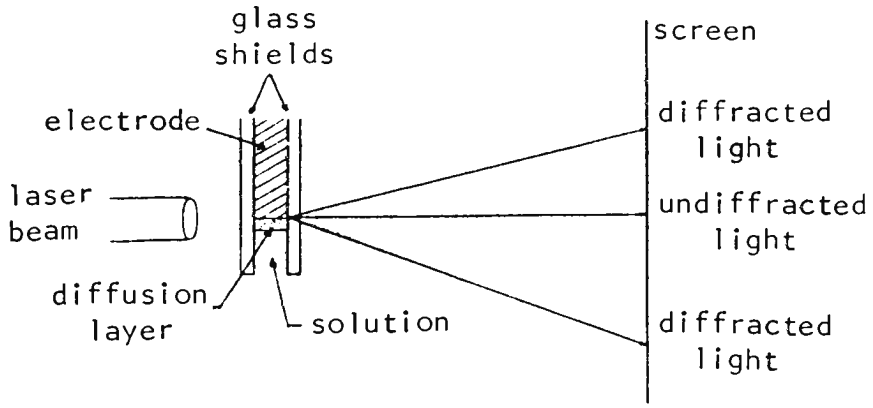

Figure 4.1 General experimental configuration for monitoring light diffracted by an electrode. Diffracted intensity is distributed symmetrically above and below the undiffracted beam.

Part of the beam strikes the electrode and part of it travels parallel to the electrode surface. Diffraction by the electrode will scatter light away from the main beam. Some diffracted intensity will appear in the shadow of the electrode as well as in the region below the beam. The major contribution to the

diffracted intensity comes from light passing close to the electrode surface. Light that passes far from the electrode will not be diffracted appreciably, and hence, to a first approximation, all the diffracted light has passed through the thin layer of interest close to the electrode surface. Thus monitoring of diffracted intensity during the generation of a chromophore will be sensitive to the concentration of that chromophore.

The diffraction pattern obtained from such an experiment is a spatial Fourier transform of the intensity distribution of the light that passes the electrode after interaction with the chromophore. Therefore, the relationship between the generation of the chromophore and the diffracted intensity is embedded in the Fourier transform. Thus, information can be gained about the chromophore generation with the aid of Fourier transform techniques.[13]

There are many advantages to this diffractive approach over absorption spectroelectrochemical methods. This method provides high sensitivity since the effective path length is limited by the electrode length rather than the thickness of the diffusion layer. Fast response times are also possible, especially if a high-powered laser is used in conjunction with a highly efficient photon receptor. Finally, a unique feature of this technique is that Fourier inversion of the diffraction pattern will yield the

chromophore distribution as a function of time. Experimental concentration profiles could be obtained with resolution on the order of the wavelength of the light employed. These profiles could be obtained under a variety of experimental conditions to establish the basis for a number of mass transport processes. Diffractive spectroelectrochemistry is a technique which is only in its infancy but it promises to evolve into an excellent probe for the diffusion layer. This is a region of extreme importance but it has been difficult to probe with conventional methods.

Riemann-Liouville Transformation[16]

The surface concentration of species O, for any electrochemical technique, is given by the expression

$$C_o(t) = C_o^* - \frac{1}{nAFD_o^{\frac{1}{2}}}\left[\frac{1}{\pi^{\frac{1}{2}}}\int_0^t \frac{i(u)}{(t-u)^{\frac{1}{2}}}\,du\right] \qquad (4.20)$$

The only restriction built into this expression is that the experiment is performed under conditions of semi-infinite linear diffusion and with an equilibrium existing prior to t=0. No assumptions have been made concerning the reversibility of the charge transfer reaction or even the dependence of surface concentrations on potential. Hence this expression is applicable for any form of excitation signal.

The bracketed term in equation (4.20) may be obtained by either of two methods. One method uses the convolution integral of Laplace transformation which has been discussed earlier. The other method uses the Riemann-Liouville transform of order $-\frac{1}{2}$. This operation is known as semiintegration and is denoted as $d^{-\frac{1}{2}}/dt^{-\frac{1}{2}}$. The equivalence that exists between the semiintegral and the convolution integral does not extend to Riemann-Liouville transforms in general.

(i) Riemann-Liouville Transform Polarography[19]

Riemann-Liouville transforms are employed in the fractional calculus in which the differential operator d^q/dt^q may be evaluated for any value of q.[20] The form of the Riemann-Liouville integral that is employed depends upon the magnitude of q. For $q<0$,

$$\frac{d^q}{dt^q}(f(t)) = \frac{1}{\Gamma(-q)}\int_0^t \frac{f(u)}{(t-u)^{q+1}}\,du \qquad (4.21)$$

and for $0 \leqq q<1$,

$$\frac{d^q}{dt^q}(f(t)) = \frac{d}{dt}\left[\frac{1}{\Gamma(1-q)}\int_0^t \frac{f(u)}{(t-u)^q}\,du\right] \qquad (4.22)$$

Algorithms have been derived which enable these expressions to be evaluated numerically.[21]

An attractive property of the Riemann-Liouville transform is its ability to render variable functions of time invariant; that is,

$$\frac{d^q}{dt^q}(kt^q) = k\Gamma(q+1) \tag{4.23}$$

which is valid for all values of q. This property may be exploited to enable the faradaic and capacitative components to be separated from a current that flows at a dropping mercury electrode. This current is described by the equation

$$i(t) = i_f(t) + i_c(t) = k_f t^{1/6} + k_c t^{-1/3} \tag{4.24}$$

in which[22]

$$k_f = 4nFC_o^* \left(\frac{7\pi D_o}{3}\right)^{\frac{1}{2}} \left(\frac{3m}{4\pi d_{Hg}}\right)^{\frac{2}{3}} \tag{4.25}$$

and

$$k_c = 2C_i(E_z - E) \left(\frac{4}{3}\pi\right)^{\frac{1}{3}} \left(\frac{m}{d_{Hg}}\right)^{\frac{2}{3}} \tag{4.26}$$

where m is the rate of mercury flow for the dropping mercury, d_{Hg} is the density of mercury, C_i is the integral capacitance of the double layer, and E_z is the potential of zero charge. Various methods have been developed in an attempt to separate $i_f(t)$ from

$i_c(t)$ but the simplicity of the Riemann-Liouville transform was only introduced recently by Soong and Maloy.[19] Transformations of order $-\frac{1}{3}$ and $+\frac{1}{6}$ were applied repetitively on $i(t)$ to determine k_f and k_c. This method enabled a linear calibration curve to be obtained for Cd^{2+} over a concentration range of 0.1 μM to 0.1 mM. This procedure has the advantage that sophisticated instrumentation required for other separation techniques may be replaced by a more versatile and less costly computer while maintaining high sensitivity.

(ii) Cottrell Filtering

Another method that uses Riemann-Liouville transforms to separate faradaic and non-faradaic currents is the Cottrell filter. This technique was developed and studied by Hempstead and Oldham but as yet remains unpublished. This method is applicable to a Cottrell experiment for which the current response is given by

$$i(t) = nAFC_o^* \left(\frac{D_o}{\pi t}\right)^{\frac{1}{2}} + f_?(t) \qquad (4.27)$$

where $f_?(t)$ is a current extraneous to the faradaic process under study. The Riemann-Liouville transform possesses the convenient properties

$$\frac{d^{\frac{1}{2}}}{dt^{\frac{1}{2}}}\left(\frac{k}{(\pi t)^{\frac{1}{2}}}\right) = 0 \qquad (4.28)$$

and

$$\frac{d^{-\frac{1}{2}}}{dt^{-\frac{1}{2}}}\left(\frac{k}{(\pi t)^{\frac{1}{2}}}\right) = k \qquad (4.29)$$

where $d^{\frac{1}{2}}/dt^{\frac{1}{2}}$ is the semidifferentiation operator and $d^{-\frac{1}{2}}/dt^{-\frac{1}{2}}$ is the semiintegration operator. These properties may be employed in the scheme outlined in Figure 4.2 to obtain $nAFC_o^{*}D_o^{\frac{1}{2}}$ which enables the faradaic component of the current to be analyzed.

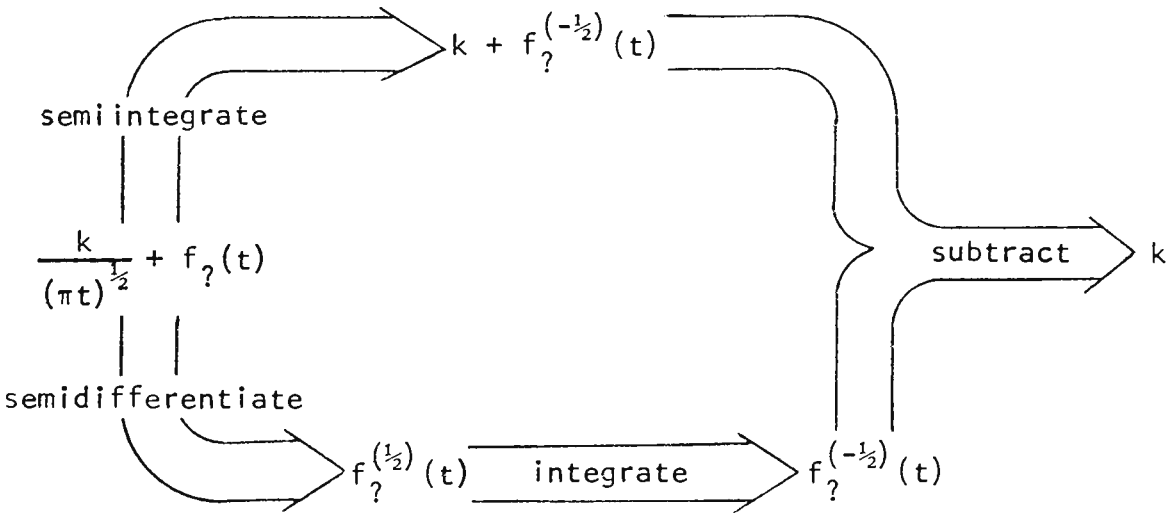

Figure 4.2 Outline for Cottrell filtering where $k = nAFC_o^{*}D_o^{\frac{1}{2}}$.

CHAPTER 5

REVERSAL TECHNIQUES IN ELECTROCHEMISTRY

It will be useful to describe some electrochemical reversal techniques so as to lay the groundwork for the study that will be described in subsequent chapters. Reversal techniques comprise a large and growing class of experiments that feature the generation of an electrochemical product followed by the reversal of electrolysis which permits the product to be examined electrochemically. These procedures are summarized by

$$O + ne \longrightarrow R \quad \text{, generation phase} \tag{5.1a}$$
$$R - ne \longrightarrow O \quad \text{, reversal phase} \tag{5.1b}$$

or alternatively

$$R - ne \longrightarrow O \quad \text{, generation phase} \tag{5.1a'}$$
$$O + ne \longrightarrow R \quad \text{, reversal phase} \tag{5.1b'}$$

Reversal techniques are especially useful for studies of complex electrode kinetics.[1] An example of a kinetic complication is illustrated in the mechanism

$$O + ne \rightleftarrows R \tag{5.2a}$$
$$R \xrightarrow{k} X \tag{5.2b}$$

The product, R, of the electrode reaction reacts to produce a species which is not electroactive at potentials where the reduction of O is occurring. This mechanism may be denoted E_rC_i to indicate a reversible electron transfer followed by an

irreversible homogeneous chemical reaction.[2]

A number of diverse reversal techniques are examined in this chapter and the effect of an E_rC_i mechanism on each is discussed.

Double Step Chronoamperometry

The simplest reversal technique is probably double step chronoamperometry. The method is illustrated in Figure 5.1. An electrode is immersed in a solution containing species O that is reversibly reduced in the vicinity of the potential $E^{\circ\prime}$. The initial potential, E_i, is much more positive than $E^{\circ\prime}$ and hence no electrolysis occurs. At t=0 the potential is changed abruptly to E_g, which is far more negative than $E^{\circ\prime}$. This induces the generation of species R under concentration polarized conditions for a period T. At t=T a second potential step shifts the electrode to the more positive value E_r. (In many cases $E_r=E_i$.) This reverses the electrolysis; hence species R is reoxidized to species O. The direct "observation" of species R after its electrogeneration permits an evaluation of R's participation in homogeneous chemical reactions on a time scale comparable to T.

The current response during the generation phase is given by the Cottrell equation[3]

$$i_g(t) = nAFC_o^*\left(\frac{D_o}{\pi}\right)^{1/2}\left[\frac{1}{t^{1/2}}\right] \quad , \quad 0<t<T \qquad (5.3)$$

whereas the current response during the reversal phase in the

absence of a homogeneous reaction such as (5.2b) is described by the equation first derived by Kambara[4]

$$-i_r(t) = nAFC_o^* \left(\frac{D_o}{\pi}\right)^{\frac{1}{2}} \left[\frac{1}{(t-T)^{\frac{1}{2}}} - \frac{1}{t^{\frac{1}{2}}}\right] \quad , \quad t>T \qquad (5.4)$$

These responses are illustrated in Figure 5.2.

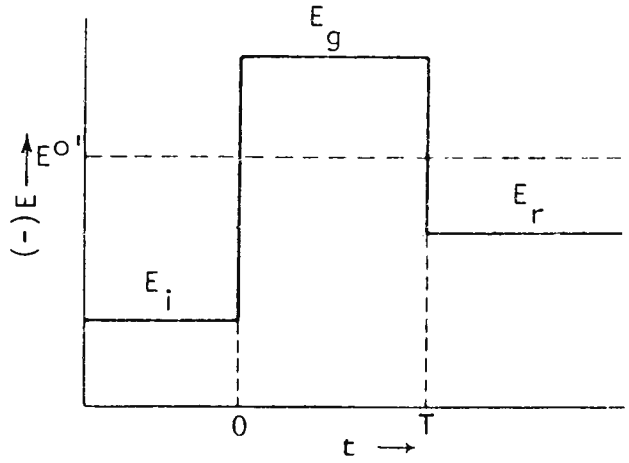

Figure 5.1 General waveform for a double step experiment

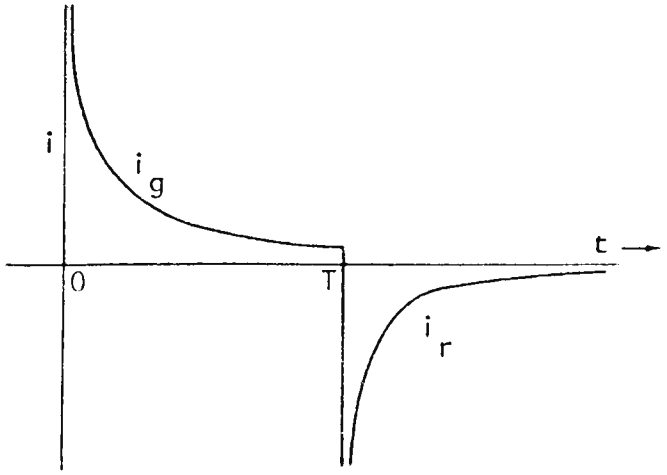

Figure 5.2 Current response for a double step experiment

The generation and reversal currents are both proportional to $C_o^* AD_o^{\frac{1}{2}}$, which is often unknown. Therefore, it is more convenient

to use a ratio of these currents, rather than their absolute values, when comparing a real experiment to the prediction. If t_g and t_r are the times at which the current measurements are made, then

$$-\frac{i_r(t_r)}{i_g(t_g)} = \left(\frac{t_g}{t_r - T}\right)^{\frac{1}{2}} - \left(\frac{t_g}{t_r}\right)^{\frac{1}{2}} \qquad (5.5)$$

A simple check for a stable system is that $-i_r(2T)/i_g(T) \simeq 0.293$. Departures from this ratio indicate kinetic complications in the electrode reaction.[5] For example, an E_rC_i mechanism would cause the reversal current to be less than predicted by equation (5.4) and hence the current ratio would also be smaller.

Double Step Chronocoulometry

The double step chronocoulometric experiment resembles the double step chronoamperometric experiment in many ways, the potential waveform being the same. The way in which these experiments differ is that chronocoulometric experiments integrate the current over time so that the charge passed, Q(t), is obtained. This method offers many advantages over the widely used chronoamperometric mode:

i) the measured signal grows with time and hence the later parts of the current transient, which are usually minute, are more accessible

ii) the operation of integration smooths random noise on the current transients and hence the signal is "cleaner"

iii) contributions to Q(t) from double-layer charging can be distinguished from those due to diffusing electroreagents. The analogous separation for chronoamperometry is not feasible.[6]

The simplest chronocoulometric experiment is analogous to the double step experiment described previously. If the double-layer charge is much smaller than Q(t), then

$$Q_g(t) = 2nAFC_o^* \left(\frac{D_o t}{\pi}\right)^{1/2} \quad , \quad 0<t<T \qquad (5.6a)$$

$$Q_r(t) = 2nAFC_o^* \left(\frac{D_o}{\pi}\right)^{1/2} \left[T^{1/2}+(t-T)^{1/2}-t^{1/2}\right] \quad , \quad t>T \qquad (5.6b)$$

in the absence of homogeneous reactions. The shapes of these response functions are shown in Figure 5.3.

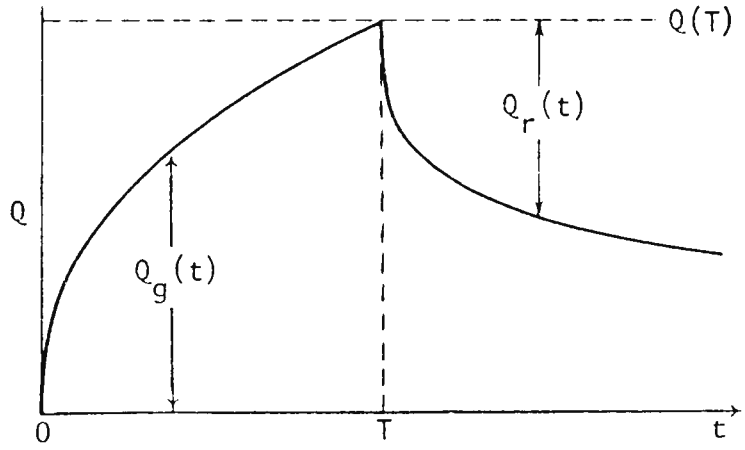

Figure 5.3 Chronocoulometric response for a double step experiment

The stability of the product species can be tested by the ratio

$$\frac{Q_r(t_r)}{Q_g(T)} = 1 + \left(\frac{t_r}{T} - 1\right)^{1/2} - \left(\frac{t_r}{T}\right)^{1/2} \qquad (5.7)$$

If the product species is stable, then $Q_r(2T)/Q_g(T) \approx 0.586$. The ratio defined by equation (5.7) is simply the fraction of the electrogenerated species that has been recaptured at the electrode. Thus, at t=2T, 58.6% of the electrogenerated species has been converted back to its precursor.

Collection Experiments

Collection experiments performed with a rotating ring-disc electrode (RRDE) incorporate similar concepts to the double step experiment except that two electrodes are used so that the reactions may occur simultaneously. A species is generated electrolytically at the disc and then collected by the ring that surrounds it (see Figure 5.4). Both processes are performed under conditions of concentration polarization.

The collection efficiency, N, is defined as

$$N = - \frac{i_R}{i_D} \tag{5.8}$$

where i_R and i_D are the currents at the ring and disc respectively. If the generated species is stable, the collection efficiency is constant for any RRDE regardless of angular velocity, C_O^*, D_O, or D_R. If the generated species reacts homogeneously at a rate sufficiently high that some is lost in its passage from the disc to the ring, then the measured kinetic collection efficiency, N_k, will be less than N. Information about the rate and mechanism of

the decomposition may then be obtained by the application of steady-state kinetics.[7-9] For typical experimental conditions, this technique is effective in measuring first order rate constants over the $0.03s^{-1}<k<10^{3}s^{-1}$ range.[10]

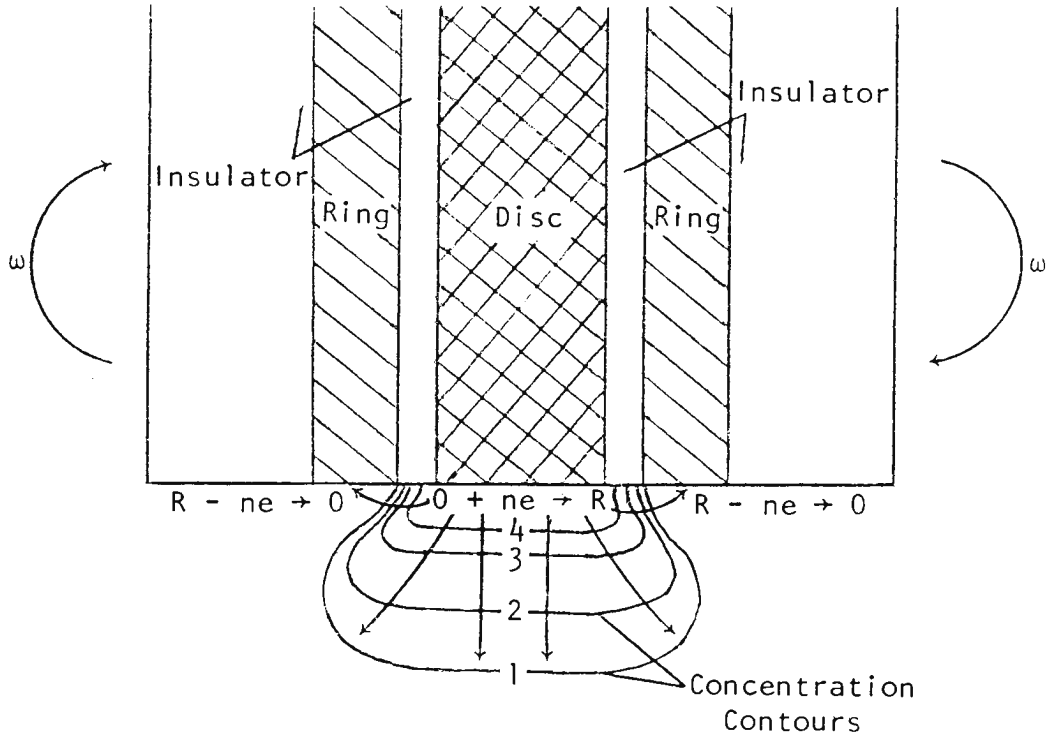

Figure 5.4 Schematic operation of RRDE. Concentration of species R increases proceeding from contours 1 to 4.

Current Reversal Potentiometry

In the previous experimental techniques, the potential was controlled and a current or charge response was monitored. Chronopotentiometric techniques control the current and monitor the potential.

The most common chronopotentiometric technique is the galvanostatic experiment in which a constant current flows through

the cell. For the electrode process, $O + ne \rightarrow R$,

$$i = nAFD_o\left(\frac{\partial C_o}{\partial x}\right)_{x=0} \tag{5.9}$$

where $D_o(\partial C_o/\partial x)_{x=0}$ denotes the flux of species O at the electrode surface.[11] Therefore, if a constant current flows, there must be a constant flux of species O, and hence the reduction occurs at a constant rate.

A galvanostatic experiment may be regarded as a "titration" of an electroactive species by a continuous flux of electrons. The concentration of the electroactive species will eventually drop to zero at the electrode surface and the flux of species O will become insufficient to accept all of the electrons that are being forced across the interface. The electrode potential will then change rapidly until a new reduction process begins. The time required before this transition occurs is denoted τ, as illustrated in Figure 5.6(a). The transition time τ is related to the concentration and diffusion coefficient of the electroactive species by the Sand equation[12]

$$i\tau^{\frac{1}{2}} = nAFC_o^{*}D_o^{\frac{1}{2}}\pi^{\frac{1}{2}}/2 \tag{5.10}$$

If the current was reversed, an oxidation reaction would occur. Species R would eventually become depleted at the electrode surface and the potential would rapidly become more positive until another oxidation process begins. This requires a second

transition time τ_2, as illustrated in Figure 5.6(b). It can be shown[13] that for a time t_1 taken prior to the first transition time, τ_1,

$$\tau_2 = t_1/3 \tag{5.11}$$

for stable R. Hence only ⅓ of the generated species R returns to the electrode up to the time τ_2. The remaining R diffuses into the bulk solution.

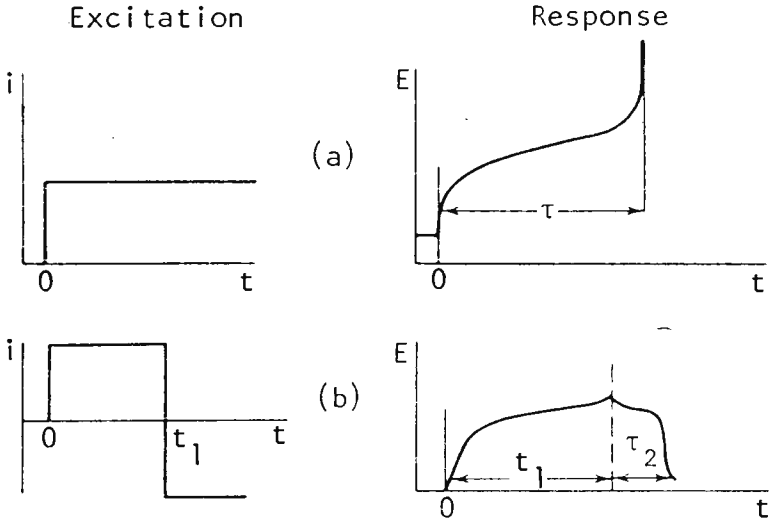

Figure 5.5 Two controlled current techniques. (a) Constant current potentiometry. (b) Current reversal potentiometry.

If kinetic complications arise in the form of an E_rC_i mechanism, then equation (5.11) becomes replaced by,[14]

$$\mathrm{erf}\left\{\left[k\left(t_1+\tau_2\right)\right]^{\frac{1}{2}}\right\} = 2\mathrm{erf}\left[\left(k\tau_2\right)^{\frac{1}{2}}\right] \tag{5.12}$$

where erf is the error function. If kt_1 is small (i.e. $R \xrightarrow{k} X$ is negligible), then equation (5.12) reduces to equation (5.11). If kt_1 is large (i.e. R decomposes rapidly), then τ_2 approaches zero.

Hence the value of k may be determined by varying t_1 and determining the ratio τ_2/t_1. This technique is applicable over the $0.1<kt_1<5$ range.[14]

Cyclic Voltammetry

Cyclic voltammetry is often used to investigate intermediates in an electrochemical reaction. The electrode potential is varied in a triangular waveform as described by[15]

$$E = E_i - \nu t \quad , \quad 0 \leq t \leq \lambda \tag{5.13a}$$

$$E = E_i - 2\nu\lambda + \nu t \quad , \quad t \geq \lambda \tag{5.13b}$$

where E_i is the initial potential, ν is the ramp rate, and λ is the switching time. Usually the current is plotted against potential, as shown in Figure 5.6(b). The product of the cathodic "hump" becomes the reactant for the anodic one. The rising current leading to the hump is caused by more favorable potentials for the electrode reaction. The falling current after the hump reflects the depletion of the reactant near the electrode surface.[16]

The current may also be plotted against time, as shown in Figure 5.7(b). Prior to $t=\lambda$ the current-time relationship is described by the Randles-Sevcik equation[17,18]

$$(i/nAFC_o^*)(RT/nFD_o\nu)^{1/2} = \pi^{1/2}\chi(x) \tag{5.14}$$

where R is the universal gas constant, T is the thermodynamic temperature, E_h is the polarographic half-wave potential of species O, and x is an abbreviation for $nF[E_h-E]/RT$. Reinmuth

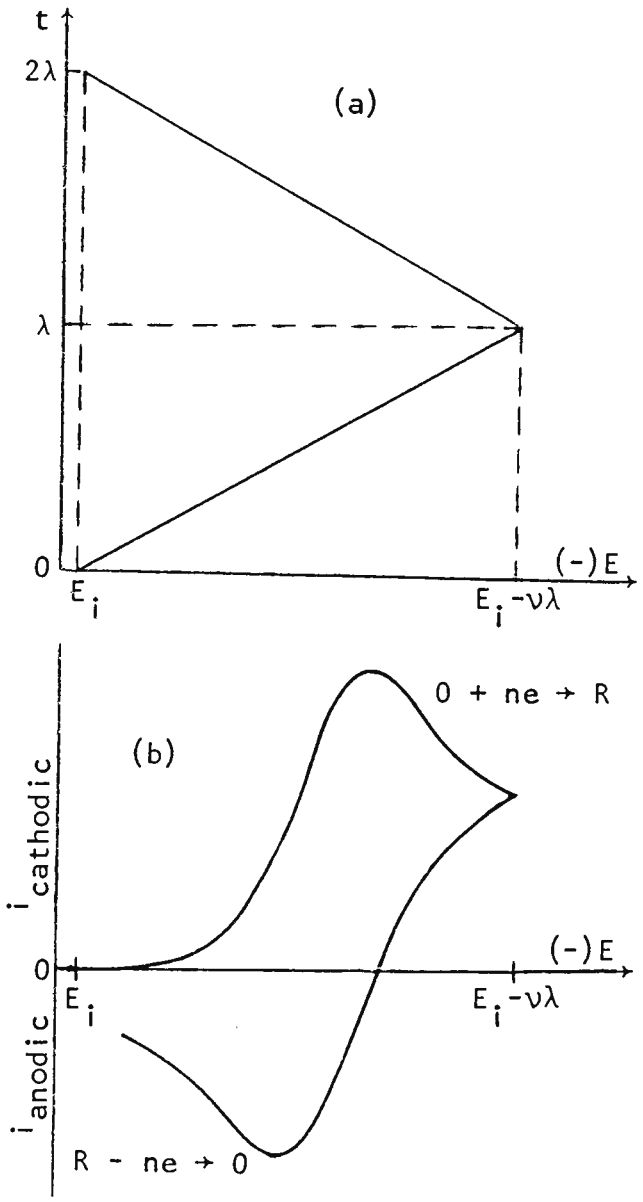

Figure 5.6 Cyclic voltammetry. (a) variation of potential with time. (b) variation of current with potential.

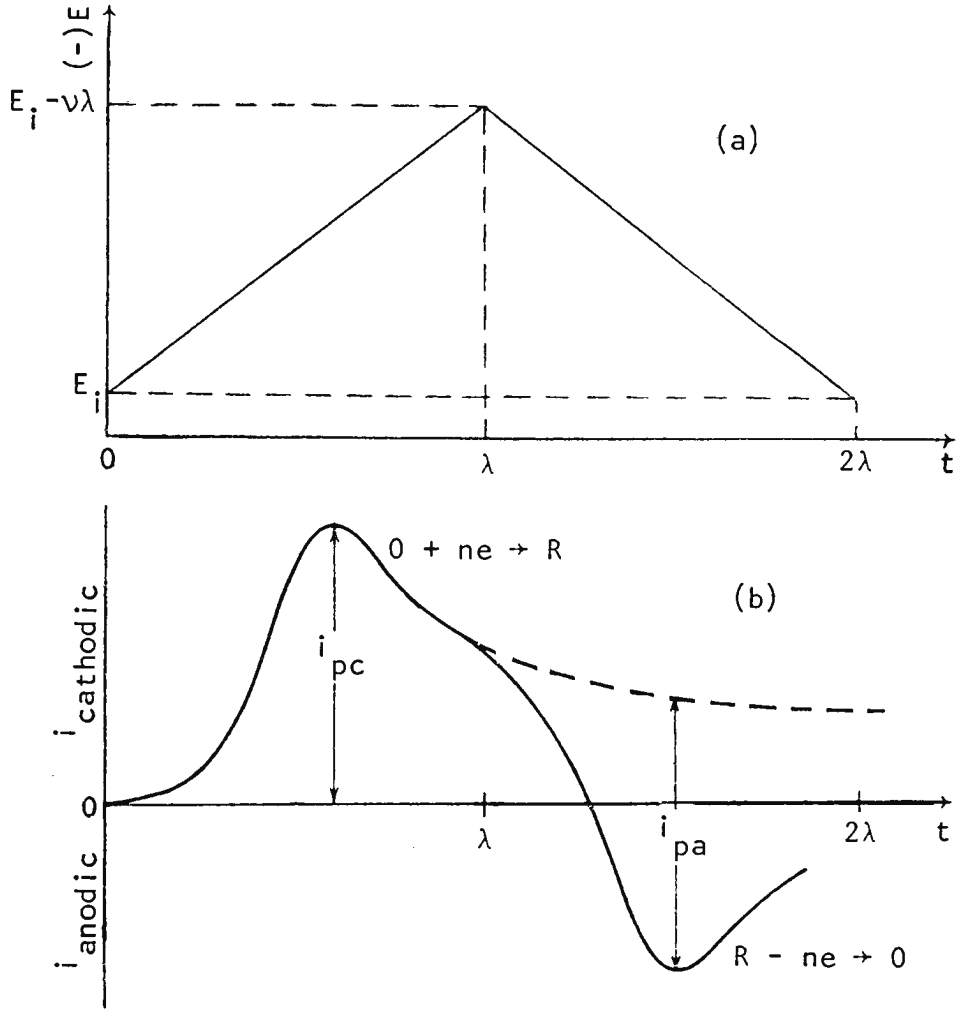

Figure 5.7 Cyclic voltammetry. (a) variation of potential with time. (b) variation of current with time. Solid line designates current for cyclic voltammogram; dashed line designates current for a linear voltage scan $E=E_i-\nu t$.

showed that for a reversible process the $\pi^{\frac{1}{2}}\chi(x)$ could be described simply as[19]

$$\pi^{\frac{1}{2}}\chi(x) = -\sum_{j=1}^{\infty} (-)^j \, j^{\frac{1}{2}} \exp(jx) \qquad (5.15)$$

which converges rapidly for negative values of x but diverges for

$x>0$. An expression that is valid for all values of x is[20]

$$\pi^{\frac{1}{2}}\chi(x) = L + Mx - Nx^2 + \left(\frac{\pi}{2}\right)^{\frac{1}{2}} \sum_{k=1}^{\infty} \left[\frac{(\beta-x)^{\frac{1}{2}}(\beta+2x)}{\beta^3} - \frac{8b^2 + 12bx - 15x^2}{8b^{7/2}} \right] \qquad (5.16)$$

where $L=0.380104813$, $M=0.118680871$, $N=0.043920560$, $b=(2k-1)\pi$, and $\beta=[b^2+x^2]^{\frac{1}{2}}$.

For times beyond $t=\lambda$ the expression for the current-time relationship is considerably more complicated. This complication arises because the electrochemical conditions upon which the current is dependent are characterized not only by $E-E_h$ but also by the total excursion that the potential has made since it first encountered E_h. This excursion may be expressed as E_h-2E_r+E, where E_r is the reversal potential. The nomenclature for the following relationships differ from that used for equations (5.14) and (5.16). The current prior to $t=\lambda$ is denoted $\overrightarrow{i}$ and the current after $t=\lambda$ is $\overleftarrow{i}$. The current-time relationship for the entire reversible cyclic voltammogram is described[21] by the equations

$$\overrightarrow{i} = \frac{nAFC_o^*}{\pi}\left(\frac{D_o nF\nu}{2RT}\right)^{\frac{1}{2}} \left\{ \lambda(3/2) - \frac{3\bar{y}}{2}\lambda(5/2) - \frac{15(\bar{y})^2}{8}\lambda(7/2) - \sum_{j=1}^{J} \frac{1}{j^{3/2}} - \frac{3\bar{y}}{2j^{5/2}} - \frac{15(\bar{y})^2}{8j^{7/2}} - \frac{\left[\bar{y}_j+\bar{y}\right]^{\frac{1}{2}}\left[\bar{y}_j-2\bar{y}\right]}{\left[\bar{y}_j\right]^3} \right\} \qquad (5.17)$$

and

$$\tilde{i} = \frac{nAFC_o^*}{\pi}\left(\frac{D_o nF\nu}{2RT}\right)^{1/2}\left\{\lambda(3/2) - \pi(2y)^{1/2} + \frac{3y^+}{2}\lambda(3/2) - \frac{15(y^+)^2}{8}\lambda(7/2)\right.$$

$$- \sum_{j=1}^{J}\frac{1}{j^{3/2}} - \frac{(128y)^{1/2}}{\pi j^2} + \frac{3y^+}{2j^{5/2}} - \frac{15(y^+)^2}{8j^{7/2}} + \sum_{s=\pm}\frac{8^{1/2}\,y^s}{\pi y^{1/2}\left[y_j^s\right]^2}$$

$$\left. - \frac{\left[y_j^s - y^s\right]^{1/2}\left[y_j^s + 2y^s\right]}{s\pi\left[y_j^s\right]^3}\arccos\frac{y-y_j^s}{s0_j^s} + \frac{\left[y_j^s + y^s\right]^{1/2}\left[y_j^s - 2y^s\right]}{\pi\left[y_j^s\right]^3}\operatorname{arccosh}\frac{y+y_j^s}{0_j^s}\right\} \tag{5.18}$$

where $y = nF(E-E_r)/\pi RT$

$\Delta = nF(E_h-E_r)/\pi RT$

$y^s = y + s\Delta$

$y_j^s = \left[j^2+(y^s)^2\right]^{1/2}$

$0_j^s = \left[j^2+(s\Delta)^2\right]^{1/2}$

and the summation index j takes odd integer values. The function $\lambda(p)$ is described[22] by

$$\lambda(p) = \sum_{j=1}^{\infty} j^{-p} = \frac{2^p-1}{2^p}\zeta(p) \qquad , j=1,3,5,\cdots , p>1 \tag{5.19}$$

where ζ is Riemann's zeta function. The relevant values of $\lambda(p)$ are given in the referenced article. Although equations (5.16) and (5.17) differ substantially in appearance, substituting equation (5.16) into equation (5.14) gives an expression that is

equivalent to equation (5.17).

A parameter of interest in a cyclic voltammogram is the ratio of the anodic peak current to the cathodic peak current (i.e. i_{pa}/i_{pc}). The measurment of i_{pa} and i_{pc} is illustrated in Figure 5.7(b). For a reversible electrode process, this ratio is unity regardless of scan rate, switching potential, or diffusion coefficients. Deviations from one indicate kinetic complications in the electrode process.

Stripping Analysis

This technique utilizes a bulk electrolysis step, commonly termed preelectrolysis, to preconcentrate an electroactive species into the small volume of a mercury electrode. After this electrodeposition step, the electroactive species is "stripped" from the electrode by some voltammetric method, usually linear sweep voltammetry. Exhaustive electrolysis of the solution may be avoided by proper calibration of the preelectrolysis step. If the conditions of the electrodeposition are maintained constant, then the voltammetric response (e.g. peak current) may be employed to determine the solution concentration. The principles of a stripping experiment are given schematically in Figure 5.8.[23]

Stripping analysis is most frequently used for the determination of metal ions by cathodic deposition followed by anodic stripping with a linear potential scan. This technique is often

called anodic stripping voltammetry or inverse polarography.

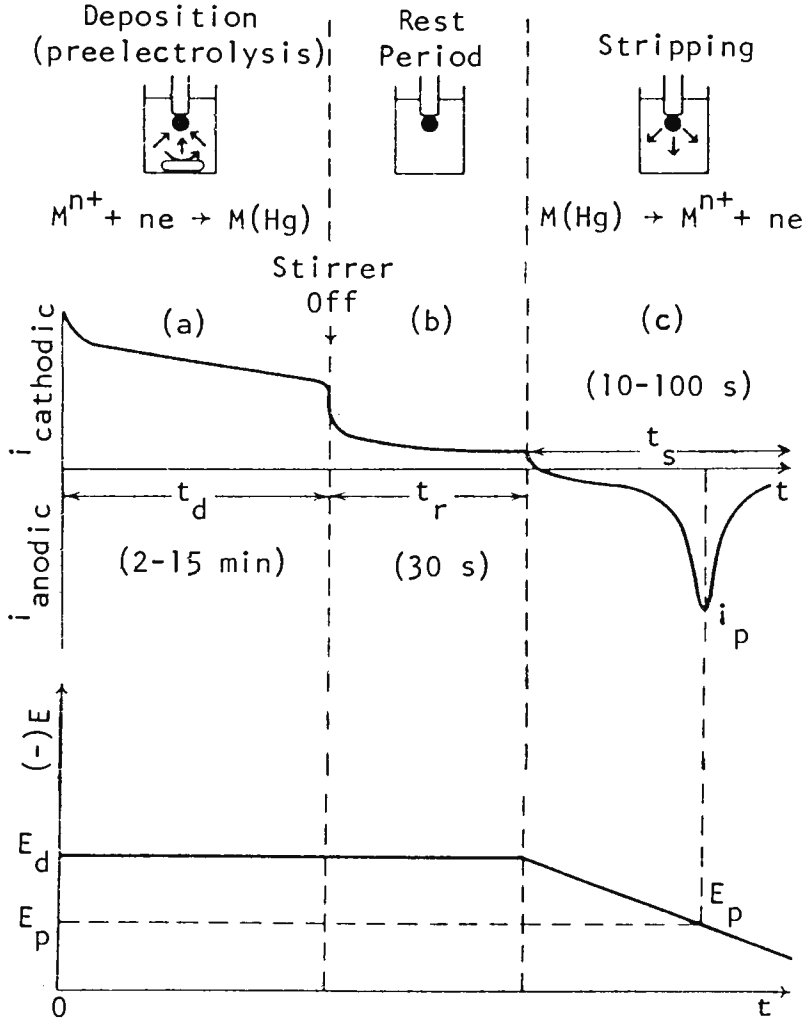

Figure 5.8 Schematic representation of an anodic stripping experiment. (a) Preelectrolysis at E_d; stirred solution. (b) Rest period; stirrer off. (c) Anodic scan (ν=10-100mV/s).

The electrodeposition step is carried out in a stirred solution at a potential E_d which is several tenths of a volt more negative than $E^{\circ\prime}$ for the least easily reduced metal ion to be determined. If the electrolysis is not exhaustive, the deposition

conditions must be the same for the sample and the standards.

After the deposition a rest period with the stirrer turned off is observed during which the solution is allowed to become quiescent, and the concentration of the metal in the amalgam becomes more uniform.

The stripping step is then initiated by scanning the potential linearly towards more positive values. If the sweep rate, ν, is sufficiently high (i.e. ν>20mV/s) then the concentration of amalgamated metal stays constant at the center of a hanging mercury drop electrode (HMDE). The analysis may therefore assume semi-infinite diffusion with a correction term for the sphericity of the HMDE. The peak current is then described by[24]

$$i_p = AD_M^{1/2}C_M^* \left(\alpha n^{3/2}\nu^{1/2} - \beta n D_M^{1/2}/r_o\right) \qquad (5.20)$$

where C_M^* is the concentration of the metal at the center of the drop, r_o is the drop radius, and α and β are constants equal to $2.69X10^5$ $Cmol^{-1}V^{-\frac{1}{2}}$ and $7.25X10^4$ $Cmol^{-1}$ respectively.

The major advantage of stripping analysis compared to direct voltammetric analysis is the preconcentration of the analyte within the electrode (by factors of 100 to more than 1000) so that the voltammetric (stripping) current is less perturbed by residual impurity or charging currents.[25] This is especially useful for the analysis of very dilute solutions ($\sim 10^{-10}$ M).

CHAPTER 6

GENERATION/RECAPTURE ANALYSIS

Consider the following electroanalytical problem. An electroactive analyte reduces, although not necessarily in a reversible manner, in the same range of potential as some interfering oxidant, such as oxygen, that it is either inconvenient or impossible to remove. The reduction current of the analyte will be obscured by that of the interferant thereby hindering analysis. If, however, the reduction product of the analyte is a soluble species that can be reoxidized under diffusion-controlled conditions at some potential at which there are no interferences, then a reoxidation current could be obtained that must be related somehow to the initial reduction current of the analyte. If the general relationship between the reduction current and the reoxidation current could be established, it should be possible to reconstruct the interference-free reduction current of the analyte from the interference free reoxidation current.

The problem may be restated, in a somewhat more general form, as follows. A solution containing an analyte, X, initially contains none of X's reduction product Y. Starting at time t=0, a potential is applied that induces the production of species Y. This reaction may be denoted

$$X + n_g e \longrightarrow Y \qquad (6.1)$$

in which n_g is the number of electrons consumed in the generation of Y. A faradaic current $i_g(t)$ will flow as Y diffuses, by semi-infinite planar diffusion, away from the electrode-solution interface. This generation phase ends at time t=T. After t=T the electrode is held at a potential (or in a range of potentials) at which species Y is reconsumed under conditions of complete concentration polarization. This reaction may similarly be denoted

$$Y + n_r e \longrightarrow Z \qquad (6.2)$$

where Z is the recapture product of Y and n_r is the number of electrons consumed in the recapture of Y. A faradaic current $i_r(t)$ will flow during this recapture phase of the experiment, t>T. The aim now is to determine a relationship between the currents $i_g(t)$ and $i_r(t)$. Establishment of such a relationship would enable the reconstruction of the generation current from the measured recapture current. The most versatile form for such a relationship would be one which does not place restrictions on the details of the generation process. However, the lack of restrictions will be reflected in the complexity of both the relationship and its development.

The simplest generation/recapture schemes are those in which the recapture reaction is the converse of the generation reaction, so that X=Z and $n_g+n_r=0$. These schemes are analogous to the

generation/reversal reactions discussed in the previous chapter with the restriction that the reversal phase must be treated as a recapture phase. [Recall that "reversal" simply implies that reaction (6.1) is followed by reaction (6.2) whereas "recapture" implies that the latter reaction occurs under conditions of complete concentration polarization and that Y is transported by semiinfinite planar diffusion]. A less common generation/recapture scheme is possible in which species Y is generated by a reduction process in one range of potential, and then further reduced in a recapture process at a more negative potential. A generation/recapture scheme of this nature would require that X be in the highest of three oxidation states. A similar scheme would be to perform successive oxidations of a species that is in the lowest of three oxidation states.

The combinations possible for reactions (6.1) and (6.2) are given in Table 6.1. The first two schemes correspond to the generation/recapture reactions in which Z corresponds to X and hence n_r is the negative of n_g. For the final two schemes, however, the generation/recapture proceeds by successive reductions, or successive oxidations, and hence Z differs from X. Therefore, both n_g and n_r would have the same sign but not necessarily the same magnitude.

generation reaction	recapture reaction	i_g	i_r	n_g	n_r
reduction	oxidation	cathodic	anodic	+	-
oxidation	reduction	anodic	cathodic	-	+
reduction	reduction	cathodic	cathodic	+	+
oxidation	oxidation	anodic	anodic	-	-

Table 6.1 Generation/recapture schemes with associated parameters

Interrelationship of the Currents

The recapture current is related to the generation current by the definite integral

$$i_r(t) = \frac{n_r}{\pi n_g (t-T)^{\frac{1}{2}}} \int_0^T \frac{i_g(\tau)(T-\tau)^{\frac{1}{2}}}{t-\tau} d\tau \qquad (6.3)$$

which is applicable for any time t greater than T. The only restrictions embodied within this expression are that

(i) both the generation and recapture reactions must be electrochemical,
(ii) species Y must initially be absent from solution,
(iii) the recapture reaction must occur under conditions of complete concentration polarization, and
(iv) transport must be by semiinfinite planar diffusion.

The proof for this expression is provided in appendix A by a rather lengthy exercise in Laplace transformation. Although the development of the interrelationship between the generation and recapture currents is rather involved, the final expression lacks

the complexity that one might have anticipated for such a general relationship. This simplicity, moreover, makes it easier to see the versatility of equation (6.3). Note that this expression enables the recapture current to be calculated by knowing only

(i) the generation current as a function of time
(ii) the duration of the generation phase, and
(iii) the ratio n_r/n_g.

Restrictions have not been placed on the potential waveform that can be imposed during the generation phase or on the electrochemical reversibility of the generation or recapture reactions. Thus equation (6.3) is more versatile than most current relationships encountered in electrochemistry.

An expression, equivalent to equation (6.3), which is valid for the first two generation/recapture schemes listed in Table 6.1 is

$$i_r(t) = - \frac{1}{\pi(t-T)^{\frac{1}{2}}} \int_0^T \frac{i_g(\tau)(T-\tau)^{\frac{1}{2}}}{t - \tau} d\tau \qquad (6.4)$$

since the ratio n_r/n_g is minus one for both of these reaction schemes. This expression is proven easily in appendix B with the aid of the fractional calculus. Although this second proof was not necessary to obtain equation (6.4), it illustrates that the fractional calculus can often offer advantages over "conventional" methods.

Since most generation/recapture experiments follow the reaction schemes in which the ratio n_r/n_g is minus one, the mathematical development that follows will be based on equation (6.4) rather than the more general equation (6.3). The assumption that the ratio n_r/n_g be minus one is not an essential restriction to this development but rather it will serve only to simplify many of the expressions that follow.

A generation/recapture experiment may be divided into three time periods. Initially, that is, for $t<0$, the system is at equilibrium during which nothing happens. Then, during $0<t<T$, species Y is created in the generation phase. Finally, for $t>T$, species Y is consumed in the recapture phase. The symmetry of the problem may be enhanced by considering the middle of the generation phase, that is, $t=T/2$, as the time origin. This new origin is established by the definition

$$g = r = \frac{2t}{T} - 1 \qquad (6.5)$$

which also undimensionalizes the independent variables g and r. Although g and r are identical, it will be convenient to use g as the independent variable of the generation current and r as the independent variable of the recapture process.

Equation (6.4) may be expressed in terms of the new independent variables as

$$i_r(r) = -\frac{1}{\pi(r-1)^{\frac{1}{2}}}\int_{-1}^{1}\frac{i_g(g)(1-g)^{\frac{1}{2}}}{r-g}\,dg \qquad (6.6)$$

in which r must be greater than one to describe the current in the recapture phase. It is convenient to define a "generation function" by the tripartite definition

$$G(g) = \left\{\begin{array}{ccc} 0 & , & g<-1 \\ (1-g)^{\frac{1}{2}} i_g(g) & , & -1<g<1 \\ 0 & , & g>1 \end{array}\right\} \qquad (6.7)$$

where the three periods correspond to the three phases of the experiment: equilibrium, generation, and recapture. Combination of this definition with equation (6.6) leads to

$$(r-1)^{\frac{1}{2}} i_r(r>1) = \frac{1}{\pi}\int_{-\infty}^{\infty}\frac{G(g)}{g-r}\,dg \qquad (6.8)$$

Thus, by referring to equation (2.10), it may be seen that the left-hand side of equation (6.8) equals the Hilbert transform of G(g) in the region r>1.

Recall that our ultimate intention is to devise a relationship which will enable the generation current to be reconstructed from the recapture current. Equation (6.8) establishes that the recapture current is proportional to the Hilbert transform of the generation function and equation (6.7) illustrates the simple manner in which the generation function is related to the generation current. The skew-reciprocity of the Hilbert transform

dictates that the generation function is described by the negative Hilbert transform of the left-hand side of equation (6.8). Calculation of the generation function will then enable the generation current to be reconstructed with the aid of equation (6.7). Unfortunately this operation is not as simple to implement as would be desired.

Consider a recapture function R(r) that is the Hilbert transform of G(g) defined by

$$H\{G(g)\} = R(r) = \left\{ \begin{array}{lll} R_1(r) & , & r<-1 \\ R_2(r) & , & -1<r<1 \\ (r-1)^{\frac{1}{2}} i_r(r) & , & r>1 \end{array} \right\} \tag{6.9}$$

where H is an operator denoting Hilbert transformation. It was shown in equation (6.8) that the Hilbert transform of G(g) is $(r-1)^{\frac{1}{2}} i_r(r)$ when r is greater than one. However, when r is less than one, that is, during the equilibrium and generation phases of the experiment, the recapture function is not zero and it has no experimental significance. Therefore $R_1(r)$ and $R_2(r)$ are unknown functions of r which are nonzero. If these functions were known, the identity

$$-H\{R(r)\} = G(g) = \left\{ \begin{array}{lll} 0 & , & g<-1 \\ (1-g)^{\frac{1}{2}} i_g(g) & , & -1<g<1 \\ 0 & , & g>1 \end{array} \right\} \tag{6.10}$$

could be used to reconstruct the generation function and thereby

the generation current $i_g(t)$.

Before trying to deal with our ignorance of $R_1(r)$ and $R_2(r)$, examples of generation/recapture experiments will be considered which illustrate the validity of this Hilbert transform relationship by deriving the functionality of $i_r(t)$ given $i_g(t)$. A number of Hilbert transform pairs are also listed in Table I as examples of recapture functions that correspond to given generation functions.

Hilbert Transform Analysis

i) Cottrellian Generation/Recapture Relationship

The current response during the generation phase of a Cottrell experiment, given by equation (5.3), may be expressed as

$$i_g(t) = nAFC^* \left(\frac{D}{\pi}\right)^{\frac{1}{2}} \left[\frac{1}{t^{\frac{1}{2}}}\right] \quad , \quad 0<t<\tau \tag{6.11}$$

This equation may be reformulated in terms of the independent variable g as

$$i_g(g) = \frac{k}{(1+g)^{\frac{1}{2}}} \quad , \quad -1<g<1 \tag{6.12}$$

where k is an abbreviation for $nAFC^*(2D/\pi T)^{\frac{1}{2}}$. The generation function, given by definition (6.7), is

$$G(g) = \left\{ \begin{array}{ccc} 0 & , & g<-1 \\ k\left(\frac{1-g}{1+g}\right)^{\frac{1}{2}} & , & -1<g<1 \\ 0 & , & g>1 \end{array} \right\} \tag{6.13}$$

The Hilbert transformation of equation (6.13) can be accomplished by performing the appropriate integrations, or, more effortlessly, by consulting Table I. The result is

$$H\{G(g)\} = \begin{cases} -k + k\left(\dfrac{-r+1}{-r-1}\right)^{\frac{1}{2}} , & r<-1 \\ -k , & -1<r<1 \\ -k + k\left(\dfrac{r-1}{r+1}\right)^{\frac{1}{2}} , & r>1 \end{cases} \qquad (6.14)$$

which is equivalent to $R(r)$.

The first two parts of the right-hand side of equation (6.14), in accordance with definition (6.9), correspond to the $R_1(r)$ and $R_2(r)$ functions that lack experimental significance. However, the third part of this solution corresponds to $(r-1)^{\frac{1}{2}} i_r(r)$. Hence the recapture current is given by

$$\begin{aligned} i_r &= \frac{-k}{(r-1)^{\frac{1}{2}}} + \frac{k}{(r+1)^{\frac{1}{2}}} && , r>1 \\ &= -nAFC^{*}\left(\frac{D}{\pi}\right)^{\frac{1}{2}}\left[\frac{1}{(t-T)^{\frac{1}{2}}} - \frac{1}{t^{\frac{1}{2}}}\right] && , t>T \end{aligned} \qquad (6.15)$$

This expression is equivalent to equation (5.4) which describes the current response in the reversal phase of a double-step chronoamperometric experiment. The reversal reaction in such an experiment occurs under conditions of complete concentration polarization and therefore satisfies the criterion for a recapture process. Hence the equivalence between equations (5.4) and (6.15) gives credibility to the Hilbert transform relationship.

ii) Galvanostatic Generation/Recapture Relationship

Consider an experiment in which species Y is generated at an electrode by a current of magnitude I that remains constant during $0<t<T$. This may require the restriction that T not exceed the transition time of the system (see current reversal potentiometry in previous chapter). The tripartite definition of the generation function,

$$G(g) = \left\{ \begin{array}{ccc} 0 & , & g<-1 \\ I(1-g)^{\frac{1}{2}} & , & -1<g<1 \\ 0 & , & g>1 \end{array} \right\} \qquad (6.16)$$

is obtained from equation (6.10) and the definition of g.

The recapture function, as given by the Hilbert transform of G(g) is

$$R(r) = -\frac{I}{\pi} \int_{-1}^{1} \frac{(1-g)^{\frac{1}{2}}}{g-r}\, dg \qquad (6.17)$$

The definite integral in this expression may be evaluated by the substitution $z^2=(1-g)/(1-r)$ or $z^2=(1-g)/(r-1)$ which leads to the tripartite result

$$R(r) = \left\{ \begin{array}{ll} K - K\left(\frac{1-r}{2}\right)^{\frac{1}{2}} \tanh^{-1}\left(\frac{2}{1-r}\right)^{\frac{1}{2}}, & r<-1 \\ K - K\left(\frac{1-r}{2}\right)^{\frac{1}{2}} \coth^{-1}\left(\frac{2}{1-r}\right)^{\frac{1}{2}}, & -1<r<1 \\ K - K\left(\frac{r-1}{2}\right)^{\frac{1}{2}} \tan^{-1}\left(\frac{2}{r-1}\right)^{\frac{1}{2}}, & r>1 \end{array} \right\} \qquad (6.18)$$

where K is the constant $2^{3/2}I/\pi$.

The first two parts of the right-hand side of equation (6.18) correspond to $R_1(r)$ and $R_2(r)$ which lack experimental significance. However, the third part yields

$$i_r = -\frac{2I}{\pi}\left[\left(\frac{2}{r-1}\right)^{\frac{1}{2}} - \tan^{-1}\left(\frac{2}{r-1}\right)^{\frac{1}{2}}\right]$$

$$= -\frac{2I}{\pi}\left[\left(\frac{T}{t-T}\right)^{\frac{1}{2}} - \tan^{-1}\left(\frac{T}{t-T}\right)^{\frac{1}{2}}\right] \qquad (6.19)$$

This expression is consistent with that obtained from the theory of the electrolysis of non-uniform solutions[1] if errors found in that article are corrected.

CHAPTER 7

CONSTRUCTION OF $i_r(t)$ FROM $i_g(t)$

Numerical Hilbert Transformation

Although the ultimate goal for this transform technique is to reconstruct an interference-free generation current from the recapture data, the construction of a recapture current from generation data will be investigated first since the mathematics required for this process is much simpler. The relationship between the recapture and generation currents was given in the previous chapter as

$$i_r(t) = -\frac{1}{\pi(t-T)^{\frac{1}{2}}} \int_0^T \frac{i_g(\tau)(T-\tau)^{\frac{1}{2}}}{t-\tau}\, d\tau \qquad (7.1)$$

The integral within this relationship is easier to evaluate numerically than are most Hilbert transforms for two reasons:

(i) the integration is performed over a finite range, whereas the Hilbert transform extends over $-\infty<\tau<\infty$

and

(ii) a singularity cannot arise in this integration because t is always greater than τ.

Equation (7.1) may also be written as

$$i_r(\rho) = \frac{1}{\pi\rho^{\frac{1}{2}}} \int_{-T}^0 \frac{i_g(\gamma)(-\gamma)^{\frac{1}{2}}}{\gamma-\rho}\, d\gamma \qquad (7.2)$$

where

$$\gamma = \rho = t - T \tag{7.3}$$

and γ is the independent variable for the generation current and ρ is the independent variable for the recapture process. Since γ and ρ are related linearly to time, equal spacing in either of these variables is equivalent to equal spacing in t.

Let the generation currents be $i_1, i_2, \cdots, i_J$ measured at times $t_1, t_2, \cdots, t_J$ which correspond to $\gamma_1, \gamma_2, \cdots, \gamma_J$. Let the spacing between all measurements be Δt but permit t_1 and $T-t_J$ to be other intervals. Equation (7.2) may be rewritten as

$$\pi\rho^{\frac{1}{2}} i_r(\rho) = \int_{-T}^{\gamma_2} \frac{i_g(\gamma)(-\gamma)^{\frac{1}{2}}}{\gamma - \rho}\, d\gamma + \sum_{j=2}^{J-2} \int_{\gamma_j}^{\gamma_{j+1}} \frac{i_g(\gamma)(-\gamma)^{\frac{1}{2}}}{\gamma - \rho}\, d\gamma + \int_{\gamma_{J-1}}^{0} \frac{i_g(\gamma)(-\gamma)^{\frac{1}{2}}}{\gamma - \rho}\, d\gamma \tag{7.4}$$

The generation current may be approximated by a linear fit between γ_j and γ_{j+1} using the expression

$$i_g(\gamma) \simeq \frac{(i_{j+1} - i_j)\gamma + i_j\gamma_{j+1} - i_{j+1}\gamma_j}{\gamma_{j+1} - \gamma_j} = \frac{a\gamma + b}{\Delta t} \tag{7.5}$$

where a and b are constants. It is then convenient to make the approximation

$$\int \frac{i_g(\gamma)(-\gamma)^{\frac{1}{2}}}{\gamma - \rho}\, d\gamma$$

$$\simeq \frac{1}{\Delta t} \int \frac{(a\gamma+b)(-\gamma)^{\frac{1}{2}}}{\gamma - \rho}\, d\gamma$$

$$= \frac{a}{\Delta t} \int (-\gamma)^{\frac{1}{2}}\, d\gamma + \frac{(a\rho+b)}{\Delta t} \int \frac{(-\gamma)^{\frac{1}{2}}}{\gamma - \rho}\, d\gamma$$

$$= -\frac{2a}{3\Delta t}(-\gamma)^{3/2} + \frac{2(a\rho+b)}{\Delta t}\left\{(-\gamma)^{\frac{1}{2}} - \rho^{\frac{1}{2}}\arctan\left[\frac{-\gamma}{\rho}\right]^{\frac{1}{2}}\right\} \qquad (7.6)$$

Equation (7.4) may now be approximated by

$$\frac{\pi\Delta t}{2} i_r(\rho)$$

$$\simeq \frac{1}{3\rho^{\frac{1}{2}}} \sum_{j=1}^{J-1} (i_{j+1}-i_j)\left[(-\gamma_j)^{3/2} - (-\gamma_{j+1})^{3/2}\right]$$

$$+ \sum_{j=1}^{J-1}\left\{(i_{j+1}-i_j)\rho + i_j\gamma_{j+1} - i_{j+1}\gamma_j\right\}$$

$$\times\left[\frac{(-\gamma_{j+1})^{\frac{1}{2}} - (-\gamma_j)^{\frac{1}{2}}}{(\rho)^{\frac{1}{2}}} - \arctan\left[\frac{-\gamma_{j+1}}{\rho}\right]^{\frac{1}{2}}\right.$$

$$\left. + \arctan\left[\frac{-\gamma_j}{\rho}\right]^{\frac{1}{2}}\right] \qquad (7.7)$$

with the stipulations that for j=1, all γ_j within square brackets must be replaced by -T and for j=J-1, all γ_{j+1} within square brackets must be replaced by zero.

At a time t selected such that t>T, the recapture current for the corresponding value of ρ, equivalent to $i_r(t)$, may be evaluated using equation (7.7). This evaluation was performed by a program called "TRNG→R" which is given in appendix C. The success of this algorithm is illustrated in Figure 7.1. Theoretical recapture data for a double step experiment are plotted along with the transform of the corresponding generation current. The agreement is so good that the difference is almost indistinguishable. This result was encouraging enough to warrant experimental study.

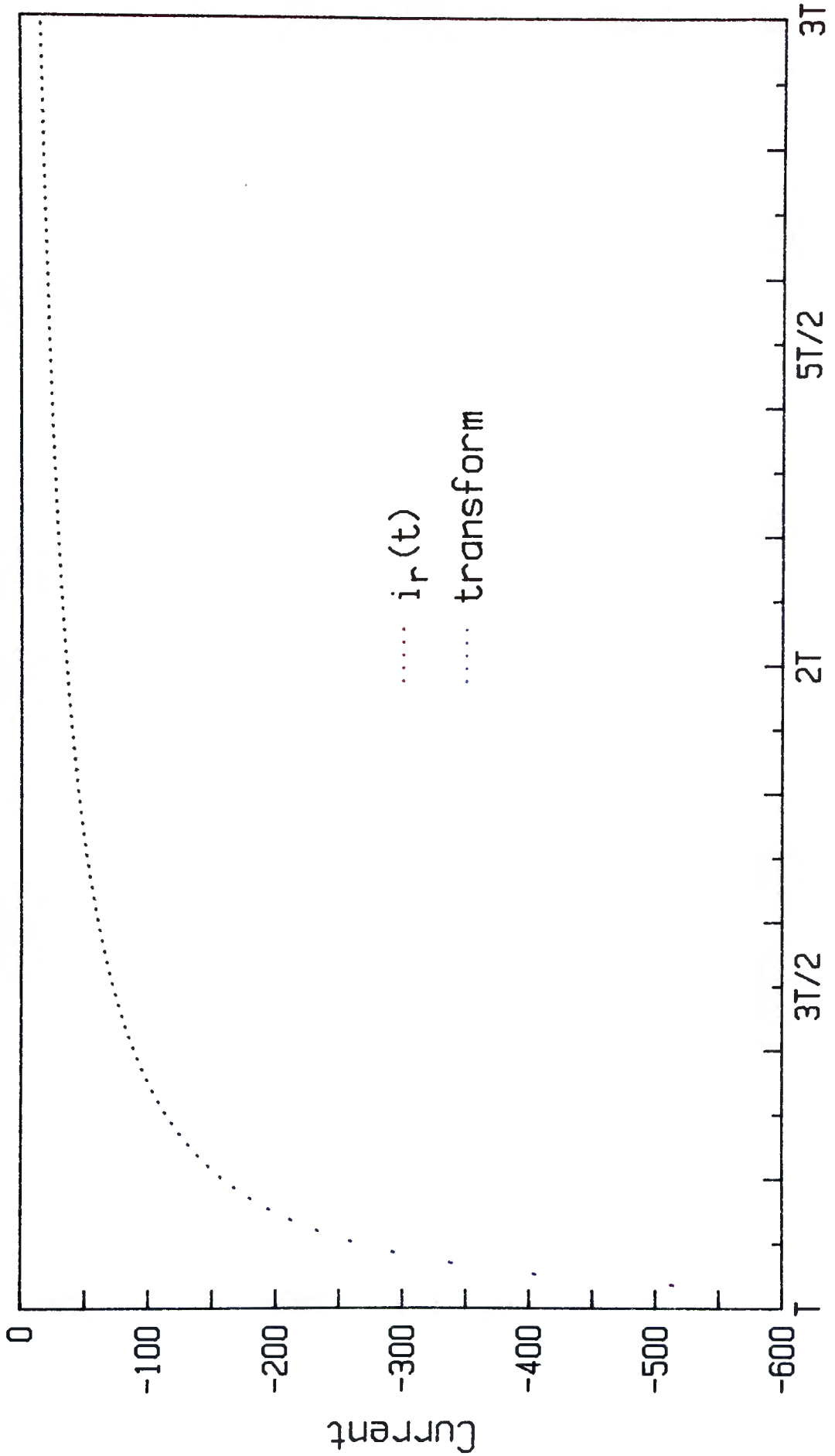

Figure 7.1 Transform of $i_g(t)$ to $i_r(t)$

Experimental Analysis

Chronoamperometric experiments on the systems

$$Fe(CN)_6^{3-} + e \rightleftarrows Fe(CN)_6^{4-} \qquad (7.8A)$$

$$Fe(C_2O_4)_3^{3-} + e \rightleftarrows Fe(C_2O_4)_3^{4-} \qquad (7.8B)$$

were performed for a variety of potential waveforms. These waveforms were designed to induce generation and, later, recapture. The generation current was Hilbert transformed using equation (7.7) to produce a curve that should correspond to the experimental recapture response. The current, $i_r[T]$, obtained from the transform will be compared graphically to the recapture data, $i_r[D]$.

The electrochemical reversibility of the two chemical systems is substantially different. The transform should produce the recapture response for a concentration polarized system regardless of its reversibility. The agreement between the transform and the recapture current will be compared for each system to establish whether the nernstian behaviour of the system is pertinent to the accuracy of this transform technique.

Reagents and Solutions

A) $Fe(CN)_6^{3-}$

Reagent grade chemicals and "polished" deionized water were used throughout. A 5.0 mM solution of $K_3Fe(CN)_6$ was prepared in a supporting electrolyte of 2.0 M KCl. The cell contents were deaerated with argon for about an hour prior to use.

B) $Fe(C_2O_4)_3^{3-}$

A supporting electrolyte of 1.0 M $K_2C_2O_4$ and 0.10 M $H_2C_2O_4$ was prepared from reagent grade chemicals and "polished" deionized water. A 5.0 mM solution of $Fe(C_2O_4)_3^{3-}$ was then prepared by dissolving triply recrystallized $K_3Fe(C_2O_4)_3 \cdot 3H_2O$ in the supporting electrolyte. The vessels used for this solution were shielded from the light since the $Fe(C_2O_4)_3^{3-}$ ion is known[1] to undergo light-catalyzed decomposition. This solution was also deaerated with argon for an hour prior to use.

Apparatus

The electrochemical cell consisted of a three-necked, round-bottomed flask. The vessel's capacity was about 200 mL but a fill line at about 100 mL was used. A platinum inlaid disc electrode (Pine Instrument Company, Model DT6) served as a stationary working electrode. This electrode had a finely machined surface consisting of a circular disc of area 46.1 mm^2 surrounded by a Teflon annulus, bringing the overall diameter to 18mm. The auxillary electrode was constructed simply of platinum foil. A commercially available (Beckman, Model 39403) saturated KCl/AgCl/Ag electrode served as the reference electrode.

The experiments were performed with a Princeton Applied Research Corporation Model 170 Electrochemistry System (hereafter abbreviated PARC 170). The PARC 170 was calibrated with a Digetec

Model 268 Millivoltmeter before each experiment. The PARC 170 was linked through an HP3497A data acquisition/control unit to an HP-85 personal computer. The HP3497A performed the digital-to-analog (D/A) and analog-to-digital (A/D) conversions which permit interaction between the cell and the HP-85 via an HP-IB interface. A schematic representation of the experimental apparatus is given in Figure 7.2.

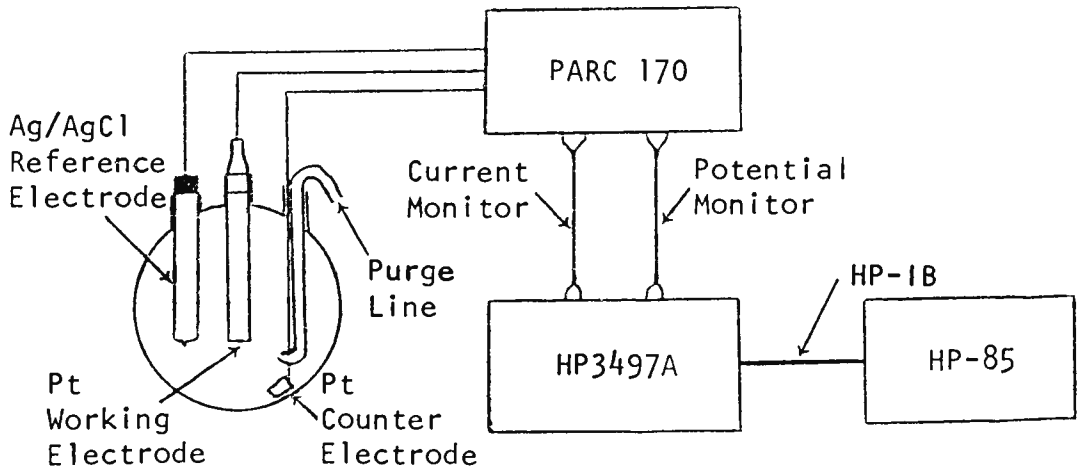

Figure 7.2 Schematic representation of the experimental apparatus

The potential waveforms that were applied in these experiments consisted of combinations of steps and linear ramps as detailed later. They were generated by the superposition of a voltage sent from the D/A of the HP3497A added to a waveform controlled by the PARC 170. For both of the step experiments, the PARC 170 applied a constant potential of -1.000 V upon which the HP3497A then applied the steps. All of the other experiments used a ramp controlled by the PARC 170 upon which steps could be applied by

the D/A of the HP3497A. There was always a potential applied to the PARC 170 from the D/A in the HP3497A, although over much of the ramp experiments, this potential was zero.

Each of the experiments started at the same potential. This potential was chosen in a region where the ferric complex is stable. Since none of the ferrous complex was present initially, the stability of the ferric complex ensures that a current cannot arise from this redox couple during the pre-electrolysis phase. There could have been other current sources, however, such as double layer charging or impurities in the system.

The initial potential, comprised of potentials from the PARC 170 and the D/A of the HP3497A, was applied to the cell by switching the selector switch on the PARC 170 from "Off" to "External Cell". While this initial potential was being applied, the program which controlled the experiment was waiting for a dummy input that would designate the start of data sampling, or time zero. A period of about ten seconds was allowed to elapse to permit the system to recover from stray currents, and then the dummy input was sent. For experiments that incorporated a ramp, the HP-85 would then send a command to the HP3497A to close a switch which grounded the external trigger on the PARC 170 thereby starting the ramp. A similar operation was not required for the step experiments. A timer within the HP-85 was then set which

provided a program interrupt whenever a data transfer across the interfacing was required. The data transfer was the most complex part of the program. A buffer containing the voltage sent by the D/A of the HP3497A was created in the HP-85. A portion of this buffer representative of a single voltage command was sent to the D/A of the HP3497A and at the same time another command was sent for the A/D of the HP3497A to take a current measurement. Calibration of the instrumentation indicated that the time between the application of the voltage and the measurement of a current was 20 ms (see appendix D). The current reading was then sent to a buffer in the HP-85. The data were stored in a packed format to improve execution time. Pointers were assigned to establish the portion of the voltage command buffer that would be sent next, and then the program waited for another timer interrupt. The duration of the data transfer routine was established at 140 ms and hence this was the fastest sampling rate (see appendix D). Upon completion of the experiment, the selector switch on the PARC 170 was returned to "Off". The current data were then unpacked and the corresponding times were calculated.

Experimental

The study of each chemical system followed a standard procedure. First a cyclic voltammogram was run to determine a suitable potential range for experimentation. Data taken from the

peaks on the cyclic voltammograms were also used to give an indication of the electrochemical reversibility of the system (see Figures 7.3A and 7.3B).

Each of the potential waveforms was applied to a solution containing first the ferricyanide or ferrioxalate, and then to the supporting electrolyte alone. "Background" was removed by subtracting the contribution from the supporting electrolyte. These background-corrected data were then Hilbert transformed using equation (7.7).

The data for each experiment were checked for consistency. Repetitive runs were performed until the experiment yielded a reproducible response. The data from this run were then stored on an HP magnetic tape cartridge for later analysis. The data for the ferricyanide or ferrioxalate only needed to be sampled two or three times to establish consistent behaviour but the data for the background took up to seven runs before a reproducible response was obtained.

A comparison between the transform and the recapture data will be presented graphically after a brief description of each experiment. The labelling adopted for these diagrams gives the experiment number followed by an "A" or a "B" to designate the system described by either equation 7.8A or 7.8B respectively.

Although the experiments lasted between 42 and 56 seconds,

only data from the first 30 seconds were plotted. The current changes the most drastically over this time period and the current at later times was not plotted since it was not as interesting. The current scale on each graph spans -600 μA to +600 μA. This range was fixed to permit variations in the current responses to be detected more easily. The data and Hilbert transform were plotted in sharply contrasting colours because, in many cases, the transform matches the recapture data so well that they are indistinguishable. In an attempt to better resolve the discrepancy between the transform and the recapture data, the later portion of the recapture graph was replotted on a scale spanning -100 μA to 0 μA. This 6:1 expansion provides sufficient magnification to show up most discrepancies.

The first few experiments implement conventional potential waveforms which were used to test the effect of electrochemical reversibility on the accuracy of this transform technique. Therefore , results from both system "A" and system "B" will be presented. Later experiments, however, were designed to illustrate the versatility of this transform technique by implementing unusual potential waveforms. The effect of electrochemical reversibility was not of interest in these experiments and hence only one system, namely system "A", was studied.

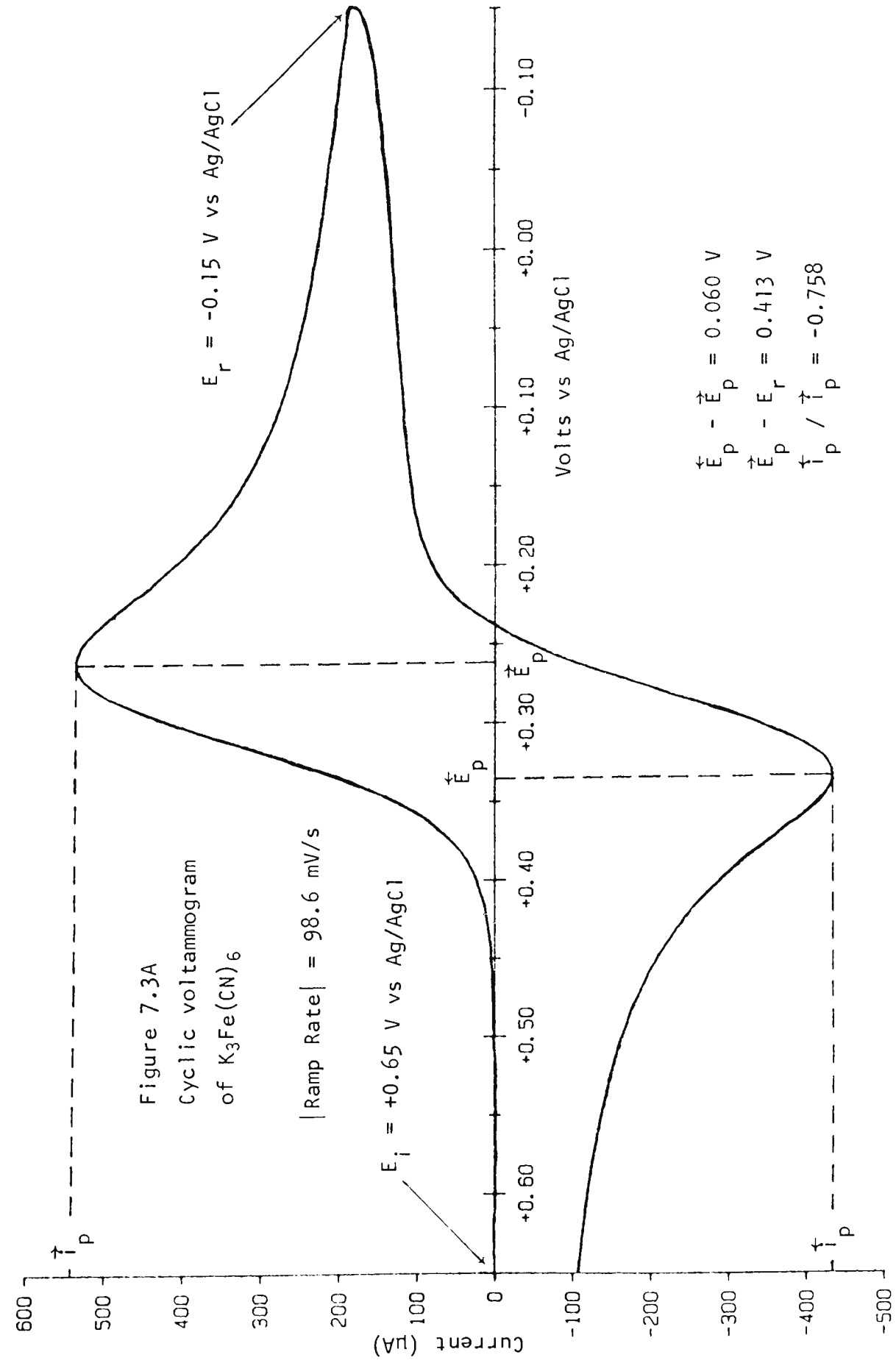

Figure 7.3A
Cyclic voltammogram
of $K_3Fe(CN)_6$

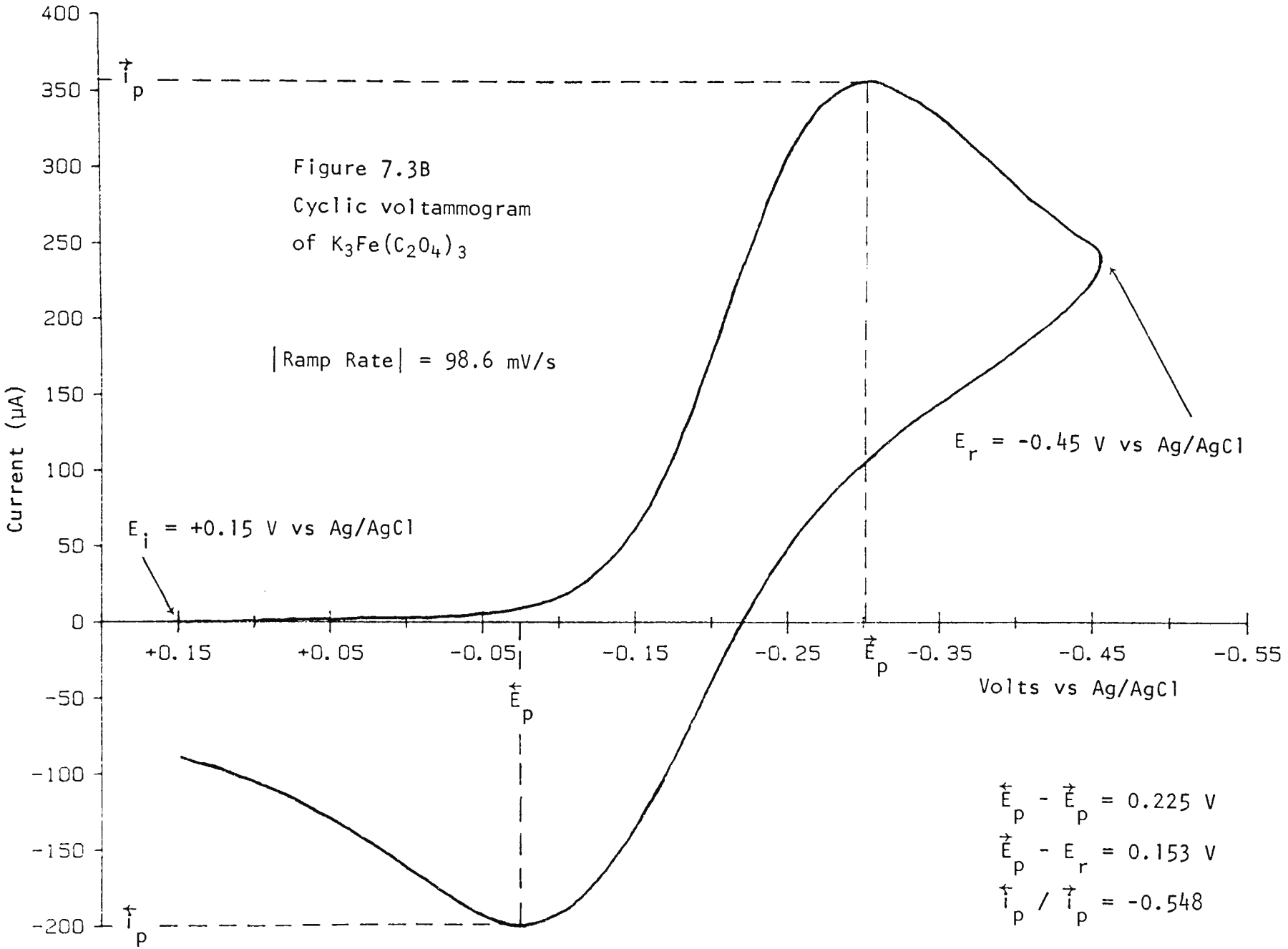
400
350
300
250
200
150
100
50
0
-50
-100
-150
-200
Current (μA)
$\vec{i}_p$
$\overleftarrow{i}_p$
Figure 7.3B
Cyclic voltammogram
of $K_3Fe(C_2O_4)_3$
|Ramp Rate| = 98.6 mV/s
E_i = +0.15 V vs Ag/AgCl
E_r = -0.45 V vs Ag/AgCl
+0.15
+0.05
-0.05
-0.15
-0.25
-0.35
-0.45
-0.55
$\vec{E}_p$
$\overleftarrow{E}_p$
Volts vs Ag/AgCl
$\overleftarrow{E}_p - \vec{E}_p = 0.225$ V
$\vec{E}_p - E_r = 0.153$ V
$\overleftarrow{i}_p / \vec{i}_p = -0.548$

E1 : Double Step Experiment

This experiment was controlled by the program "DSCHEM" (see appendix C). The potential waveform that was applied is illustrated in Figure 7.4.

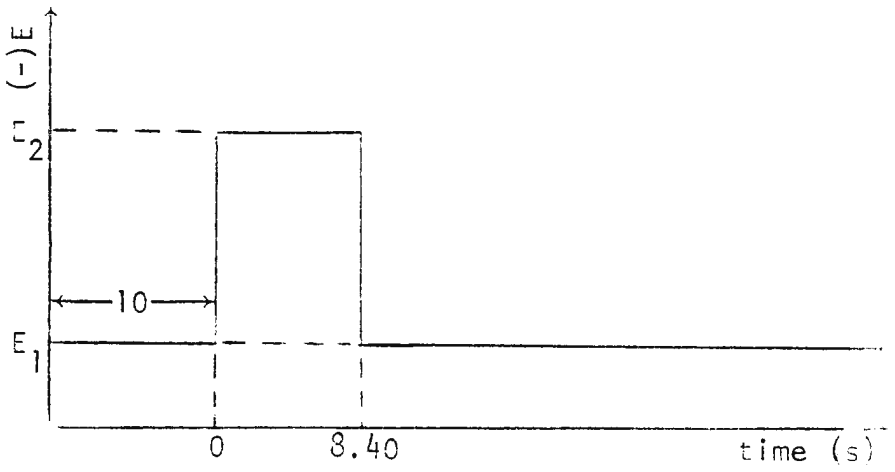

Figure 7.4 Potential waveform for double step experiment

The potentials E_1 and E_2 designate the initial and reversal potentials utilized for the cyclic voltammograms. These potentials are in the regions of concentration polarization for the redox reactions of the ferric/ferrous couples. At the potential E_1, the ferric complex is electrochemically stable; whereas it is the ferrous complex that is stable at E_2.

After time zero, designated by the application of E_2, the ferric complex was reduced to its ferrous partner. The generation of the ferrous complex proceeded for 8.4 seconds and then the potential was restored to E_1. The ferric complex was thereby recaptured under concentration polarized conditions. The results

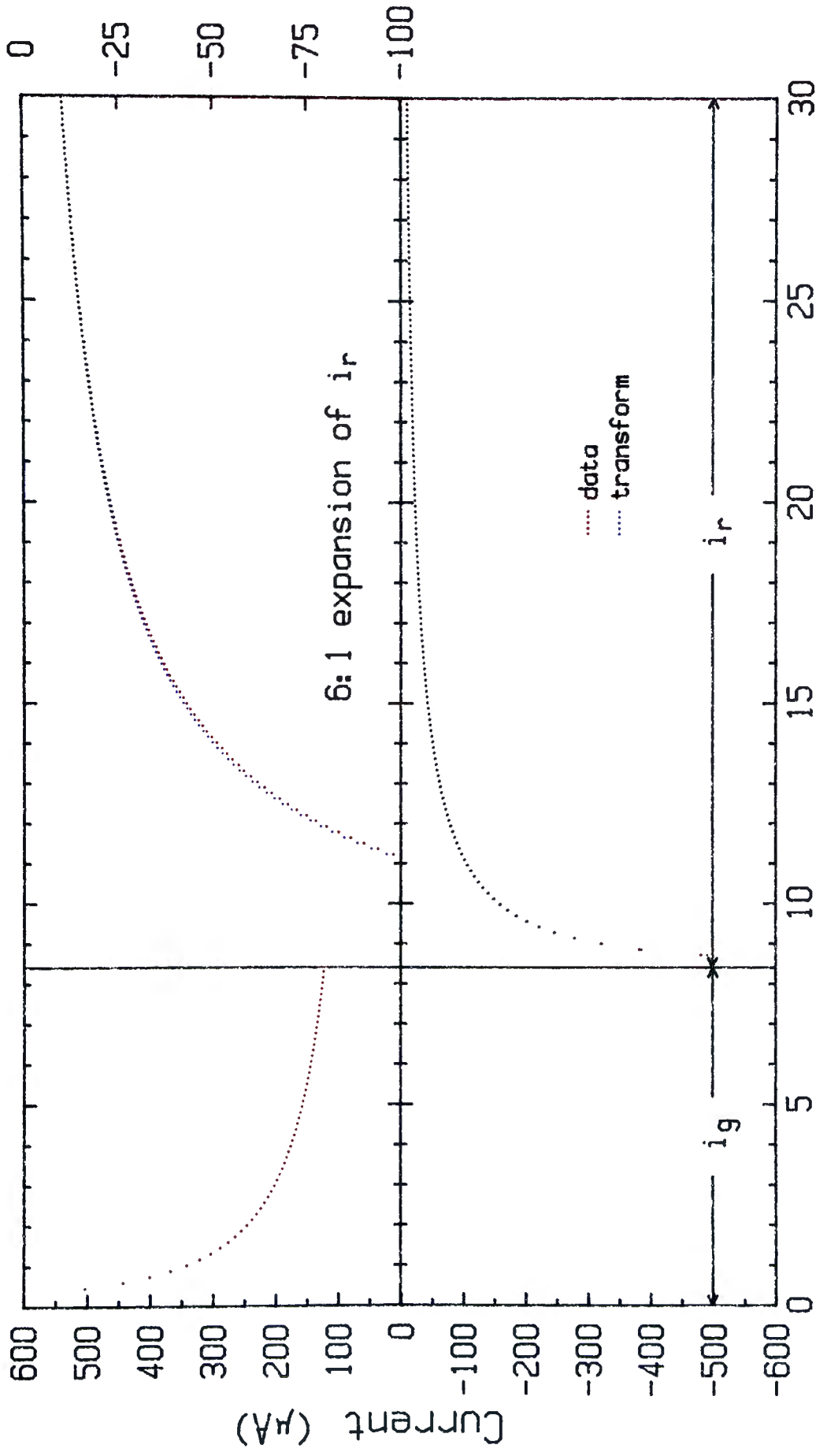

Figure E1A Double Step Experiment (cyanide)

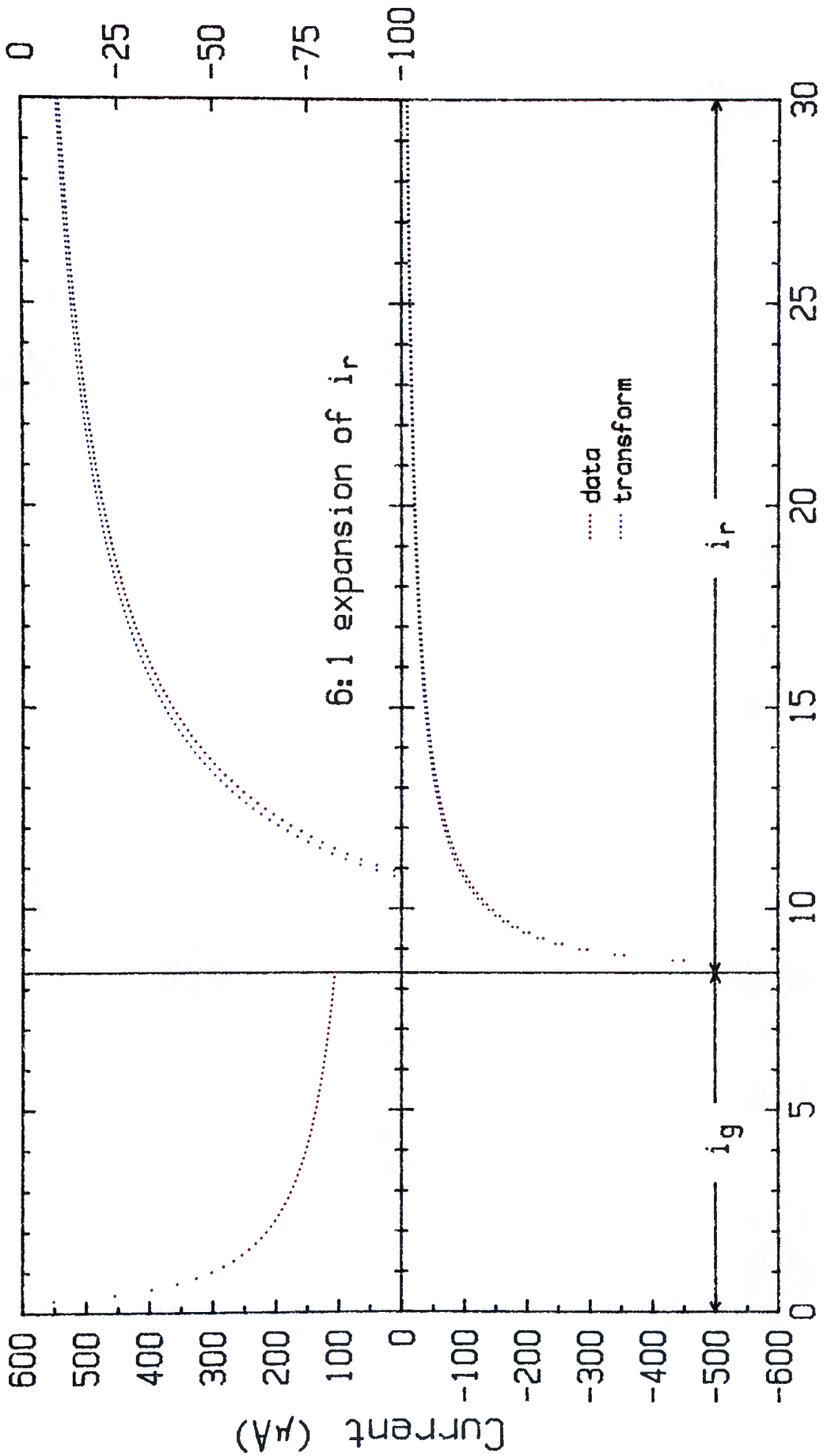

Figure E1B Double Step Experiment (oxalate)

of the double step experiment are presented in Figures E1A and E1B.

E2 : Ramp-Step Experiment

This experiment was controlled by the program "RSCHEM" (see appendix C). The potential waveform that was applied is shown in Figure 7.5.

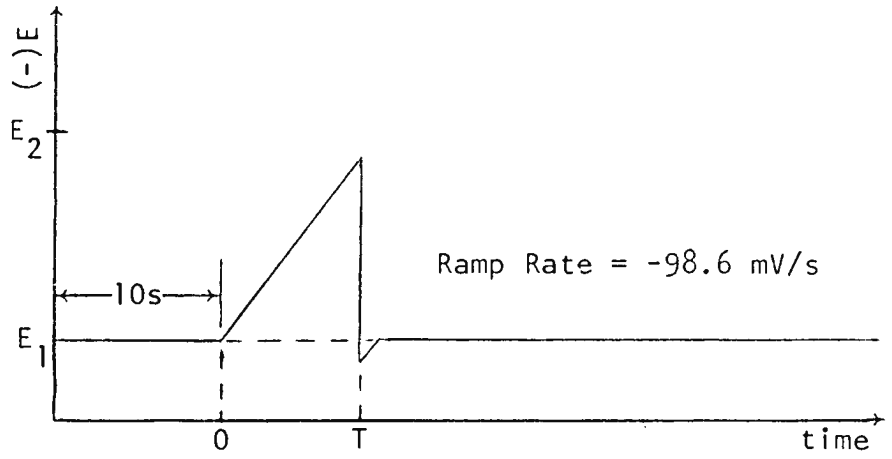

Figure 7.5 Potential waveform for ramp-step experiment

The step was applied just before the potential reached E_2. This was necessary to avoid a plateau. The step pushed the potential slightly beyond E_1 but the system responded the same as it would at E_1 since it was in the region of concentration polarization.

As the potential was ramped from E_1 to E_2, the ferrous complex was generated under increasingly more favourable conditions. The application of the step then induced recapture.

Since the potential range for the two systems differed and and the ramp rate was constant, the value of T (see Figure 7.5)

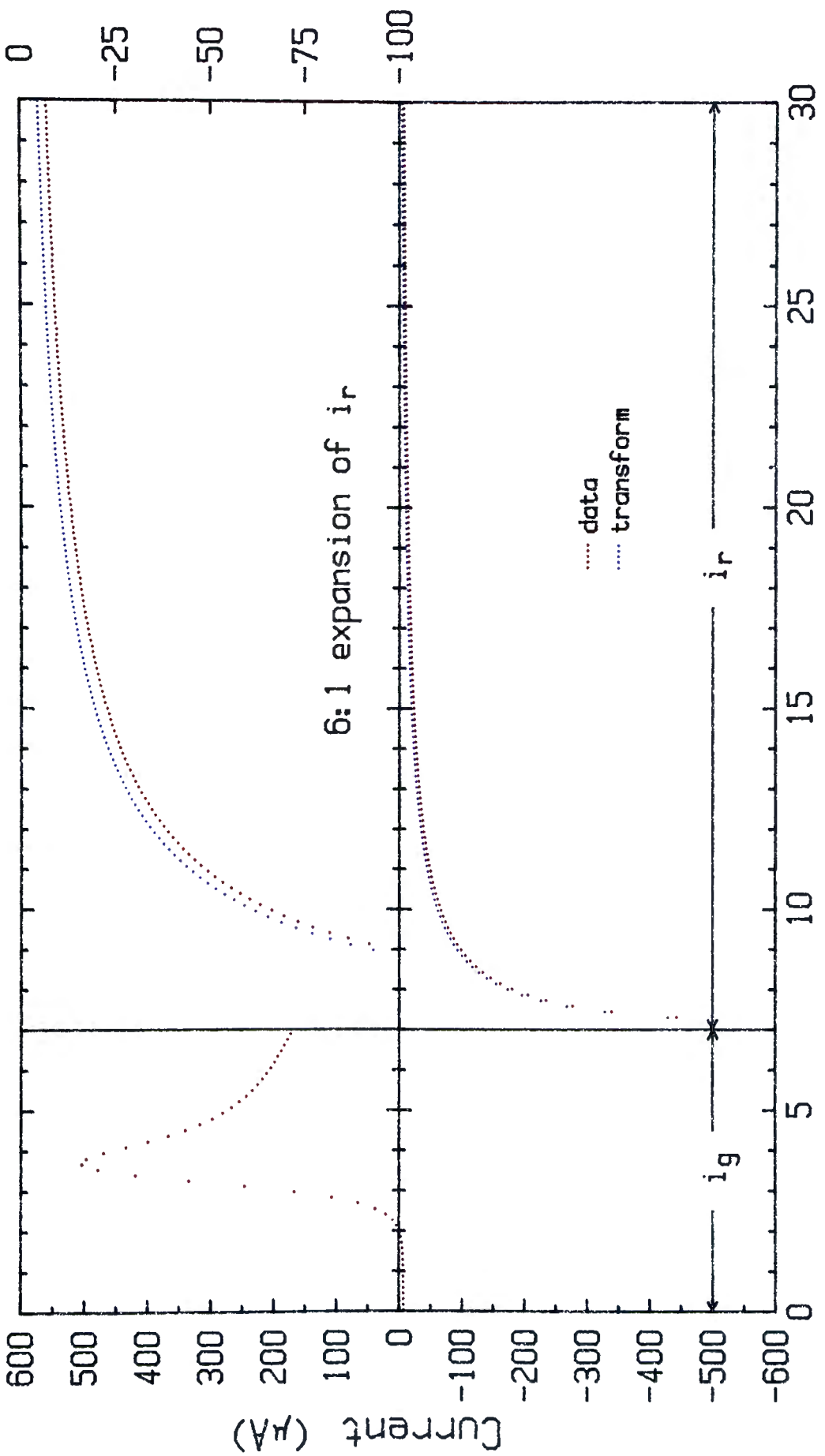

Figure E2A Ramp-Step Experiment (cyanide)

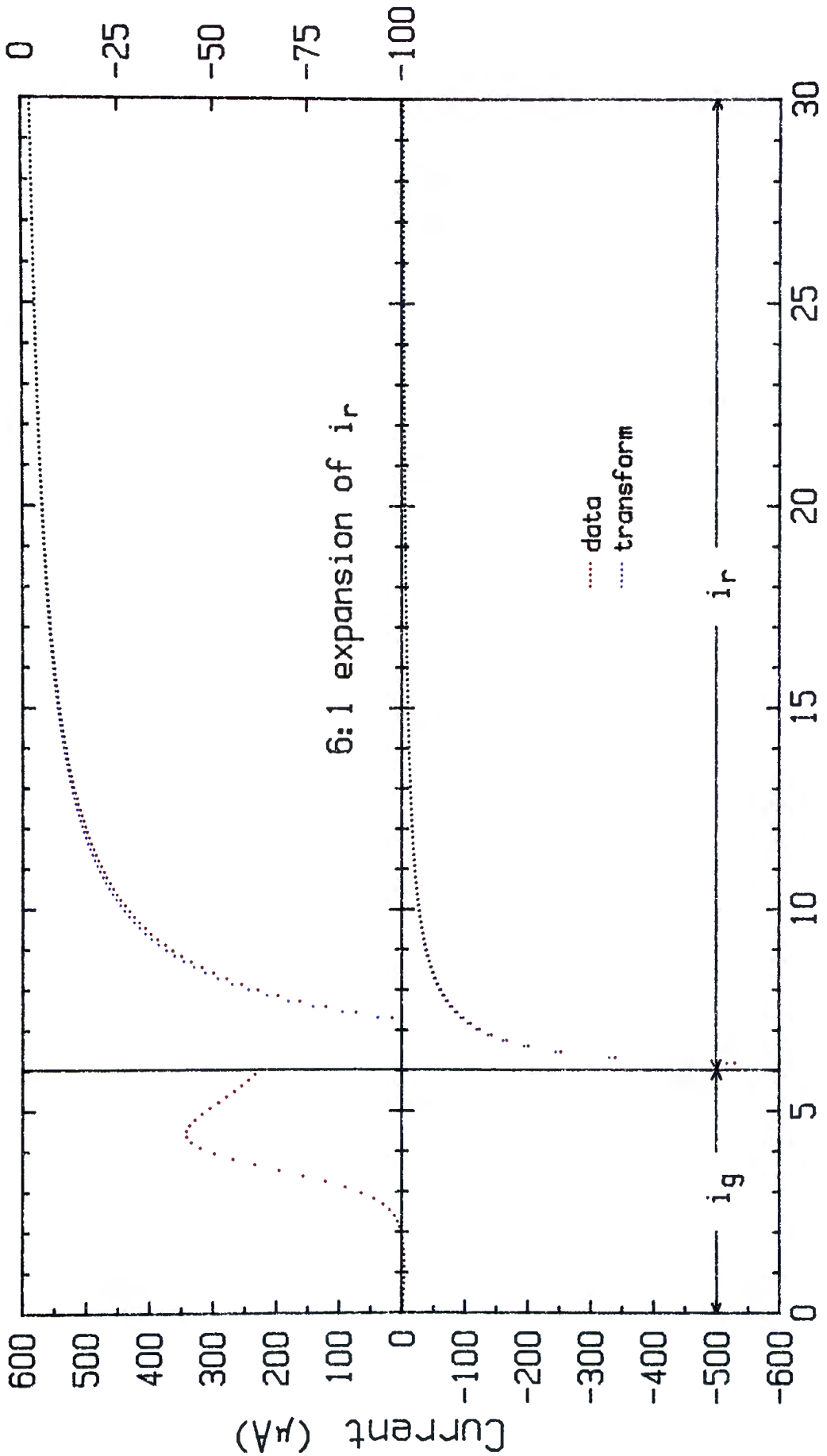

Figure E2B Ramp-Step Experiment (oxalate)

differed for the two systems. For the $Fe(CN)_6^{3-}$ system, the ramp must span 0.8 volts and T was selected as 7.00 seconds. For the $Fe(C_2O_4)_3^{3-}$ system, the ramp only needed to span 0.6 volts and hence T was shortened to 6.02 seconds.

The results of the ramp-step experiments are presented in Figures E2A and E2B.

E3,E4,E5 : Cyclic Ramp Experiments

These experiments were also controlled by the program "RSCHEM". In each experiment the potential was ramped through one cycle and then held at the initial value. The symmetry of the potential waveform was varied between experiments. The waveform symmetry is expressed as the ratio of the backward ramp rate to the forward ramp rate. The normal mode for a cyclic voltammogram is to use a symmetry of 1:1, but, in addition to this ratio, symmetries of 5:1 and 10:1 were also tested. As this ratio increases, the potential waveform deviates from that typical of a cyclic ramp experiment towards that of a ramp-step experiment. This transition is illustrated in Figure 7.6.

As with the ramp-step experiments, the value of T was changed between systems. In an attempt to optimize performance, T was selected at the earliest possible time that would correspond to a potential within the concentration polarization range. Therefore, T occurs slightly before the end of the ramping cycle.

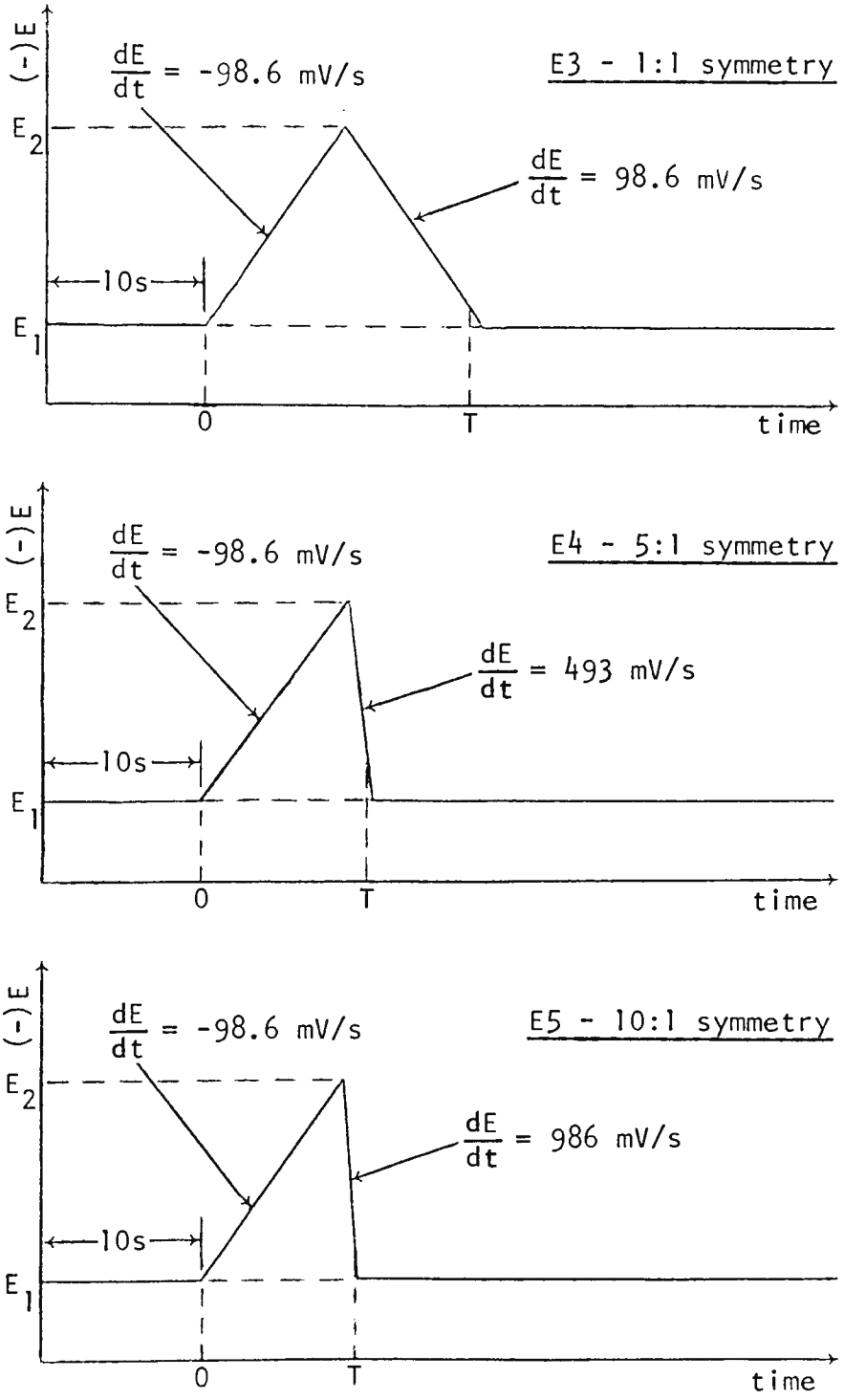

Figure 7.6 Potential waveforms for cyclic ramp experiments

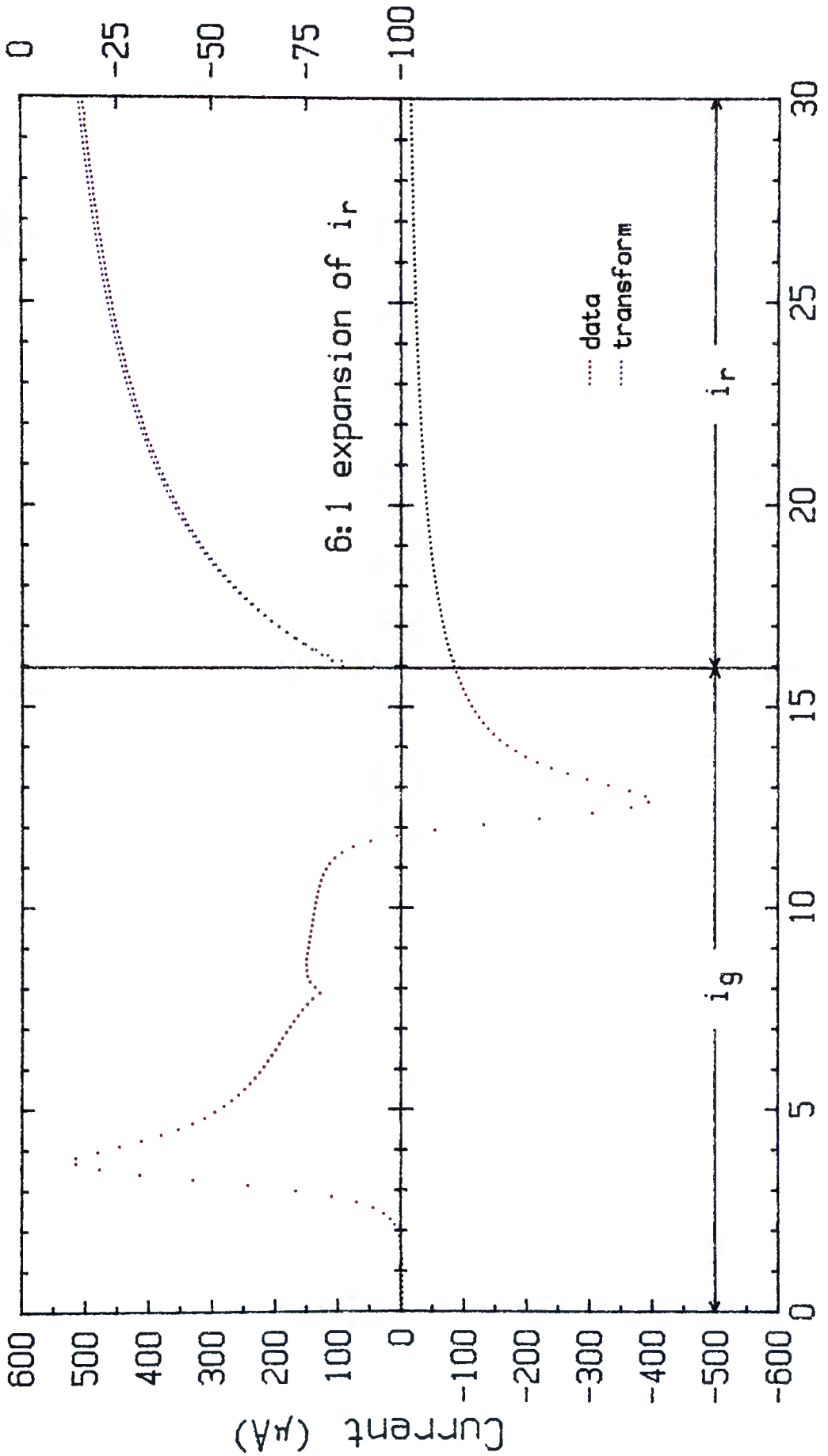

Figure E3A (1:1) Ramp Experiment (cyanide)

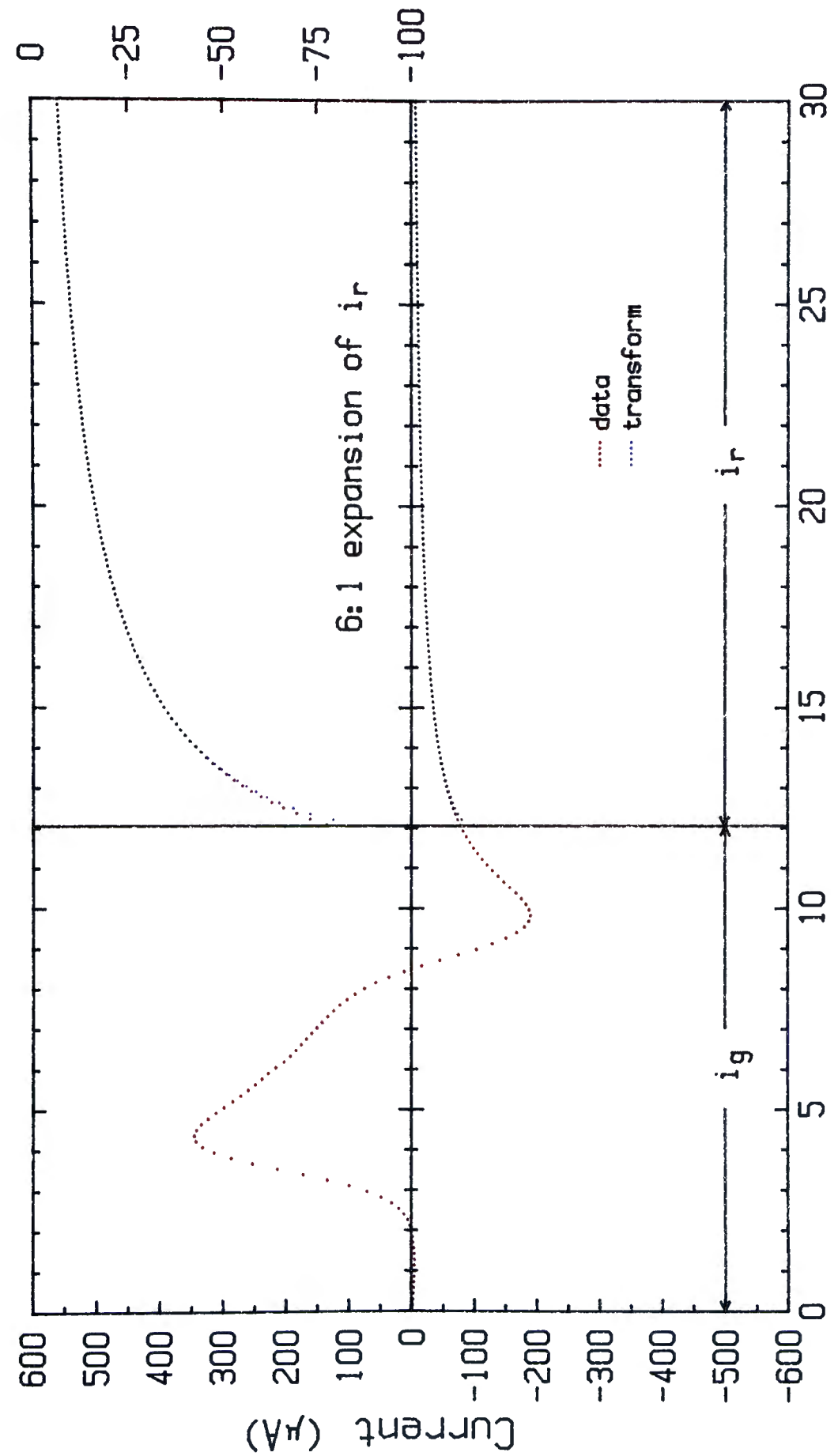

Figure E3B (1:1) Ramp Experiment (oxalate)

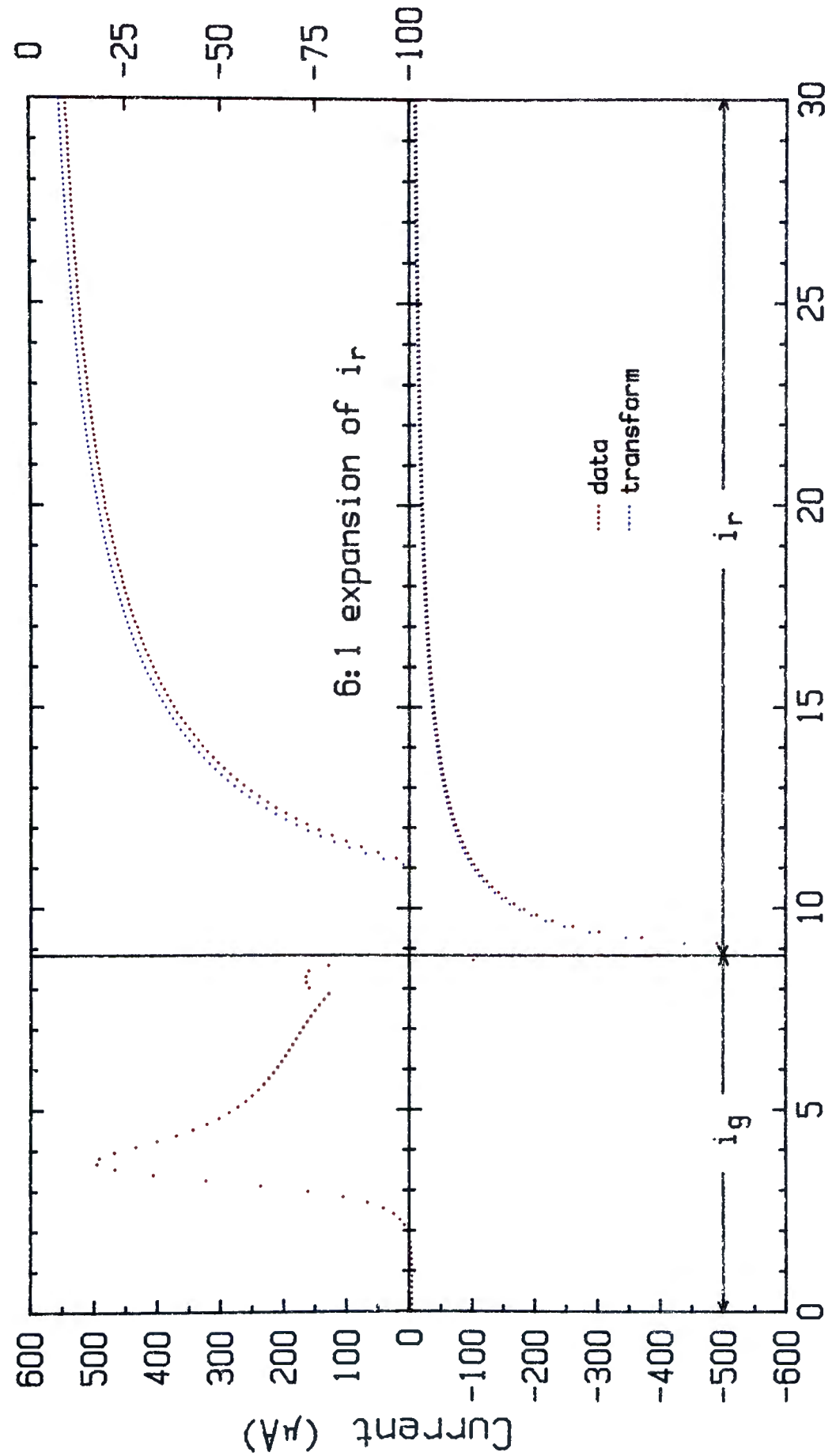

Figure E4A (5:1) Ramp Experiment (cyanide)

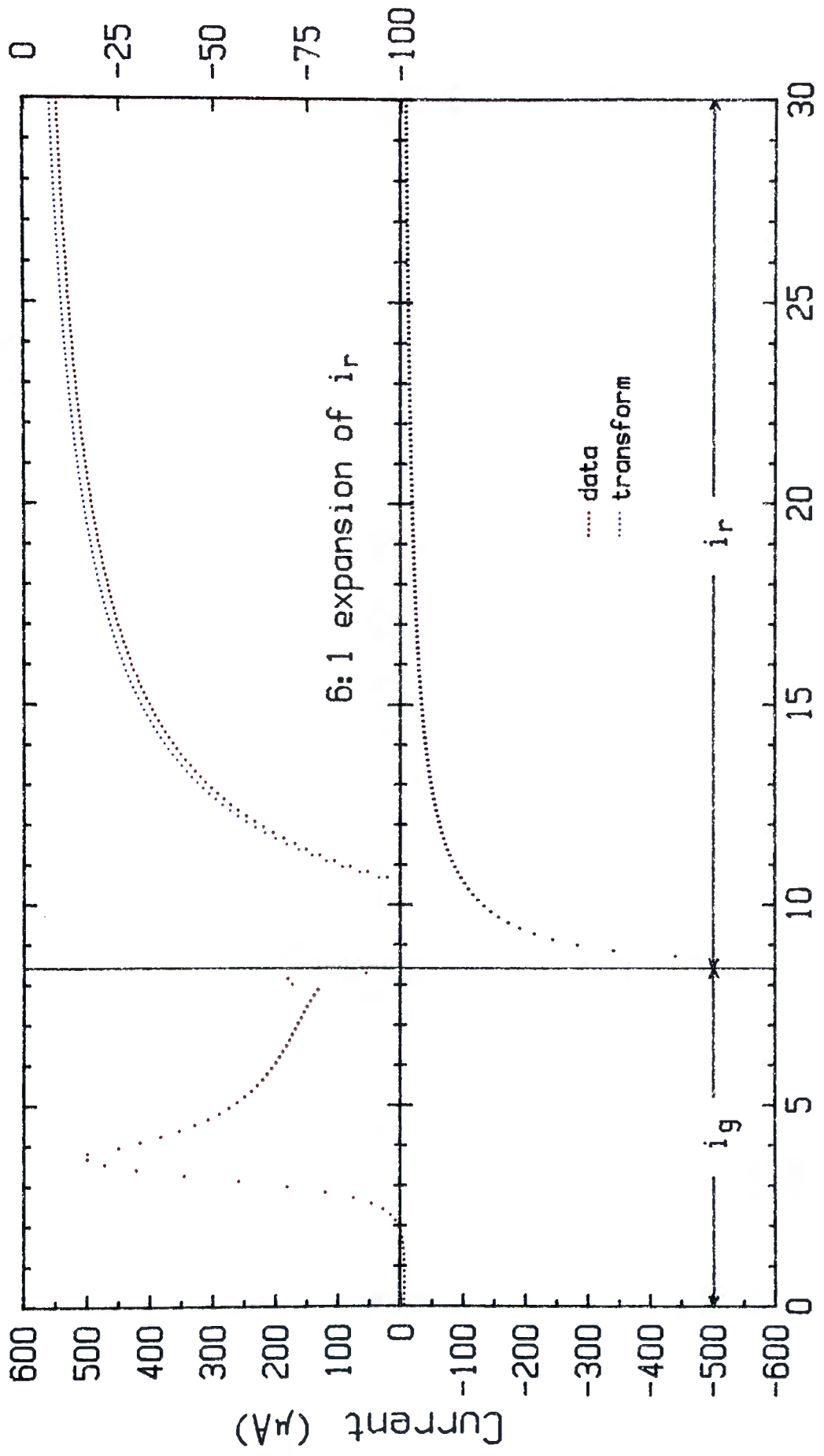

Figure E5A (10:1) Ramp Experiment (cyanide)

The results of these experiments are presented in Figures E3A through E5A.

E6 : Ramp-Hold-Step Experiment

This experiment was very similar to the ramp-step experiment except that the step was applied after the ramp had stopped at E_2. The potential waveform is shown in Figure 7.7.

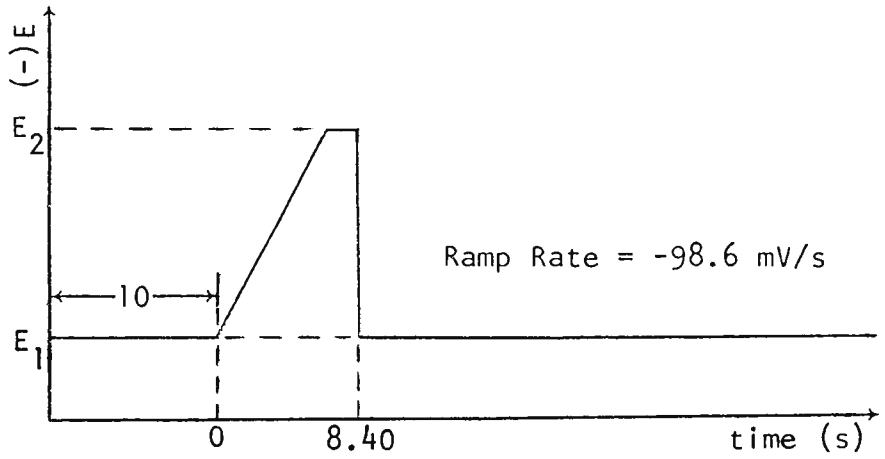

Figure 7.7 Potential waveform for ramp-hold-step experiment

The value chosen for T was 8.40 seconds. This selection was made for comparitive purposes with the double step experiment. Figure E6A shows the result of this experiment.

E7 : Multistep Experiment

The waveform applied in this experiment was the most unusual of all. It is illustrated in Figure 7.8. This waveform was applied by the program "DSCHEM" with a manually open-circuited period in the middle of the generation phase. While the cell was open-circuited, no current could flow and hence the cell would

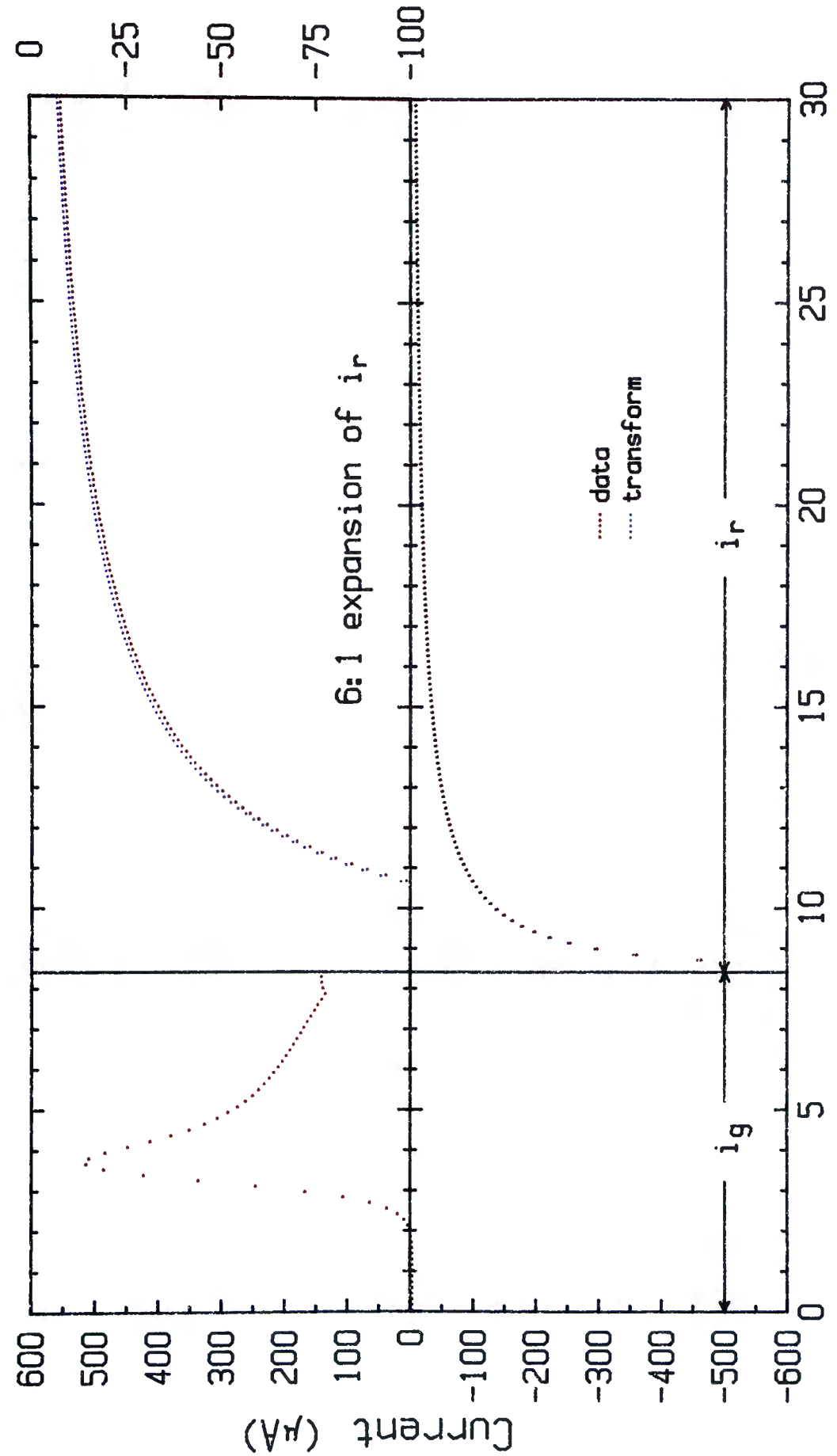

Figure E6A Ramp-Hold-Step Experiment (cyanide)

be at E_n, the null potential, which varies with time.

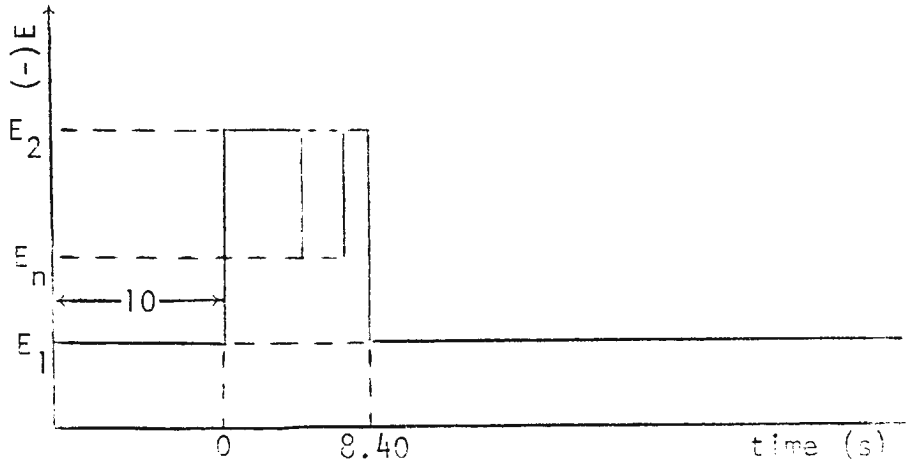

Figure 7.8 Potential waveform for multistep experiment

The cell was open-circuited by switching the selector switch on the PARC 170 from "External Cell" to "Off". The timing for this manual operation could not be reproduced accurately enough to enable a background correction to be performed and therefore these data are presented uncorrected.

The data and transform are presented in Figure E7A.

The cottrellian dependence of the generation current was studied by testing the constancy of $i_g(t)t^{\frac{1}{2}}$. The variation in this parameter was limited to $\pm 1\%$ demostrating that the contribution from extraneous sources, such as non-linear diffusion, was very small.

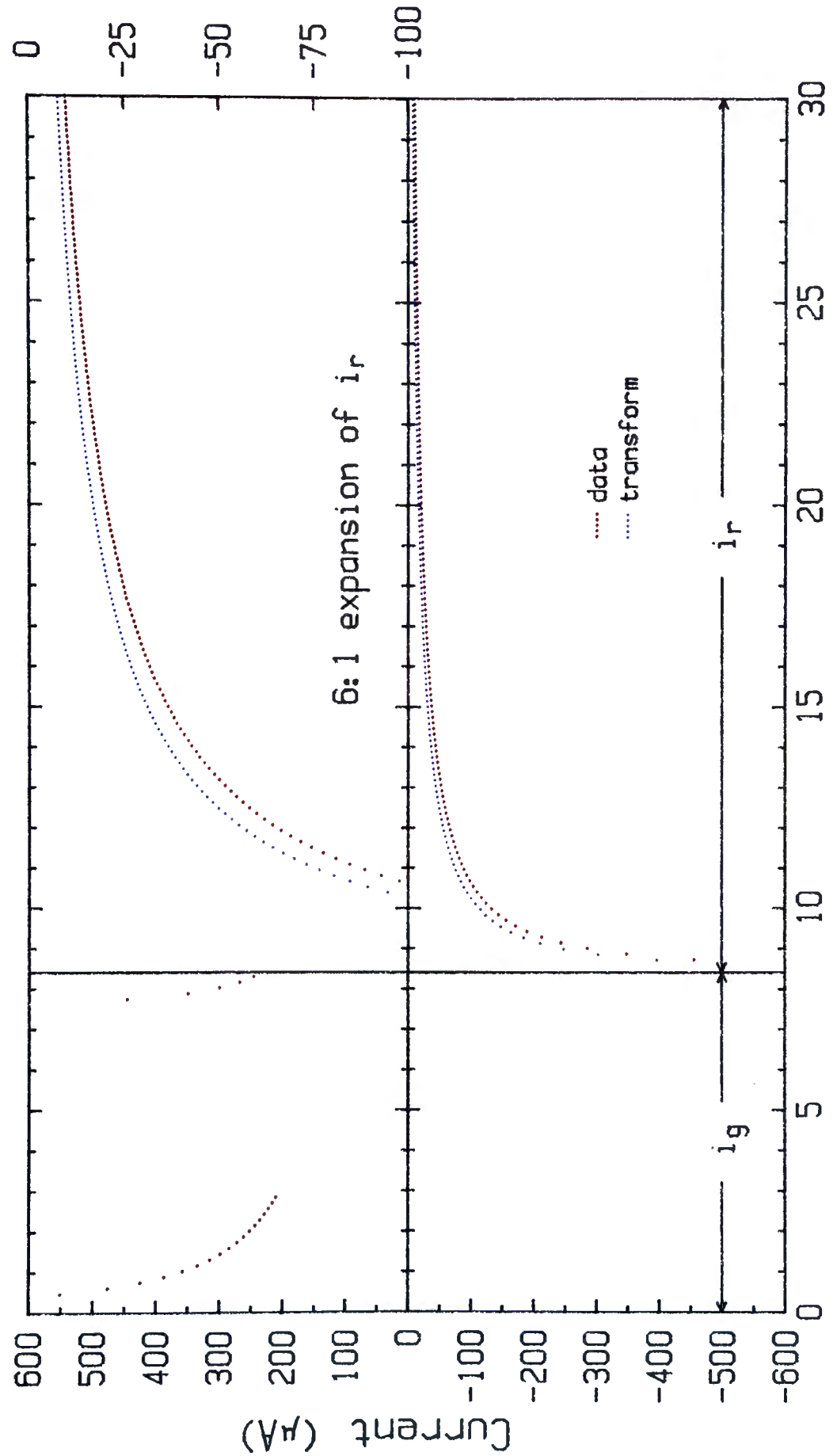

Figure E7A Multistep Experiment (cyanide)

Error Analysis

The preceding graphs, Figures E1A through E7A, clearly illustrate the success of this transform technique. The curve obtained by Hilbert transformation matches the recapture data so well that for many of the experiments, discrepancies can only be detected on the expanded scale. This degree of precision is encouraging since, in addition to the usual experimental errors, an error is imposed by an approximation made within the algorithm. The contributions from each of these error sources has been investigated to determine their weighting.

The algorithmic error was investigated with synthetic data representative of a double potential step. The choice of this experiment was necessitated by the lack of analytical solutions for recapture following other waveforms. The synthetic data were generated with the same time parameters that were used for sampling the experimental systems. The ratio of the current, $i_r[T]$, obtained from the transform compared to the recapture data, $i_r[D]$, is presented in Figure 7.9 to illustrate the relative error introduced by the transform algorithm.

The line denoted $i_r[D]/i_r[D]$ serves as a reference against which the transforms can be compared. The curve "ALL(0)" designates the relative error for the transform of the data set that contains all 400 points that were generated. The error in

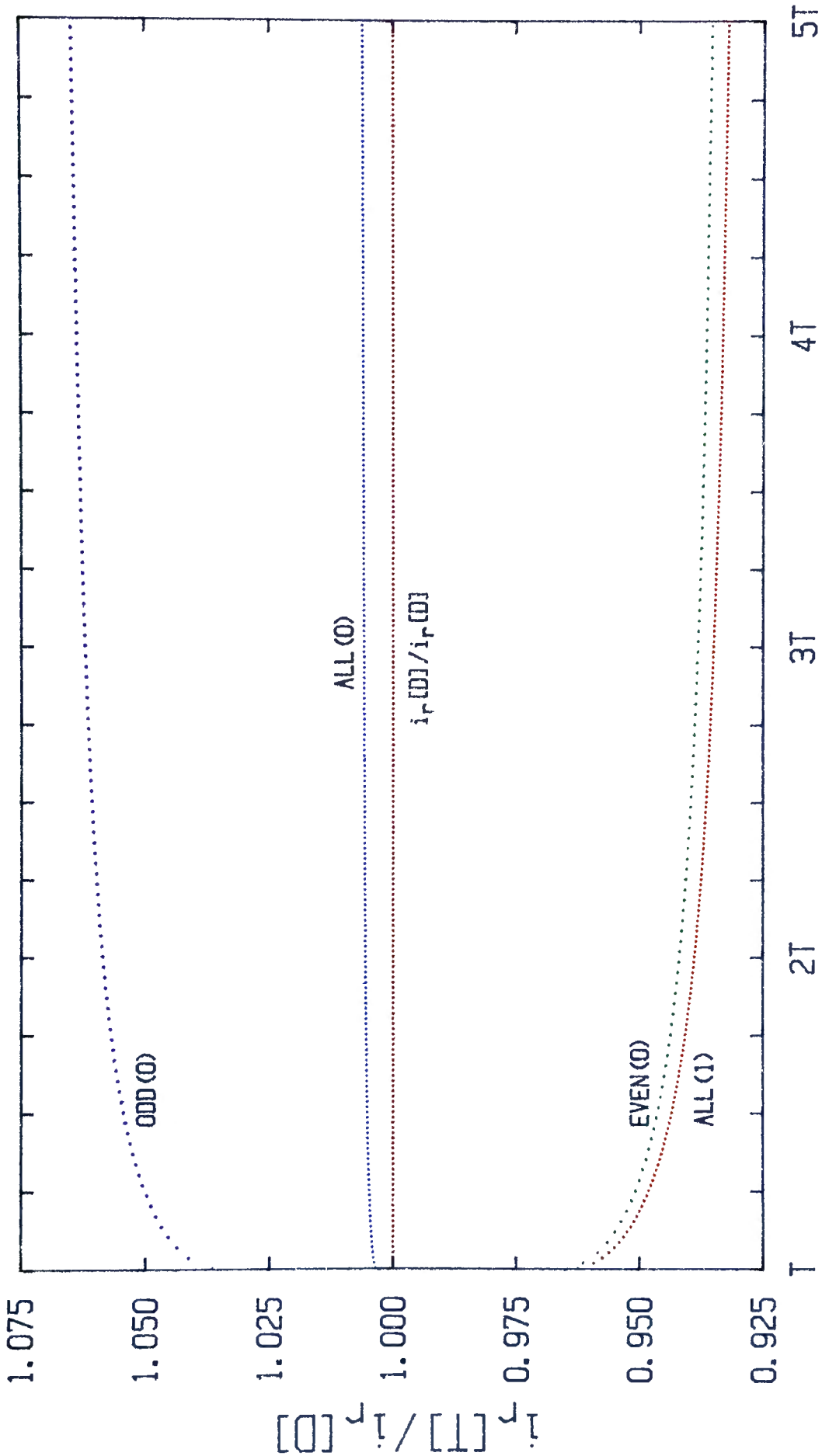

Figure 7.9 Relative Error in Transform Algorithm

this transform was only 0.6% at the time 5T. The curve "ALL(1)" was derived from the same data set that was used for "ALL(0)" except that the first generation point was omitted. This data set formulation is similar to that used for both of the double step experiments in which the first data point was beyond the range of the measuring instrument and therefore unknown. Hence the "ALL(1)" curve reflects the algorithmic error inherent in the experimental transforms. Ignorance of the first data point increased the algorithmic error at the time 5T to 7%. This increase by an order of magnitude was apparently caused by the linear fitting routine within the algorithm. The algorithm approximates the curve by fitting straight lines between consecutive points. At both ends of the curve, the fit to the boundaries of the generation region is obtained by extrapolating the line described by the two closest points.

The current for a double step experiment is proportional to $t^{-\frac{1}{2}}$ and hence it falls rapidly from an initial value of infinity. This produces a curve which looks like the falling edge of a spike. A linear fit between two points on such a curve will describe a line which will lie above the curve for all intervening points. An extrapolation of such a fit, however, will define an endpoint that is too low. Therefore, a linear fit establishes a delicate balance between high and low approximations to the curve.

For the "ALL(0)" data set, the overall fit must have been slightly high whereas the fit for the "ALL(1)" data set was too low. The lowering of the overall fit to the "ALL(1)" data set could have been predicted since the omission of the first data point would lower the extrapolation at time zero. The magnitude of this effect, however, was a surprise. Even so, the error is still less than seven percent.

Two new data sets were formed by taking alternate points from the original data set. One data set consisted of the odd-numbered points and the relative error in its transform is designated "ODD(0)". The other data set consisted of the even-numbered points and the relative error in its transform is designated by "EVEN(0)". The "ODD(0)" and "ALL(0)" data sets have the same initial data point but the sampling interval, Δt, for the former data set is twice that of the latter. The "EVEN(0)" and "ALL(1)" are related in a similar fashion.

Incorporated into the transform algorithm is the assumption that Δt is small. The approximation made by this assumption improves as Δt approaches zero and hence the increased error in "ODD(0)" over "ALL(0)" reflects this dependence. Another dependence, that of the extrapolation at time zero, is reinforced by the similarities of the curves "EVEN(0)" and "ALL(1)".

The spikes encountered in the generation region of the double

step and multistep experiments are approximated very poorly by the linear fit used in the transform algorithm. A linear approximation of the peaks for the various ramp experiments would also not be very accurate, but this error could still not approach that encountered for an extrapolation over a spike. Based on this assumption, the algorithmic error in the ramp experiments should be less than the 7% found for the double step experiment. The error in the multistep experiment, however, would surely be more than this since two spikes must be approximated; one without the benefit of an extrapolation. The error in the transform for the multistep experiment does appear to be larger than that found in any other experiment, but this could also be due to background-uncorrected data being analysed.

The errors attributed to experimental measurements would be difficult to segregate but at least some idea of the reproducibility of the data may be gained from Figure 7.10. In this diagram, data are presented for five distinct ramp experiments with the cyanide system. Over the first seven seconds of these experiments, the potential was ramped at the same rate and over the same range. Hence the data for these experiments should be identical over this region.

The timing for the sampling of this data appears to be quite reproducible since the peak location remains constant. However

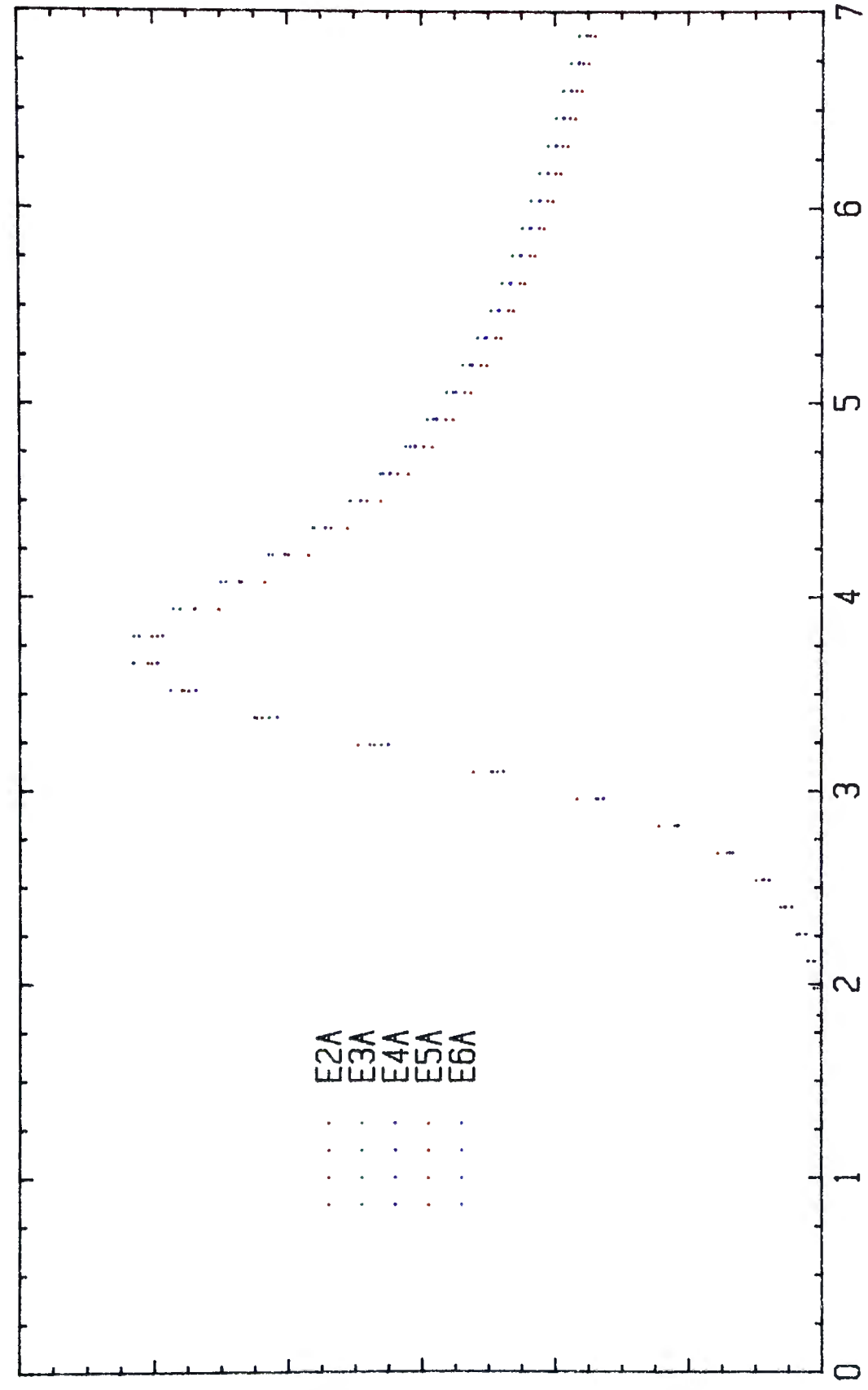

Figure 7.10 Reproducibility Of Ramp Data

there is some variation in the currents that were measured. The current data presented in Figure 7.10 are background-corrected and hence reflect errors incorporated into measurements on two solutions.

At any given time, the current displays a variation of about 8% over the five sets of data. Each of the signals, however, intermingles with the others and none is consistently high or low. As an example, the current for experiment E5A crosses all the other experimental currents. Initially it was the largest, near the peak it obtained a median value and then, on the tail extending beyond the peak, it became the smallest current.

Since the experimental error outweighs the algorithmic error, most of the discrepancy between the transform and recapture data must have arisen from experimental sources. These sources would include capacitative currents that are produced by the charging and discharging of the electrode double layer, currents that originate from non-linear diffusion, and stray currents that are the result of instrumental noise. Background subtraction would help to remove some of these extraneous currents but the correction would not be perfect. A technique that could have improved the agreement would have been to average the output signal over several runs. This would have improved the correction for the capacitative currents although other components may have still been a problem.

Even though this averaging technique was not used, the similarity between the transform and recapture data is still satisfactory.

Discussion

As mentioned earlier, these seven experiments were divided into two classes, each with its own purpose. The first three were intended to test the dependence of the transform on the electrochemical reversibility of the system whereas the last four were designed to illustrate the versatility of this transform technique.

The extent of the reversibility of each of the systems was established by comparison of parameters taken from the cyclic voltammograms (Figures 7.3A and 7.3B) with those predicted by reversible theory.[2] The values are provided in Table 7.1. The theoretical values assume that the system is completely reversible.

System	$\frac{nF}{RT}\left(\vec{E}_p - E_r\right)$	Parameter	Experiment	Reversible Theory
A	16.074	$\frac{nF}{RT}\left(\overleftarrow{E}_p - \vec{E}_p\right)$	2.33	2.23
		$\overleftarrow{i}_p \,/\, \vec{i}_p$	-0.758	-0.788
B	5.955	$\frac{nF}{RT}\left(\overleftarrow{E}_p - \vec{E}_p\right)$	8.76	2.27
		$\overleftarrow{i}_p \,/\, \vec{i}_p$	-0.548	-0.687

Table 7.1 Reversibility parameters for the experimental systems. The peak current and peak potential are denoted by i_p and E_p respectively. The ramp direction at the peak is denoted by the arrow.

The parameters for system "A" are in much better agreement with theory than are the parameters for system "B" and hence the $Fe(CN)_6^{3-}/Fe(CN)_6^{4-}$ couple was more reversible than the $Fe(C_2O_4)_3^{3-}/Fe(C_2O_4)_3^{4-}$ couple at the platinum electrode. Table 7.1 also illustrates that the peak separation is more sensitive to the electrochemical reversibility than is the ratio of the peak heights.

If the transform is dependent upon electrochemical reversibility, then the results for system "A" should be better than those for system "B". This was true for the double step experiment in which the agreement for system "B" was good but that for system "A" was even better. For the ramp-step experiment, however, the roles are reversed. The transform for system "B" was very good whereas the error in the system "A" transform was about the largest of any experiment. The transform for the 1:1 ramp experiment was excellent for both systems but the shape of the curve for system "B" was slightly better than that for system "A". A probable source of error for the transform of system "A" was an unexplained "dip" in the current that occurred near the reversal potential. It would appear that, based on these three experiments, the transform has no dependence on the electrochemical reversibility since each system scored a win, a loss, and a tie.

The discrepancy between $i_r[T]$ and $i_r[D]$ for the remaining four experiments was still fairly small but it appeared to be a function

of the quality of the background correction. The data for the ramp-hold-step experiment were the smoothest of the four experimental curves and therefore appear to have been corrected the most efficiently. The discrepancy between $i_r[T]$ and $i_r[D]$ was also smaller for this experiment than for any other. As mentioned earlier, the technique by which the multistep waveform was applied prevented background subtraction. The lack of this correction was apparently responsible for the relatively large discrepancy between $i_r[T]$ and $i_r[D]$ for this experiment. The discrepancies between $i_r[T]$ and $i_r[D]$ for these four experiments were larger than those for the conventional waveforms. The recapture current for each of these experiments, however, was still described quite accurately by the Hilbert transform.

Comments

The versatility of this transform technique has been illustrated by the lack of dependence on both the nernstian behaviour of the system and the potential waveform that is applied to it. As suggested earlier, a method incorporating signal averaging could be used to improve the signal quality and therefore increase the accuracy of the Hilbert transform. This procedure would be the most beneficial for experiments in which the transform was to be applied for analytical purposes.

CHAPTER 8

RECONSTRUCTION OF $i_g(t)$ FROM $i_r(t)$

It was shown in chapter 6 that the negative Hilbert transform of the recapture function, R(r), will give the generation function, G(g), from which $i_g(t)$ may be calculated. Recall, however, that the recapture function was defined as

$$R(r) = \left\{ \begin{array}{lll} R_1(r) & , & r<-1 \\ R_2(r) & , & -1<r<1 \\ (r-1)^{\frac{1}{2}} i_r(r) & , & r>1 \end{array} \right\} \qquad (8.1)$$

where $R_1(r)$ and $R_2(r)$ are unknown functions of r which have no experimental significance. Since the Hilbert transform spans $-\infty<r<\infty$, R(r) must be known over this range to permit the transform to be performed. Hence a method had to be devised that could deal with the ignorance of $R_1(r)$ and $R_2(r)$ to exploit the Hilbert transform as a means of reconstructing the generation current.

I) Curve Fitting

The recapture function in the recapture phase, denoted $R_3(r)$, and the generation function in the generation phase, denoted $G_2(g)$, are given by

$$R_3(r) = (r-1)^{\frac{1}{2}} i_r(r) \qquad (8.2)$$

and

$$G_2(g) = (1-g)^{\frac{1}{2}} i_g(g) \tag{8.3}$$

Hence $R_3(r)$ may be calculated from the recapture current and $G_2(g)$ may be used to calculate the generation current.

If the functional form of $G_2(g)$ was set, then, since the generation function is zero elsewhere, the functions $R_1(r)$, $R_2(r)$, and $R_3(r)$ would be known from the Hilbert transform of $G_2(g)$. If a weighting was applied to $G_2(g)$ then the same weighting would be applied to each of the functions $R_1(r)$, $R_2(r)$, and $R_3(r)$. Similarly, if $G_2(g)$ was composed of a series of functions with given weightings, the functions $R_1(r)$, $R_2(r)$, and $R_3(r)$ could be determined by Hilbert transformation of these functions followed by application of the corresponding weightings. However, the only $R_n(r)$ function which has experimental significance is $R_3(r)$. If $R_3(r)$ is fitted to a series of functions which are Hilbert transforms of functions used to describe $G_2(g)$ then it may be possible to extract the weightings which are required to reconstruct $G_2(g)$ and thence the generation current.

A curve fitting routine was designed to fit $R_3(r)$ to analytical functions that were Hilbert transforms of functions selected to describe $G_2(g)$. The function $R_3(r)$ was approximated by

$$R_3(r) \simeq \sum_{n=1}^{N} A_n f_n(r) \tag{8.4}$$

for which the N coefficients A_n were determined for the functions $f_n(r)$ by a program given in appendix C. Once these coefficients were determined, the function $G_2(g)$ could be approximated by

$$G_2(g) \simeq \sum_{n=1}^{N} A_n h_n(g) \tag{8.5}$$

where $h_n(g)$ are analytical functions selected with the functionality of the generation current in mind. The domains for $f_n(r)$ and $h_n(g)$ are shown in Table 8.1.

G(g)	R(r)
0 , g<-1	$R_1(r)$, r<-1
$h_n(g)$, -1<g<1	$R_2(r)$, -1<r<1
0 , g>1	$f_n(r)$, r>1

Table 8.1 Domains of analytical functions that comprise the generation and recapture functions.

Although the functions $R_1(r)$ and $R_2(r)$ will be known for a given $h_n(g)$, these functions did not participate in the fitting operation since only data in experimentally significant regions were fitted.

The selection of fitting functions was limited to those for which the Hilbert transform relationship was known. Hence there

was not a great deal of choice in this selection. The selection of functions was based on assumptions about the form of $G_2(g)$. The results for two sets of fitting functions follow.

(i) Power Series

It has been shown previously that the generation current for a Cottrell experiment is dependent upon $t^{-\frac{1}{2}}$ and hence an appropriate power series to describe $i_g(t)$ would be

$$i_g(t) \simeq a_{-1}t^{-\frac{1}{2}} + a_0 + a_1 t^{\frac{1}{2}} + a_2 t + \cdots \tag{8.6}$$

This expression may be rewritten as

$$i_g(g) \simeq A_{-1}(1+g)^{-\frac{1}{2}} + A_0 + A_1(1+g)^{\frac{1}{2}} + A_2(1+g) + \cdots \tag{8.7}$$

where

$$A_n = \left(\frac{2}{T}\right)^{n/2} a_n \tag{8.8}$$

Therefore, from equation (8.3),

$$G_2(g) \simeq \sum_{j=1}^{\infty} A_{j-2}(1+g)^{j/2-1}(1-g)^{\frac{1}{2}} \tag{8.9}$$

The Hilbert transform of equation (8.9) may be found in Table I. This establishes $R_3(r)$ as

$$R_3(r) \simeq -\sum_{j=1}^{\infty} A_{j-2} \frac{2^{j/2-\frac{1}{2}}\Gamma(j/2)}{(r-1)\pi^{\frac{1}{2}}\Gamma(j/2+\frac{3}{2})} {}_2F_1\left[1, \tfrac{3}{2}; j/2+\tfrac{3}{2}; -\frac{2}{r-1}\right. \tag{8.10}$$

The functionality of $h_n(g)$ and $f_n(r)$ as dictated by equations (8.9) and (8.10) was determined for the first five members of these series. The derivations are presented in the first part of appendix E and the corresponding curves are plotted in Figures 8.1 and 8.2.

The functions $f_n(r)$ were evaluated over the range $1<r<5$ at intervals of 0.1 and then filed on the computer to form a data base named GUS. Synthetic recapture data were then generated from known combinations of the $f_n(r)$ functions. The numbers within the data base and the recapture datafiles contained fourteen significant figures. However, experimental recapture data would not possess any more than four significant figures. Therefore, additional datafiles were created which possessed numbers with only four significant figures.

The fits to the datafiles S-IT03 and 4S-IT03 are given in appendix F. These datafiles were generated by summing all five of the $f_n(r)$ functions with equal weighting. The former of these files contains numbers with fourteen significant figures whereas the latter file contains numbers with only four. The coefficients from these fits along with the sample variance, s^2, are summarized in Table 8.2. The sample variance, equivalent to the reduced chi-square, is defined as

$$s^2 = \frac{1}{J-N-1} \sum_{j=0}^{J} (\Delta j)^2 \qquad (8.11)$$

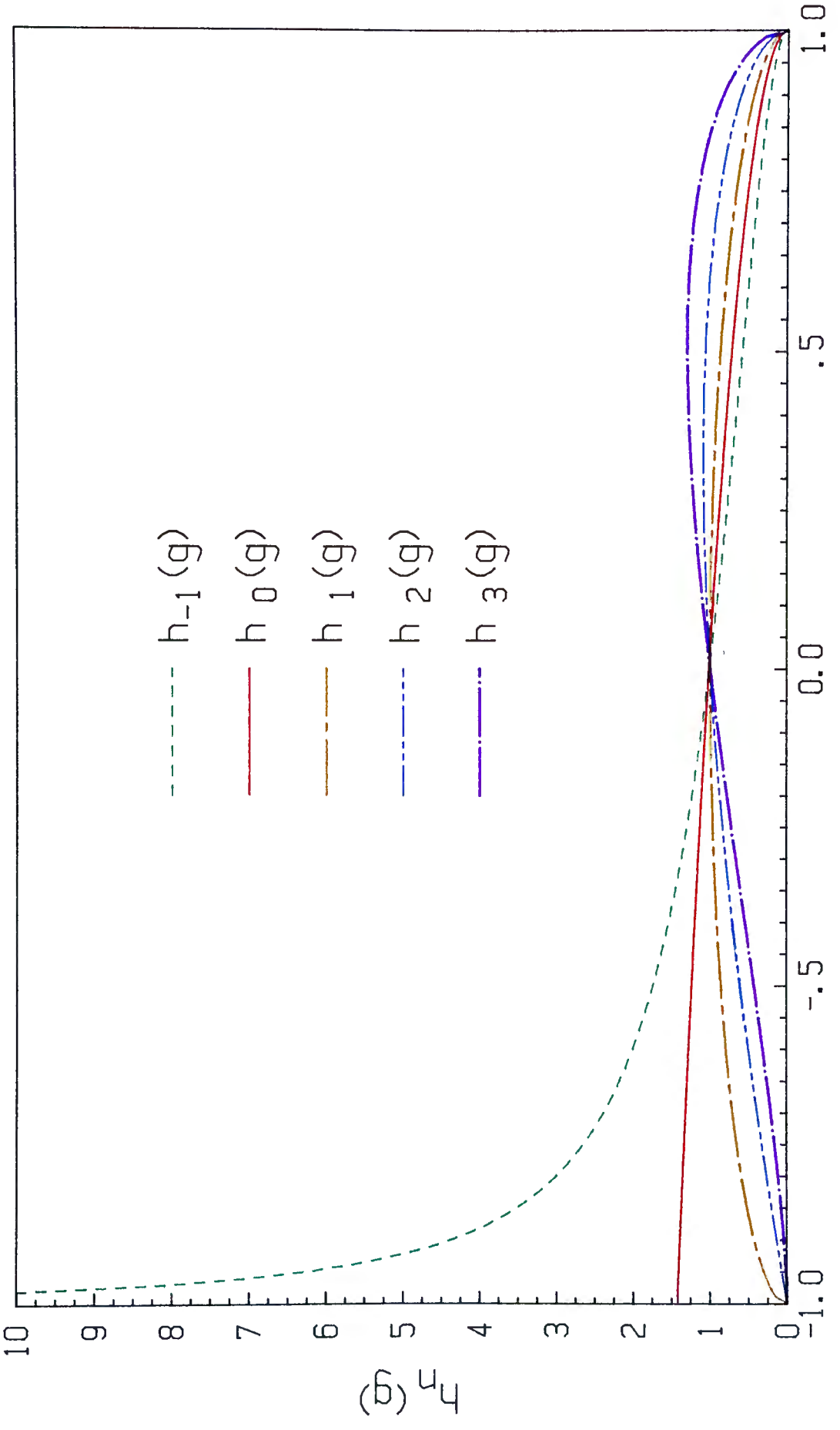

Figure 8.1 $G_2(g)$ fitting functions

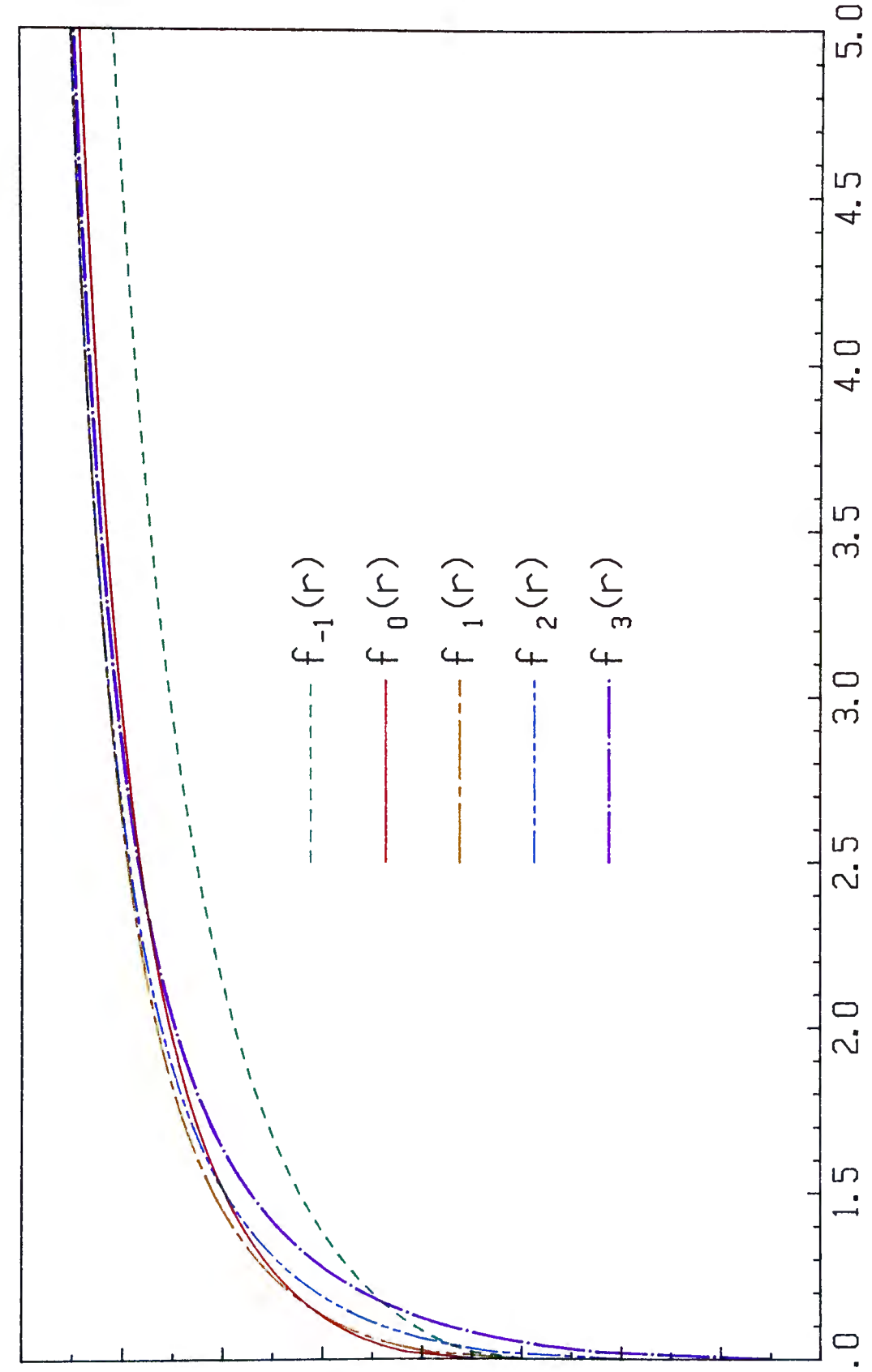

Figure 8.2 $R_3(r)$ fitting functions

where J is the number of data points, N is the order of the fit, and Δj is the difference between the fit and the data at the jth data point. Therefore a small s^2 indicates a good fit to the data.

Datafile	S-1T03	4S-1T03
A_{-1}	0.9994	-13.68
A_0	1.0055	127.59
A_1	0.9875	-285.56
A_2	1.0105	245.41
A_3	0.9970	-69.78
s^2	$8.25X10^{-12}$	$7.13X10^{-8}$

Table 8.2 Summary of coefficients and sample variance for some power series fits.

The s^2 for both of these fits is quite small and therefore indicates that these are good fits to the data. However, the coefficients which describe the fits differ significantly. All of the coefficients were expected to be unity based on the manner in which these datafiles were generated. The coefficients for the fit to S-1T03 met this expectation quite well but those for the fit to 4S-1T03 were very surprising. Although the fit to 4S-1T03 matches the data very well, the coefficients which describe the fit could be misleading if used to infer properties of the generation process. As an example, the coefficient A_{-1} is related to the contribution from a cottrellian generation current. Although the file 4S-1T03 was generated with A_{-1} equal to unity,

the fit indicates that the contribution from a cottrellian generation current is negative and far from unity. Therefore this could induce erroneous assumptions about the generation process.

It appeared that these fitting functions could not be used to describe data representative of experimental accuracy and therefore another set of fitting functions was investigated.

(ii) Orthogonal Polynomials

Neither of the series described by equations (8.9) and (8.10) is comprised of orthogonal functions. However, it may be advantageous to consider a set of orthogonal functions for reasons given in chapter 2. Consider the approximation

$$i_g(g) \simeq \sum_{n=1}^{N} A_n P_n^{(\frac{1}{2},0)}(g) \tag{8.12}$$

where $P_n^{(\frac{1}{2},0)}(g)$ are Jacobi polynomials which are orthogonal in the range $-1<g<1$. Then, from equation (8.3),

$$G_2(g) \simeq \sum_{n=1}^{N} A_n (1-g)^{\frac{1}{2}} P_n^{(\frac{1}{2},0)}(g) \tag{8.13}$$

The Hilbert transform of equation (8.13) is given in Table I which lists $R_3(r)$ as

$$R_3(r) \simeq -\frac{2}{\pi} \sum_{n=1}^{N} A_n (r-1)^{\frac{1}{2}} Q_n^{(\frac{1}{2},0)}(r) \tag{8.14}$$

where $Q_n^{(\frac{1}{2},0)}(r)$ are Jacobi functions of the second kind. This

expression may then be incorporated into equation (8.2) to yield

$$-\frac{\pi}{2} i_r(r) \simeq \sum_{n=1}^{N} A_n Q_n^{(\frac{1}{2},0)}(r) \qquad (8.15)$$

The fitting routine was applied to equation (8.15) rather than equation (8.14) since it was a simpler expression to deal with. The functional forms of the first seven members of $P_n^{(\frac{1}{2},0)}(g)$ and $Q_n^{(\frac{1}{2},0)}(r)$ are determined in the second part of appendix E. These functions have been plotted in Figures 8.3 and 8.4 as visual aids.

The functions $Q_n^{(\frac{1}{2},0)}(r)$ were evaluated over the range $1<r<5$ at intervals of 0.1 and then filed to form a data base denoted JACOBI7. Synthetic recapture data were generated once more and filed with both four and fourteen significant figures.

The fits for the files Q0T06 and 4Q0T06 are listed in appendix D. These files were generated by summing all of the $Q_n^{(\frac{1}{2},0)}(r)$ functions with unity weighting. The latter of these files contained numbers with only four significant figures. The coefficients and sample variance for these fits are summarized in Table 8.3. The fit to Q0T06 is much better than that to 4Q0T06 and the coefficients are also closer to the expected values of unity. The fit to 4Q0T06, however, describes the recapture current fairly accurately and hence there was still hope that the generation current could be reconstructed with the coefficients

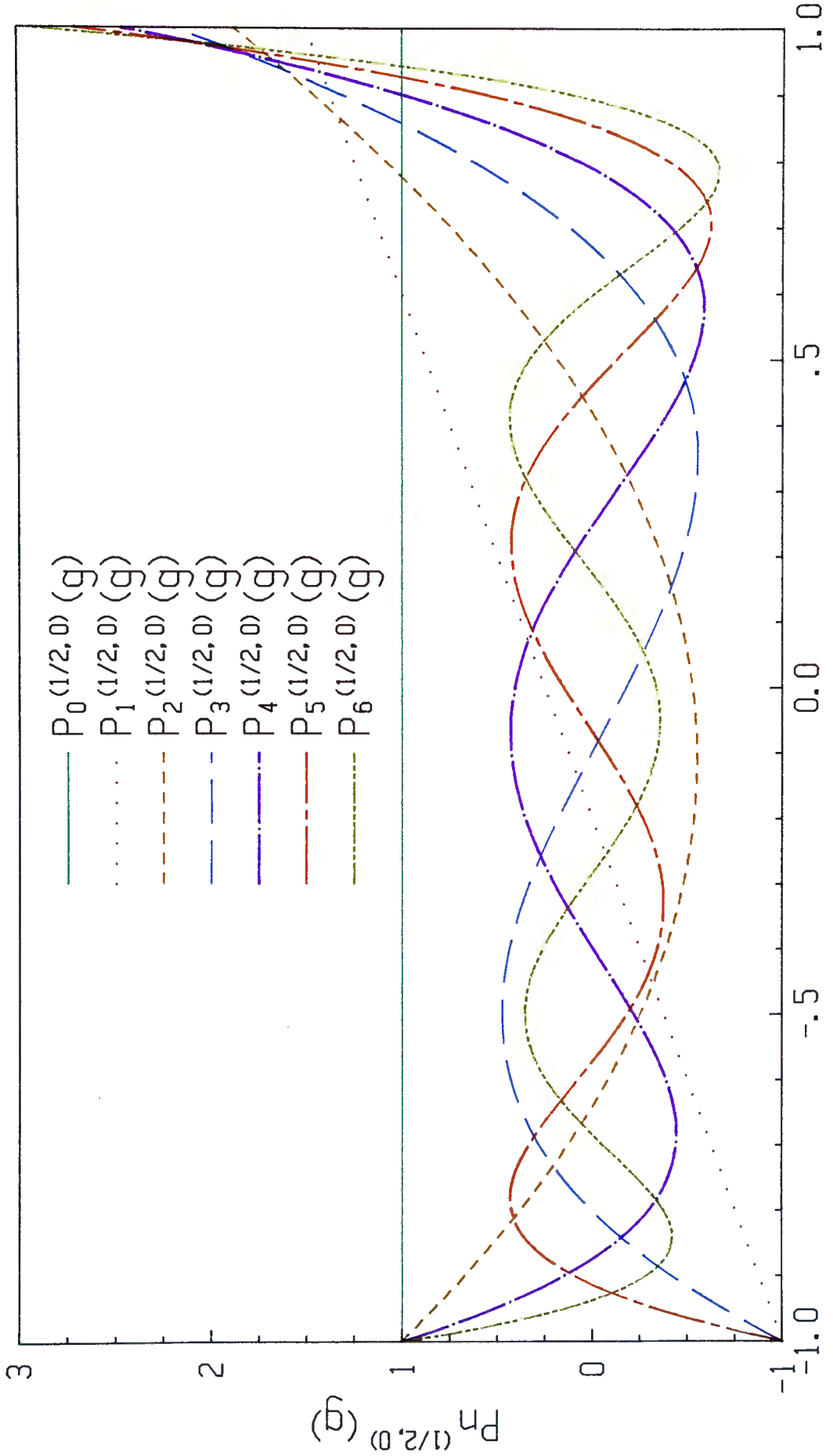

Figure 8.3 Jacobi Polynomials

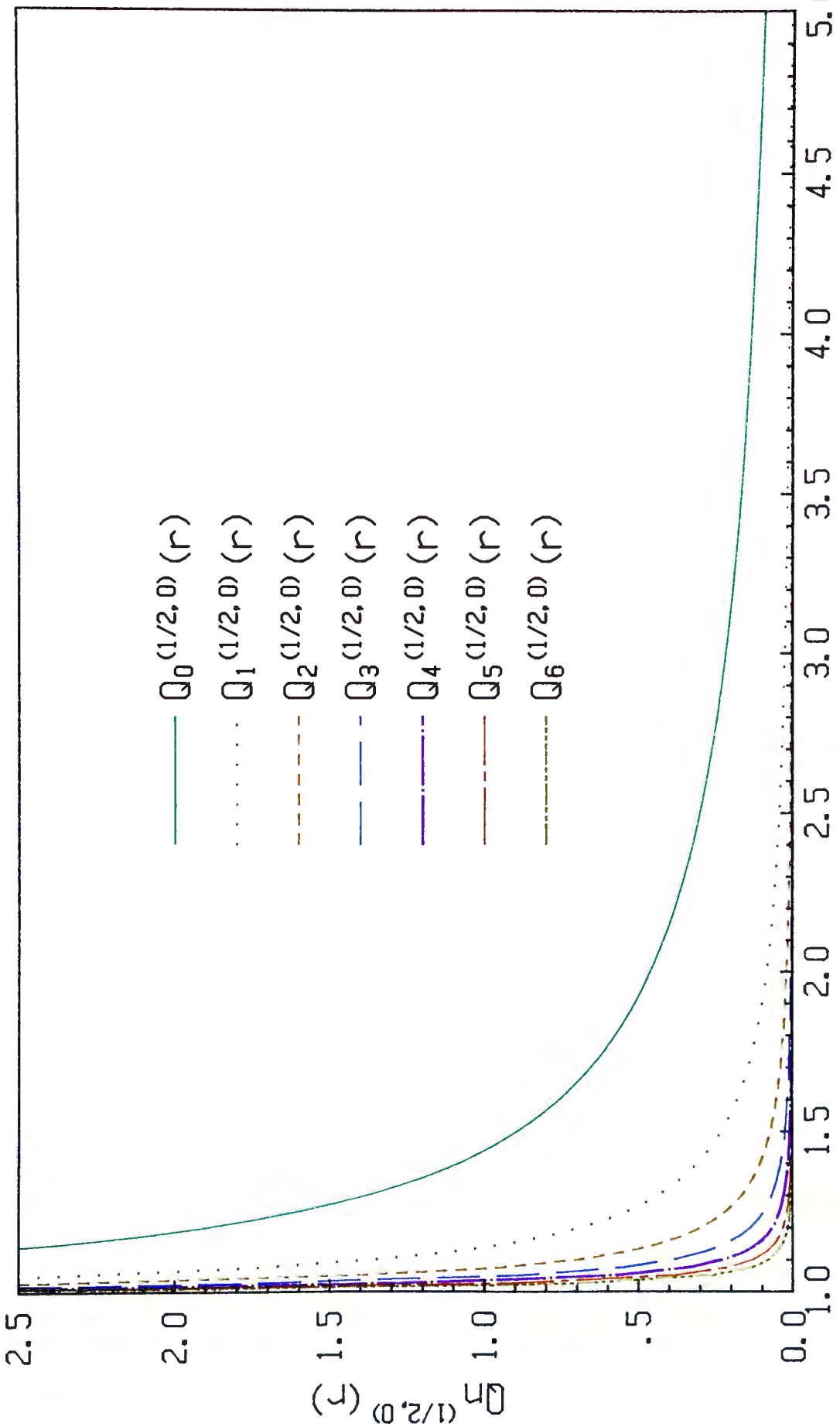

Figure 8.4 Jacobi Functions of the second kind

Datafile	Q0T06	400T06
A_0	1.0001	1.015
A_1	0.9976	0.498
A_2	1.0260	6.485
A_3	0.8715	-26.719
A_4	1.3171	71.805
A_5	0.6190	-87.554
A_6	1.1774	44.030
s^2	$7.18X10^{-12}$	$4.43X10^{-9}$

Table 8.3 Summary of coefficients and sample variance for some Jacobi function fits.

from the fit to the recapture current when applied to the corresponding $P_n^{(\frac{1}{2},0)}(g)$ functions.

Datafiles designated GALVAN-R and GALVAN-4R were built to represent the recapture current following galvanostatic generation. Since $P_0^{(\frac{1}{2},0)}(g)$ is equivalent to a galvanostatic generation current, $Q_0^{(\frac{1}{2},0)}(r)$ would be representative of the corresponding recapture current and hence the fit to the forementioned datafiles should give unity for A_0 and zero for the remaining coefficients. The coefficients and sample variance for these fits are summarized in Table 8.4.

The fit to GALVAN-R adhered to our expectations with A_0 being very close to unity and all remaining coefficients being less than 10^{-5}. These coefficients were then used to reconstruct the generation current GALVAN-G, as shown in appendix F. The

Datafile	GALVAN-R	GALVAN-4R
A_0	0.99999998	0.99979
A_1	$1.1869X10^{-7}$	-0.01737
A_2	$1.7181X10^{-6}$	0.44435
A_3	$-8.6690X10^{-6}$	-3.39992
A_4	$9.7835X10^{-6}$	11.28159
A_5	0	-16.89685
A_6	0	9.34476
s^2	$1.532X10^{-17}$	$6.170X10^{-10}$

Table 8.4 Summary of coefficients and sample variance for Jacobi function fits to recapture data corresponding to galvanostatic generation.

reconstructed generation current, denoted Fit_1, along with the exact solution are illustrated in Figure 8.5. This graph demonstrates that this is an excellent approximation of the generation current. The sample variance for the reconstructed generation current was $3X10^{-11}$. Hence Figure 8.5 may also serve as an aid for comparing previously quoted sample variances.

The coefficients for the fit to GALVAN-4R were not near those that were expected but they were used to reconstruct the generation current GALVAN-4G to learn how well this fitting routine would work with data representative of experimental accuracy. The reconstructed generation current has been plotted in Figure 8.6 as Fit_2. The reconstructed generation current is clearly not representative of the exact solution and it could not be used to gain information about the generation process.

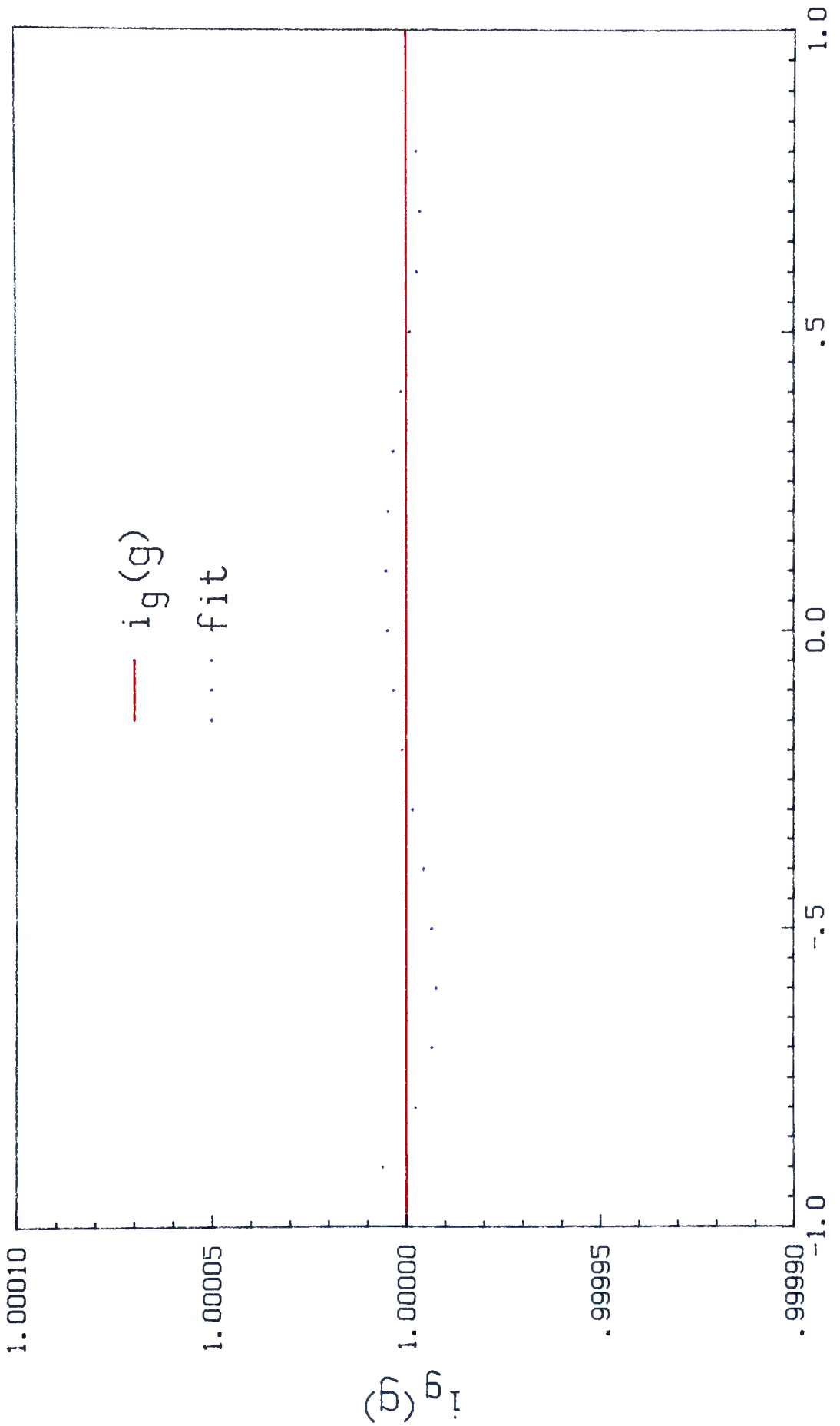

Figure 8.5 Fit1 for a galvanostatic current

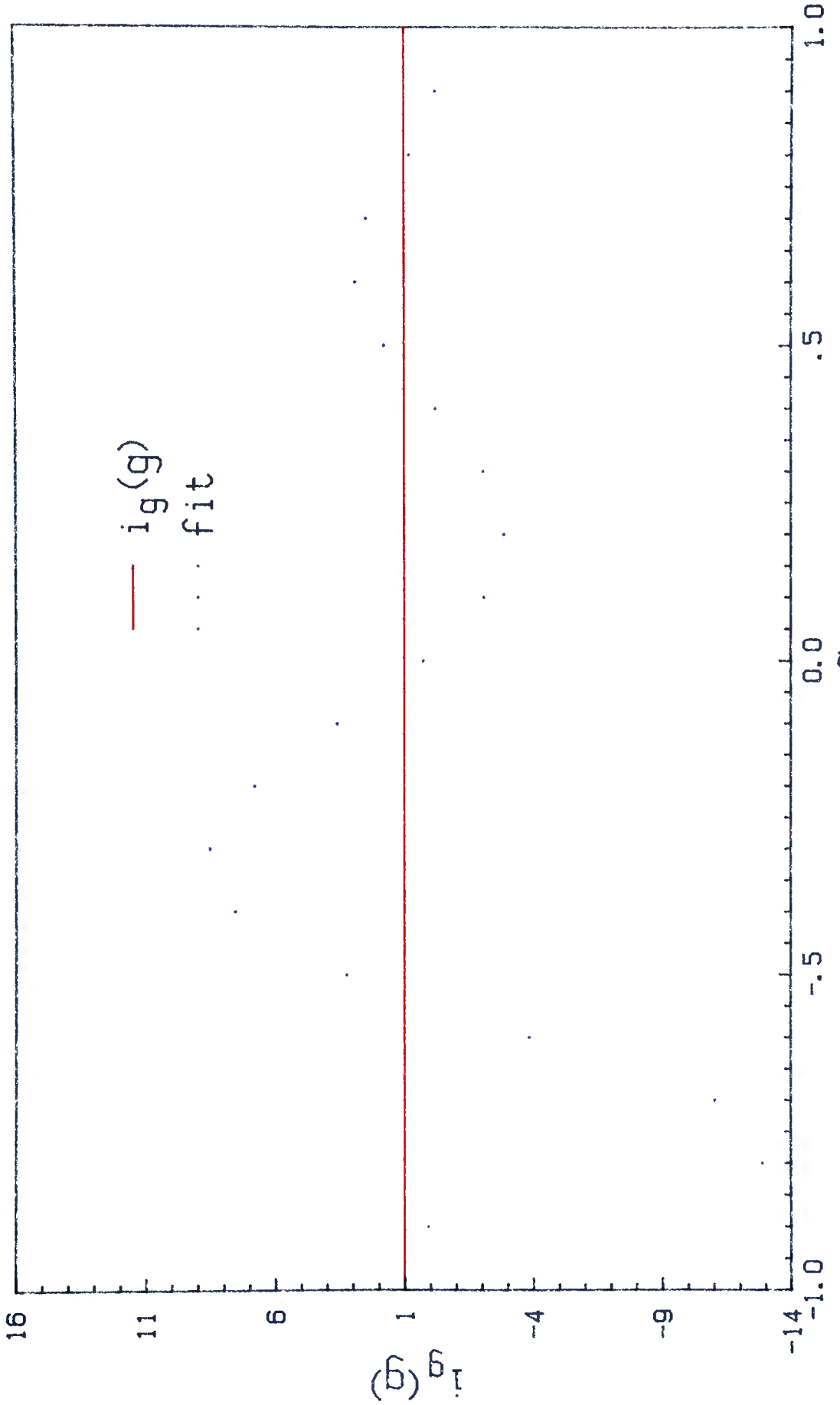

Figure 8.6 Fit$_2$ for a galvanostatic current

It appears that the second selection of fitting functions was not much better than the first for representing data that were designed to simulate the precision of experimental measurements. Another set of fitting functions was sought that would be orthogonal in the recapture domain, since the coefficients for the fit are calculated from data in this domain. (Note that the Jacobi functions were orthogonal only in the generation domain.) This search was unsuccessful and hence another approach was taken.

Summary of Curve Fitting

The reconstruction of the generation current based on coefficients obtained from a fit of the recapture current has been shown to be successful for data of high precision. However, the level of precision is beyond instrumental capability and hence another approach was necessary.

II) Iterative Hilbert Transformation

The state of knowledge of the three regions of the generation and recapture functions is summarized in Table II. Despite the extensive ignorance of these functions, it may be possible to make use of the known regions to improve a guessed generation function. The procedure is represented diagrammatically by the flowchart given as Figure 8.7. Each step in the algorithm is described below:

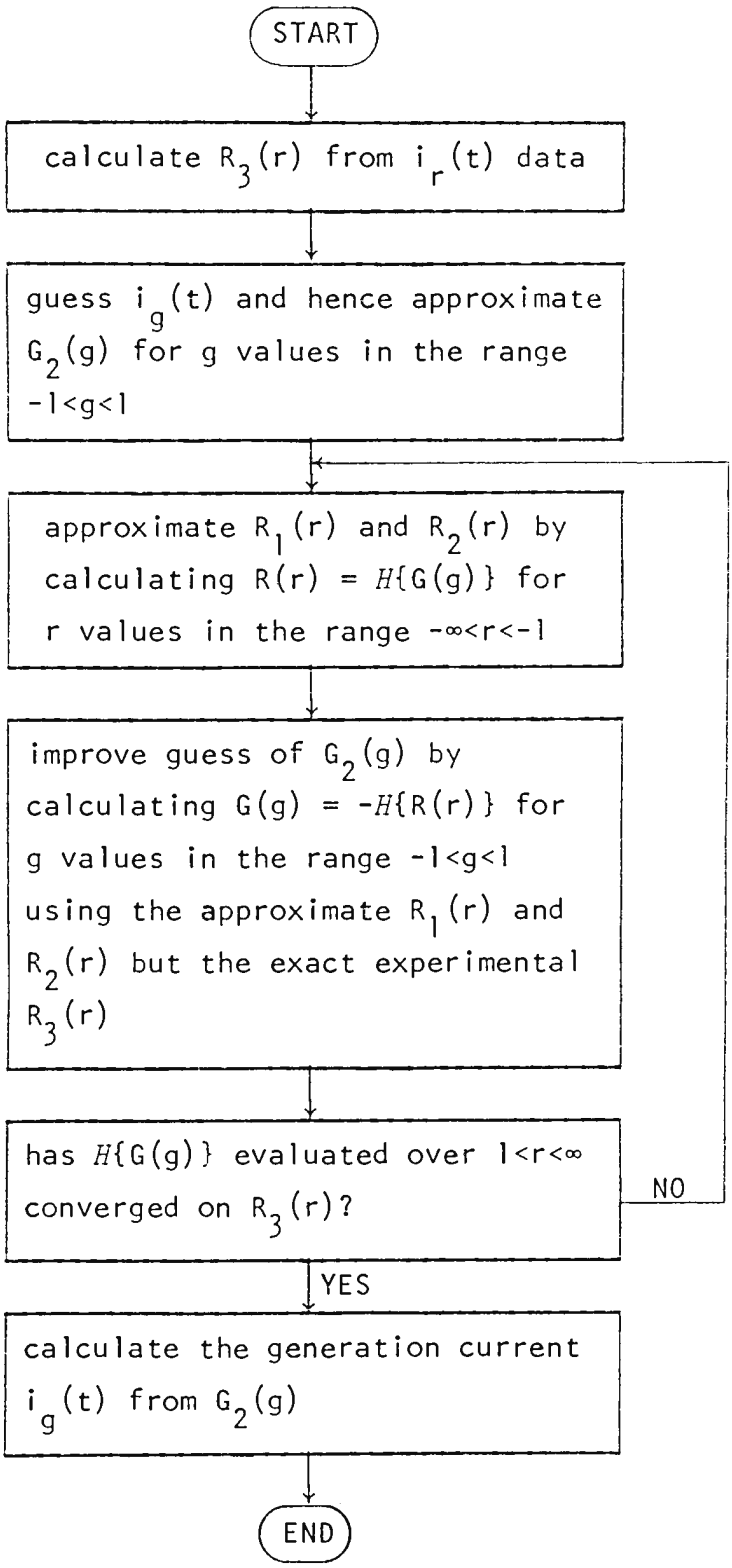

Figure 8.7 Flowchart of an iterative scheme to calculate $i_g(t)$ from $i_r(t)$

(i) Calculate the recapture function R(r) for r>1 from the measured recapture current $i_r(t)$. This part, $R_3(r)$, of the recapture function is henceforth assumed to be known exactly and precisely.

(ii) Make a guess concerning $i_g(t)$ and hence calculate an approximate $G_2(g)$ function for $-1<g<1$. Note that the generation function outside of this g domain is zero.

(iii) Use the approximate $G_2(g)$ function to implement the Hilbert transformation

$$R(r) = H\{G(g)\} = \frac{1}{\pi}\int_{-1}^{1} \frac{G_2(g)}{g-r}\,dg \qquad (8.16)$$

for r values in the range $-\infty<r<1$, thereby producing approximate values for the $R_1(r)$ and $R_2(r)$ portions of the recapture function.

(iv) Use these $R_1(r)$ and $R_2(r)$ functions, together with the exact $R_3(r)$ function to implement the negative Hilbert transformation

$$G(g) = -H\{R(r)\} = -\frac{1}{\pi}\int_{-\infty}^{\infty} \frac{R(r)}{r-g}\,dr \qquad (8.17)$$

for g values in the range $-1<g<1$, thereby improving the $G_2(g)$ approximation.

(v) The convergence of $G_2(g)$ can be tested by comparing the Hilbert transform of $G_2(g)$ with the exact solution of $R_3(r)$.

(vi) If $G_2(g)$ has not converged, repeat steps (iii) and (iv).

(vii) If $G_2(g)$ has converged, calculate the generation current $i_g(t)$.

This iterative approach required a numerical method for performing the Hilbert transformtion. This necessitated a method

that could deal with both an infinite integration range and the singularities that arise when g and r are equal. Applying the substitutions

$$r = \tan \phi \tag{8.18a}$$

and

$$g = \tan \theta \tag{8.18b}$$

to equations (8.16) and (8.17) yields

$$R(\phi) = \frac{1}{\pi} \int_{-\pi/4}^{\pi/4} G_2(\theta)[\cot(\theta-\phi)+\tan\theta]\, d\theta \tag{8.19a}$$

and

$$G(\theta) = -\frac{1}{\pi} \int_{-\pi/2}^{\pi/2} R(\phi)[\cot(\phi-\theta)+\tan\phi]\, d\phi \tag{8.19b}$$

where the angles are in radian measure. The integrals in these equations may be approximated by summations giving

$$R(\phi) \simeq \frac{1}{120} \sum_{j=0}^{59} G_2(\theta)[\cot(\theta-\phi)+\tan\theta] \quad , \quad \theta = -44\tfrac{1}{4} + 1\tfrac{1}{2}j \tag{8.20a}$$

and

$$G(\theta) \simeq -\frac{1}{120} \sum_{j=0}^{119} R(\phi)[\cot(\phi-\theta)+\tan\phi] \quad , \quad \phi = -89\tfrac{1}{4} + 1\tfrac{1}{2}j \tag{8.20b}$$

where the angles are measured in degrees and the summations are evaluated over data spaced at $1\frac{1}{2}^{\circ}$ intervals. The singularity that arises at $\theta=\phi$ may be compensated for by omitting the cotangent term from these expressions. Hence the preceding equations permit the Hilbert transformations to be evaluated by finite summations.

The iterative scheme was tested using equations (8.20a) and (8.20b) with data generated at $1\frac{1}{2}^{\circ}$ intervals for a cottrellian generation/recapture scheme. The solutions for $G(\theta)$ and $R(\phi)$ are illustrated in Figure 8.8. It was discovered that after only one iteration the new $G_2(\theta)$ diverged from the true solution even though the exact solution had been used for the guess of $G_2(\theta)$. In an attempt to learn what the transform was doing to the data, the entire $G(\theta)$ function was calculated rather than just $G_2(\theta)$. The new $G(\theta)$ function was slightly improved when calculated from data at a spacing of $\frac{3}{4}^{\circ}$ but this was still not very satisfactory, as illustrated in Figure 8.9. The transformation apparently smooths the generation function at the discontinuities. This smoothing continues with progressive iterations until $G_2(\theta)$ converges to the completely erroneous shape shown in Figure 8.10.

Several generation/recapture function pairs were tested with this algorithm and all displayed smoothing after a sufficient number of iterations. Therefore it was assumed that smoothing was inherent to this particular algorithm. Since a discontinuity

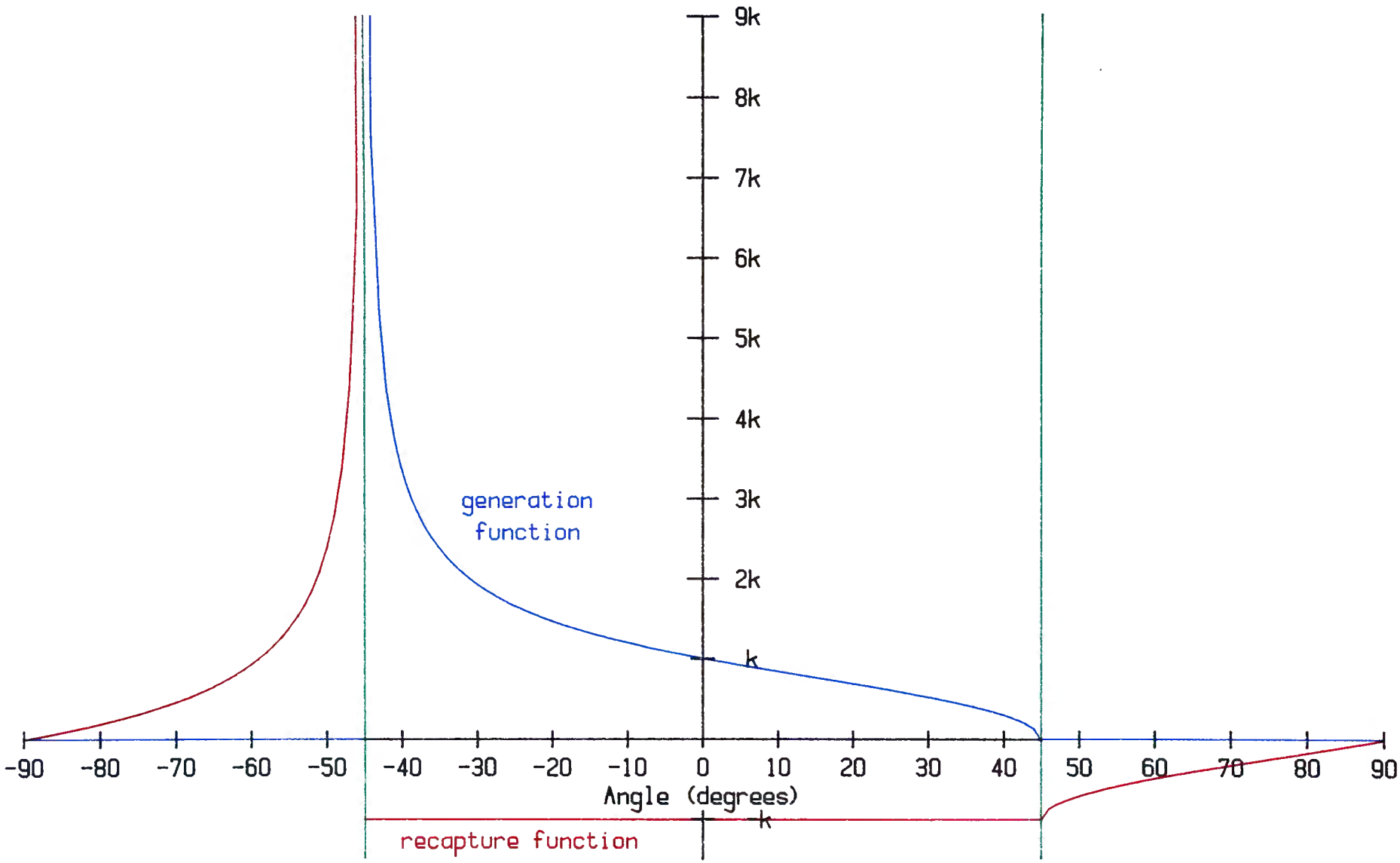

Figure 8.8 Cottrell generation and recapture functions

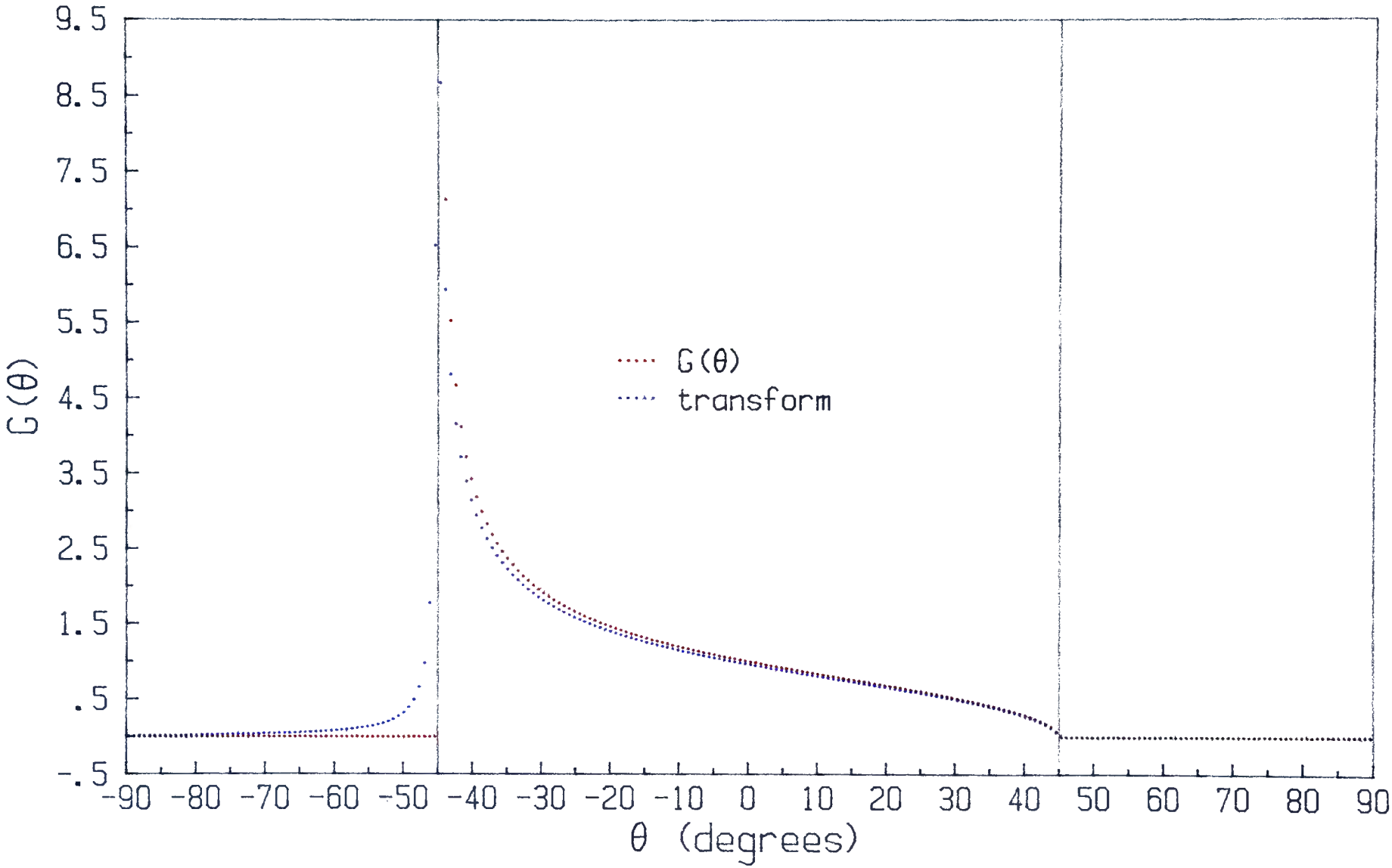

Figure 8.9 Transform of R(Ø) to G(θ)

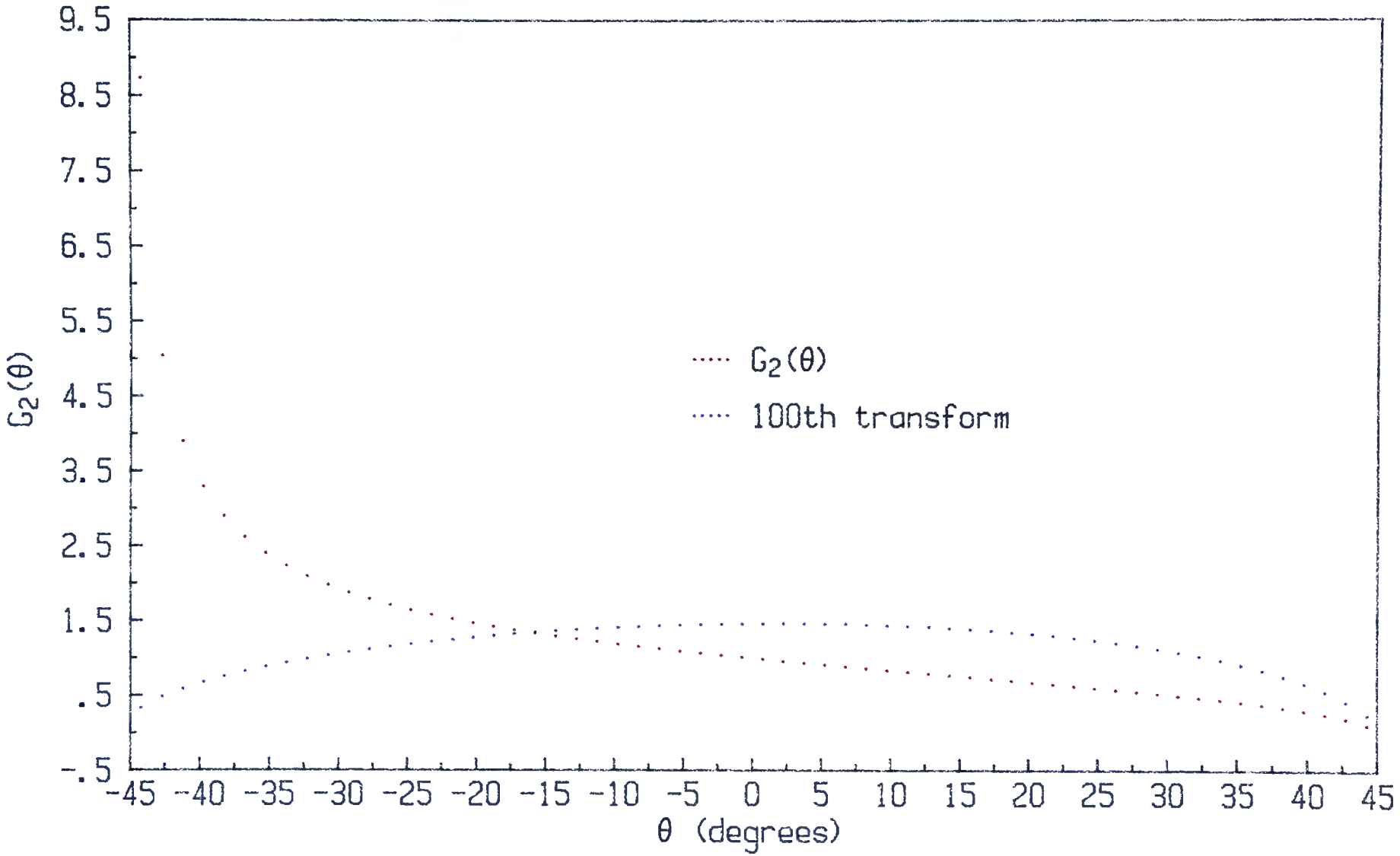

Figure 8.10 Divergence of $G_2(\theta)$ after 100 iterations

often arises in the generation function at either the beginning or end of the generation phase, a smoothing operation is undesirable.

Summary of Iterative Hilbert Transformation

The failure of this method was very disappointing since the idea behind it appeared to have been quite sound. However, it may be possible to improve this iterative approach by studying new algorithms for performing the numerical Hilbert transform. A thorough study of such algorithms may lead to a successful method for reconstructing the generation current.

CHAPTER 9

AN APPLICATION OF GENERATION/RECAPTURE ANALYSIS

Generation/recapture reaction schemes have rarely been applied for analytical purposes. One technique that does use this scheme is liquid chromatography / electrochemistry (LCEC).[1] In LCEC, the analyte is transported by a mobile phase and hence the recapture process is not controlled purely by diffusion. Therefore this system would not be suitable for Hilbert transform analysis. However, a description of LCEC can illustrate the advantages that a generation/recapture scheme can offer.

LCEC versus GC/MS

Many problems arise for trace analysis in complex samples. In biomedical research, for instance, complex samples such as biological fluids can contain thousands of individual compounds that are of no interest to the analysis under consideration. The amount of sample is often limited necessitating measurements of individual compounds in the picomole range and below.[2] Recently, established techniques have been combined to provide extremely sensitive and selective analytical methods. For example, the combination of gas chromatography and mass spectrometry (GC/MS) has revolutionized the analyst's ability to handle extremely complex mixtures. Unfortunately, this technique may not be

suitable for involatile or thermally labile samples. In addition, the expense and complexity of the instrumentation can make this system impractical for many laboratories.

The coupling of liquid chromatography with electrochemistry provides numerous advantages.[3] This technique is particularly useful for samples that cause problems in the gas phase but are well suited for analysis in a liquid medium. The LCEC system has many parallels with the GC/MS system and the detection limits achievable for both techniques are about the same.[2] Although GC/MS is more versatile and has better molecular specificity, LCEC is considerably less expensive and is more convenient for many analyses.

There are three standard configurations for the electrodes in a LCEC system as illustrated in Figure 9.1. The simplest configuration incorporates a thin-layer cell with a single working electrode whereas the remaining configurations incorporate two working electrodes. These two working electrodes may be arranged either in parallel, where they are side-by-side, or in series, where one electrode is upstream of the other. Each configuration has specific advantages, but only the dual electrode series configuration will be discussed in more detail since it is the only one that lends itself to the generation/recapture scheme.

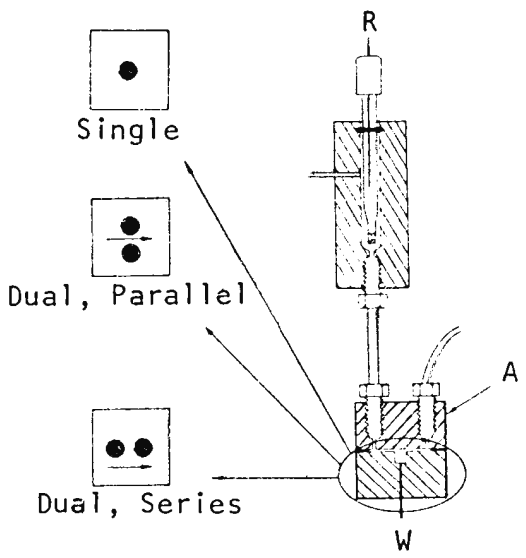

Figure 9.1 Electrode configurations for LCEC systems. The working electrode (W) is situated in a thin layer region. The reference electrode (R) and auxillary electrode (A) are located in a separate compartment outside the thin layer.

Elimination of Dissolved Oxygen Interference

The majority of applications for LCEC have been directed towards analytes which are electrochemically oxidizable. Reductive applications have been hindered by the presence of dissolved oxygen in mobile phase mixtures and sample solutions. Solutions in equilibrium with the atmosphere typically contain 10^{-3} to 10^{-4}M oxygen[1] which can make trace analysis impossible because of unacceptably high residual currents. The oxygen concentration for the mobile phase can usually be lowered to acceptable levels by appropriate methods but handling of the sample is more restricted and hence total oxygen removal is

often impossible.

One method for removing oxygen from the sample is illustrated in Figure 9.2. This method relies on the electrochemical reversibility of the analyte redox couple and the irreversibility of the oxygen/peroxide/water redox system. The upstream electrode, which serves as a generator, is set at a potential which is sufficiently negative to induce the reduction of the analyte and the dissolved oxygen. The downstream electrode, which serves as a detector, is set at a potential which is sufficiently positive to reoxidize the analyte reduction product but not the peroxide or water. Hence the current that flows at the detector will be free of interference from oxygen.

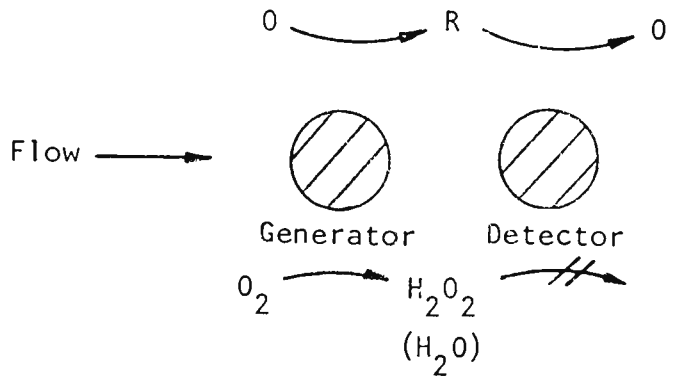

Figure 9.2 "Removal" of dissolved oxygen via dual series LCEC.

Although in this technique the generation and recapture reactions occur simultaneously at separate electrodes, the concept is essentially the same as the Hilbert transform approach.

CHAPTER 10

SUMMARY

The benefits of several transform techniques have been presented and a new application for the Hilbert transform has been developed. The Hilbert transform relationship was proven theoretically and then employed numerically to demonstrate that the recapture current could be described quite accurately by the transform of the generation current. This operation was very successful with closely spaced synthetic data and almost as successful with experimental data. It was tested with experimental data that were obtained with two chemical systems under a variety of excitation waveforms to illustrate its versatility. However, a successful algorithm was not devised that would enable an interference-free generation current to be reconstructed from a recapture current and this transform will not have fulfilled its potential until such an algorithm is developed.

APPENDIX A

The operation of Laplace transformation is applied routinely in electrochemistry [see reference (1) for examples]. A proof of equation (6.3) will be provided here which relies upon this transform.

The three phases of the experiment are summarized in Table A.1.

Phase	Electrode Reaction	Time Period
Equiiibrium	none	$-\infty<t<0$
Generation	$X + n_g e \rightarrow Y$	$0<t<T$
Recapture	$Y + n_r e \rightarrow Z$	$T<t<\infty$

Table A.1 Summary of experimental phases.

Let $C(x,t)$ denote the concentration of species Y at a distance x from the electrode at a time t in the interval $0<t<T$. The following conditions can be applied to Y during the generation phase:

(i) Y is transported in accordance with Fick's second law of diffusion

$$D \frac{\partial^2}{\partial x^2} C(x,t) = \frac{\partial}{\partial t} C(x,t) \qquad (A.1)$$

(ii) initially, Y is absent from solution

$$C(x,0) = 0 \qquad (A.2)$$

(iii) at a sufficient distance from the electrode, Y will remain absent from solution

$$C(\infty,t) = 0 \tag{A.3}$$

(iv) the total number of electrons transferred at the electrode in a unit time must be proportional to the quantity of Y that reaches the electrode in that time period

$$\frac{\partial}{\partial x} C(0,t) = - \frac{i_g(t)}{n_g AFD} \tag{A.4}$$

The Laplace transform of $C(x,t)$ with respect to t will be denoted $\overline{C}(x,s)$, s being a dummy variable. Transformation of equation (A.1) followed by substitution of equation (A.2) yields

$$D \frac{d^2}{dx^2} \overline{C}(x,s) = s\overline{C}(x,s) - C(x,0) = s\overline{C}(x,s) \tag{A.5}$$

Transformation of equations (A.3) and (A.4) give

$$\overline{C}(\infty,s) = 0 \tag{A.6}$$

$$\frac{d}{dx} \overline{C}(0,s) = - \frac{\overline{i}_g(s)}{n_g AFD} \tag{A.7}$$

where $\overline{i}_g(s)$ is the Laplace transform of $i_g(t)$.

Equation (A.5) is a second order ordinary differential equation that can be solved in terms of two arbitrary constants $B_1(s)$ and $B_2(s)$ as

$$\overline{C}(x,s) = B_1(s)\exp[-(s/D)^{\frac{1}{2}}x] + B_2(s)\exp[(s/D)^{\frac{1}{2}}x] \tag{A.8}$$

but, if equation (A.6) is to be satisfied, $B_2(s)$ must be zero.

Differentiation then gives

$$\frac{d}{dx}\bar{C}(x,s) = -(s/D)^{\frac{1}{2}}B_1(s)\exp[-(s/D)^{\frac{1}{2}}] \qquad (A.9)$$

which upon comparison with equation (A.7) establishes $B_1(s)$ as $\bar{i}_g(s)/[n_g AF(sD)^{\frac{1}{2}}]$. Equation (A.8) may now be written as

$$\bar{C}(x,s) = \left[\frac{\bar{i}_g(s)}{nAF}\right]\left[\frac{\exp[-(s/D)^{\frac{1}{2}}x]}{(Ds)^{\frac{1}{2}}}\right] \qquad (A.10)$$

Inversion of equation (A.10) is possible with the aid of the convolution integral of Laplace transformation.[2] Application of this integral to equation (A.10) gives

$$C(x,t) = \int_0^t \left[\frac{i_g(\tau)}{n_g AF}\right]\left[\frac{1}{[\pi D(t-\tau)]^{\frac{1}{2}}}\exp\left\{\frac{-x^2}{4D(t-\tau)}\right\}\right] d\tau$$

$$= \frac{1}{n_g AF(\pi D)^{\frac{1}{2}}}\int_0^t \frac{i_g(\tau)}{(t-\tau)^{\frac{1}{2}}}\exp\left\{\frac{-x^2}{4D(t-\tau)}\right\} d\tau \qquad (A.11)$$

The concentration profile during the generation phase cannot be determined from equation (A.11) unless the functional form of $i_g(t)$ is known. However, this equation is useful in its present form since it is applicable to any generation current.

Now consider the recapture phase of the experiment. Conditions (A.1) and (A.3) are still applicable but (A.2) and (A.4) are not, and therefore must be replaced. The recapture reaction is initiated at time t=T. At this instant, the concentration profile is given by

$$C(x,T) = \frac{1}{n_g AF(\pi D)^{\frac{1}{2}}} \int_0^T \frac{i_g(\tau)}{(T-\tau)^{\frac{1}{2}}} \exp\left\{\frac{-x^2}{4D(T-\tau)}\right\} d\tau \qquad (A.12)$$

according to equation (A.11). A new boundary condition,

$$C(0,t) = 0 \qquad (A.13)$$

now arises as a consequence of Y being consumed under conditions of complete concentration polarization for t>T. The recapture current is given by

$$i_r(t) = n_r AFD \frac{\partial}{\partial x} C(0,t) \qquad (A.14)$$

which is the analogue of equation (A.4) in the recapture phase. Therefore, the evaluation of the recapture current does not require a complete expression C(x,t) for the concentration profile; only the surface gradient $\partial C(0,t)/\partial x$ need be known.

Using σ as the dummy variable for Laplace transformation with respect to t-T, the transforms of equations (A.1), (A.3), and (A.13) are

$$D \frac{d^2}{dx^2} \overline{C}(x,\sigma) = \sigma \overline{C}(x,\sigma) - C(x,T) \qquad (A.15)$$

$$\overline{C}(\infty,\sigma) = 0 \qquad (A.16)$$

and

$$\overline{C}(0,\sigma) = 0 \qquad (A.17)$$

Equation (A.15) is an inhomogeneous second order ordinary

differential equation that can be solved by standard methods[3] to give

$$\bar{C}(x,\sigma) = \frac{\exp[-(\sigma/D)^{\frac{1}{2}}x]}{2(D\sigma)^{\frac{1}{2}}}\left[B_1(\sigma) + \int_0^x C(\rho,T)\exp[(\sigma/D)^{\frac{1}{2}}\rho]\,d\rho\right] + \frac{\exp[(\sigma/D)^{\frac{1}{2}}x]}{2(D\sigma)^{\frac{1}{2}}}\left[B_2(\sigma) - \int_0^x C(\rho,T)\exp[-(\sigma/D)^{\frac{1}{2}}\rho]\,d\rho\right] \quad (A.18)$$

where $B_1(\sigma)$ and $B_2(\sigma)$ are arbitrary. Application of condition (A.16) establishes that

$$B_2(\sigma) = \int_0^\infty C(\rho,T)\exp[-(\sigma/D)^{\frac{1}{2}}\rho]\,d\rho \quad (A.19)$$

while condition (A.17) establishes $B_1(\sigma)$ as the negative of $B_2(\sigma)$. Hence equation (A.18) may be written as

$$\bar{C}(x,\sigma) = \frac{\exp[-(\sigma/D)^{\frac{1}{2}}x]}{2(D\sigma)^{\frac{1}{2}}}\int_0^x C(\rho,T)\exp[(\sigma/D)^{\frac{1}{2}}\rho]\,d\rho - \frac{\exp[-(\sigma/D)^{\frac{1}{2}}x]}{2(D\sigma)^{\frac{1}{2}}}\int_0^\infty C(\rho,T)\exp[-(\sigma/D)^{\frac{1}{2}}\rho]\,d\rho + \frac{\exp[(\sigma/D)^{\frac{1}{2}}x]}{2(D\sigma)^{\frac{1}{2}}}\int_x^\infty C(\rho,T)\exp[-(\sigma/D)^{\frac{1}{2}}\rho]\,d\rho \quad (A.20)$$

Differentiation of equation (A.20) with respect to x leads to

$$2D\frac{d}{dx}\bar{C}(x,\sigma) = -\exp[-(\sigma/D)^{\frac{1}{2}}x]\int_0^x C(\rho,T)\exp[(\sigma/D)^{\frac{1}{2}}\rho]\,d\rho + \exp[-(\sigma/D)^{\frac{1}{2}}x]\int_0^\infty C(\rho,T)\exp[-(\sigma/D)^{\frac{1}{2}}\rho]\,d\rho + \exp[(\sigma/D)^{\frac{1}{2}}x]\int_x^\infty C(\rho,T)\exp[-(\sigma/D)^{\frac{1}{2}}\rho]\,d\rho \quad (A.21)$$

which simplifies to

$$\frac{d}{dx}\,\overline{C}(0,\sigma) = \frac{1}{D}\int_0^\infty C(x,T)\exp[-(\sigma/D)^{\frac{1}{2}}x]\,dx \qquad (A.22)$$

on setting x equal to zero. Substitution of C(x,T) from equation (A.12) gives

$$\frac{d}{dx}\,\overline{C}(0,\sigma) = \frac{1}{n_g AF\pi^{1/2}D^{3/2}}\int_0^T \frac{i_g(\tau)}{(T-\tau)^{\frac{1}{2}}}\int_0^\infty \exp\left\{-x\left(\frac{\sigma}{D}\right)^{\frac{1}{2}} - \frac{x^2}{4D(T-\tau)}\right\}dx\,d\tau \qquad (A.23)$$

after the order of the two integrations is reversed. The inner integral may be more easily evaluated after a change of variable to $\{\sigma(T-\tau)\}^{\frac{1}{2}}+x/[2\{D(T-\tau)^{\frac{1}{2}}\}]$. This leads to

$$\frac{d}{dx}\,\overline{C}(0,\sigma) = \frac{1}{n_g AFD}\int_0^T i_g(\tau)\exp[\sigma(T-\tau)]\,\mathrm{erfc}[\sigma(T-\tau)]^{\frac{1}{2}}\,d\tau \qquad (A.24)$$

as the final expression for the transform of the surface concentration gradient during the recapture phase.

Tables of Laplace transforms[4] give the inversion

$$L^{-1}\{\exp(ks)\,\mathrm{erfc}(ks)^{\frac{1}{2}}\} = \frac{1}{\pi(t+k)}\left(\frac{k}{t}\right)^{\frac{1}{2}} \qquad (A.25)$$

for k a positive constant. Recalling that σ is the dummy variable corresponding to t-T, the inversion of equation (A.24) is

$$\frac{\partial}{\partial x}\,C(0,t) = \frac{1}{\pi n_g AFD(t-T)^{\frac{1}{2}}}\int_0^T \frac{i_g(\tau)\,(T-\tau)^{\frac{1}{2}}}{t-\tau}\,d\tau \qquad (A.26)$$

Combination of this expression with equation (A.14) leads to

$$i_r(t) = \frac{n_r}{\pi n_g (t-T)^{\frac{1}{2}}} \int_0^T \frac{i_g(\tau)\,(T-\tau)^{\frac{1}{2}}}{t - \tau}\, d\tau \qquad \text{(A.27)}$$

which completes the proof.

APPENDIX B

A proof of equation (6.4) is provided here using the fractional calculus. It will be assumed that the generation and recapture are mutual converses. This generation/recapture scheme may be expressed as

$$X + ne \rightleftarrows Y \tag{B.1}$$

where n is positive for a reductive generation reaction, and negative for an oxidative one.

If an electroactive species, initially present at a uniform concentration C^*, is transported to and/or from an electrode by semiinfinite planar diffusion, then its concentration at the electrode surface is given by[1]

$$C(0,t) = C^* + \frac{m(t)}{nAFD^{\frac{1}{2}}} \tag{B.2}$$

where m(t) is the faradaic semiintegral and D is the diffusion coefficient of the electroactive species. The faradaic semiintegral may be defined as

$$m(t) = \frac{1}{\pi^{\frac{1}{2}}} \int_0^t \frac{i(\tau)}{(t-\tau)^{\frac{1}{2}}} d\tau = \frac{d^{-\frac{1}{2}}}{dt^{-\frac{1}{2}}} i(t) \tag{B.3}$$

where i(t) is the faradaic cathodic current flowing at time t.

For species Y in this equilibrium/generation/recapture experiment, C^* is zero. In addition, the recapture reaction

proceeds under conditions of concentration polarization and hence C(0,t>T) is also zero. Therefore, it follows from equation (B.2) that m(t>T) must also be zero. The convolution integral defining the semiintegral in equation (B.3) may be split into two components thereby defining m(t>T) as

$$m(t>T) = \frac{1}{\pi^{\frac{1}{2}}} \int_0^T \frac{i(\tau)}{(t-\tau)^{\frac{1}{2}}} d\tau + \frac{1}{\pi^{\frac{1}{2}}} \int_T^t \frac{i(\tau)}{(t-\tau)^{\frac{1}{2}}} d\tau = 0 \qquad (B.4)$$

The second of these integrals represents the operation of semi-integrating the current starting at time t=T and therfore it may be referred to as the "recapture semiintegral". This integral may be written in the notation of the fractional calculus as

$$m_r(t) = \frac{d^{-\frac{1}{2}}}{[d(t-T)]^{-\frac{1}{2}}} i(t) = \frac{1}{\pi^{\frac{1}{2}}} \int_T^t \frac{i(\tau)}{(t-\tau)^{\frac{1}{2}}} d\tau \qquad (B.5)$$

It then follows that

$$\frac{d^{-\frac{1}{2}}}{[d(t-T)]^{-\frac{1}{2}}} i(t) = - \frac{1}{\pi^{\frac{1}{2}}} \int_0^T \frac{i(\tau)}{(t-\tau)^{\frac{1}{2}}} d\tau \quad , \quad t>T \qquad (B.6)$$

by combining equations (B.4) and (B.5).

In the same way that the derivative of an integral of a function is the function itself, the semiderivative of the semi-integral of a function will also be the function itself.[2] Therefore, if equation (B.6) is semidifferentiated using T as the

lower limit, then

$$i(t>T) = -\frac{1}{\pi^{\frac{1}{2}}}\frac{d^{\frac{1}{2}}}{[d(t-T)]^{\frac{1}{2}}}\int_0^T \frac{i(\tau)}{(t-\tau)^{\frac{1}{2}}}\,d\tau$$

$$= -\frac{1}{\pi^{\frac{1}{2}}}\int_0^T i(\tau)\left\{\frac{d^{\frac{1}{2}}}{[d(t-T)]^{\frac{1}{2}}}\frac{1}{(t-\tau)^{\frac{1}{2}}}\right\}d\tau \qquad (B.7)$$

The term in braces may be evaluated by making the substitution $z = (t-T)/(T-\tau)$ which simplifies it to $(T-\tau)^{-1}d^{\frac{1}{2}}(1+z)^{-\frac{1}{2}}/dz^{\frac{1}{2}}$. The semiderivative of $(1+z)^{-\frac{1}{2}}$ may be found in standard tables[2] to be $[(\pi z)^{\frac{1}{2}}(1+z)]^{-1}$ and hence the embraced term in equation (B.7) is $(T-\tau)^{\frac{1}{2}}/[\{\pi(t-T)\}^{\frac{1}{2}}(t-\tau)]$. Equation (B.7) then becomes

$$i(t>T) = -\frac{1}{\pi(t-T)^{\frac{1}{2}}}\int_0^T \frac{i(\tau)(T-\tau)^{\frac{1}{2}}}{t-\tau}\,d\tau \qquad (B.8)$$

which, apart from minor notational differences, is identical to equation (6.4) and hence completes the proof.

APPENDIX C

This appendix contains some of the programs that were essential for this research. The first program that is given is written in FORTRAN and was run on a Honeywell CP-5 computer. The remaining programs are written in BASIC and were run on a HP-85 personal computer. Comments have been embedded throughout these programs to aid in their interpretation.

```
C     *-------------------------------------------------------------*
C     * PROGRAM: FITMOD                                             *
C     *     ROM: FITMOD-ROM                                         *
C     *                                                             *
C     * REFERENCE: Data Reduction and Error Analysis for the       *
C     *            Physical Sciences, by Philip R. Bevington        *
C     *                                                             *
C     *     This program fits data up to seven parameters. The      *
C     * datafile must be input with the value of the argument       *
C     * in column one and the function value in column two. A       *
C     * file must also be input which contains the fitting          *
C     * basis comprised of seven columns of fitting functions       *
C     * evaluated over the range of the argument.                   *
C     *     A file is eventually output which contains the co-      *
C     * efficients for the fit, their standard deviations, and      *
C     * Chi-square as well as data for the fitted curve.            *
C     *                                                             *
C     *                    LAST REVISED: AUGUST 1982                *
C     *                                 BY: Mike Hempstead          *
C     *                                                             *
C     *-------------------------------------------------------------*
C
C Set variable types and storage
C
      IMPLICIT DOUBLE PRECISION (A-H,O-Z)
      DIMENSION DATA(60,2),RF(60,7),NPS(20)
      DIMENSION A(7),FIT(60),Y(60),SIGMAA(7),F(7)
      CHARACTER*11 INFILE(20),OUTFILE(20),RFILE(20),ANS
      LOGICAL EXIST1,EXIST2,EXIST3
C
C Initialize file counter
C
      NFILE=1
C
C Initialize arrays
C
    1 DO 2 I=1,7
      F(I)=0.0D0
    2 CONTINUE
      DO 3 I=1,60
      FIT(I)=0.0
    3 CONTINUE
C
C Input datafile
C
```

```
   10 OUTPUT ' ';OUTPUT 'INPUT-FILE NAME (MAX. 11 CHAR; ESC F TO END)'
      READ(105,15,END=120) INFILE(NFILE)
      INQUIRE (FILE=INFILE(NFILE),EXIST=EXIST1)
      IF (.NOT. EXIST1) OUTPUT 'FILE DOES NOT EXIST';GOTO 10
      OPEN (UNIT=55,FILE=INFILE(NFILE),USAGE='INPUT')
      OUTPUT ' INPUT THE NUMBER OF DATA POINTS'
      READ(105,55)NPS(NFILE)
      IF (NPS(NFILE).GT.60)
     1     OUTPUT '* * * WARNING : ONLY FIRST 60 POINTS READ';
     2     NPS(NFILE)=60
      DO 100 I=1,NPS(NFILE)
      READ(55,65) (DATA(I,J),J=1,2)
  100 CONTINUE
      CLOSE (UNIT=55)
C
C Enter fitting functions
C
   11 OUTPUT'  ';OUTPUT'INPUT-FILE FOR FITTING FCNS (MAX. 11 CHAR.)'
      READ(105,15,END=120) RFILE(NFILE)
      INQUIRE (FILE=RFILE(NFILE),EXIST=EXIST2)
      IF (.NOT. EXIST2) OUTPUT 'FILE DOES NOT EXIST';GOTO 11
      OPEN (UNIT=55,FILE=RFILE(NFILE),USAGE='INPUT')
      DO 200 I=1,NPS(NFILE)
      READ(55,66) (RF(I,J),J=1,7)
  200 CONTINUE
      CLOSE (UNIT=55)
C
C Prepare data for fitting
C
      DO 4 I=1,NPS(NFILE)
      Y(I)=DATA(I,2)
    4 CONTINUE
C
C Prompt for order of fit
C
  999 OUTPUT 'What order of fit is desired'
      READ(105,55) NORDER
C
C Zero all coefficents
C
      DO 6 J=1,7
      A(J)=0.0D0
      SIGMAA(J)=0.0D0
    6 CONTINUE
C
```

```
C Perform the fitting routine
C
      CALL BETAFIT (Y,RF,NPS(NFILE),NORDER-1,0,0,F,FIT,A,SIGMAA,CHISQR
C
C Output Chisquare
C
      WRITE(105,90) CHISQR
C
C Test for repetitive fit
C
      OUTPUT 'Would you like a different order of fit'
      READ(105,15) ANS
      IF (ANS(1:3).EQ.'YES') GO TO 999
C
C Output the fitted curve
C
   20 OUTPUT' ';OUTPUT'OUTPUT-FILE NAME FOR FITTED CURVE (MAX 11 CHAR.
'
      READ(105,15,END=120) OUTFILE(NFILE)
      INQUIRE (FILE=OUTFILE(NFILE),EXIST=EXIST3)
      IF (.NOT.EXIST3) OUTPUT ' '; GOTO 30
      WRITE(108,25) OUTFILE(NFILE)
      READ(105,15) ANS
      IF (ANS(1:3).NE.'YES') GOTO 20
      OUTPUT ' ';OUTPUT '* * * FILE WILL BE OVERWRITTEN * * *'
   30 OPEN (UNIT=66,FILE=OUTFILE(NFILE),USAGE='OUTPUT')
      WRITE(66,75) INFILE(NFILE),RFILE(NFILE)
      DO 14 I=1,7
      J=I-1
      WRITE(66,85) J,A(I),SIGMAA(I)
   14 CONTINUE
      WRITE(66,90) CHISQR
      WRITE(66,95)
      DO 16 I=1,NPS(NFILE)
      WRITE(66,105) (DATA(I,J),J=1,2),FIT(I)
   16 CONTINUE
      CLOSE (UNIT=66)
C
C Step file counter
C
      NFILE=NFILE+1
      IF (NFILE.LT.21) WRITE(108,35)  ;GOTO 1
      OUTPUT 'PROGRAM CAN ONLY HANDLE TWENTY FILES AT A TIME'
C
C Output analysis summary
C
```

```
  120 NFILE=NFILE-1
      WRITE(108,45) NFILE
      DO 17 J=1,NFILE
      WRITE(108,46) INFILE(J),RFILE(J),OUTFILE(J),NPS(J)
   17 CONTINUE
    5 FORMAT(F4.2,5(1X,E14.8))
   15 FORMAT(A11)
   25 FORMAT(2/,5X,'*** WARNING : FILE ',A11,'ALREADY EXISTS.',/,
     1' DO YOU WANT TO OVERWRITE IT.(YES/NO)')
   35 FORMAT(2/,40'-',/,1H1)
   45 FORMAT(4X,G,'FILE(S) PROCESSED :',//T5,'INPUT-FILE',T20,
     1'BASIS-FILE',T35,'OUTPUT-FILE',T50,'# OF DATA PTS',/)
   46 FORMAT(T5,A11,T20,A11,T35,A11,T55,G)
   55 FORMAT(G)
   65 FORMAT(2G)
   66 FORMAT(7G)
   75 FORMAT(T5,'This file lists the fit for ',A11,/,
     1T5,'The corresponding fitting function data is '
     2'given in ',A11,2/,T5,'Coefficents',T35,'S.D. AJ')
   85 FORMAT(T5,'A(',I1,')= ',1PE15.8,T31,1PE15.8)
   90 FORMAT(2/,T5,'The value of Chi-square is ',1PE15.8)
   95 FORMAT(2/,4X,'Data generated by fit',/,T6,'r',T19,'ir',T38,'fit'
  105 FORMAT(4X,F4.2,4X,1PE15.8,4X,1PE15.8)
      STOP
      END
C *****************************************************
C
C Function fitting subroutine
C
C *****************************************************
      SUBROUTINE BETAFIT(Y,P,NPTS,NORDER,NEVEN,MODE,
     1 FTEST,YFIT,A,SIGMAA,CHISQR)
      IMPLICIT DOUBLE PRECISION (A-H,O-Z)
      DIMENSION Y(60),FTEST(7),YFIT(60),
     1 A(7),SIGMAA(7),B(7),SIGMAB(7)
      DIMENSION P(60,7),BETA(7),ALPHA(7,7)
   10 NTERMS=1
      NCOEFF=1
      JMAX=NORDER+1
C
C Accumulate matrices ALPHA and BETA
C
  120 DO 130 J=1,NTERMS
      BETA(J)=0.
      DO 130 K=1,NTERMS
```

```
  130 ALPHA(J,K)=0.
  140 DO 150 I=1,NPTS
      DO 150 J=1,NTERMS
      BETA(J)=BETA(J)+P(I,J)*Y(I)
      DO 150 K=J,NTERMS
      ALPHA(J,K)=ALPHA(J,K)+P(I,J)*P(I,K)
  150 ALPHA(K,J)=ALPHA(J,K)
C
C Delete fixed coefficients
C
  160 IF (NEVEN) 170,230,200
  170 DO 190 J=3,NTERMS,2
      BETA(J)=0.
      DO 180 K=1,NTERMS
      ALPHA(J,K)=0.
  180 ALPHA(K,J)=0.
  190 ALPHA(J,J)=1.
      GO TO 230
  200 DO 220 J=2,NTERMS,2
      BETA(J)=0.
      DO 210 K=1,NTERMS
      ALPHA(J,K)=0.
  210 ALPHA(K,J)=0.
  220 ALPHA(J,J)=1.
C
C Invert curvature matrix ALPHA
C
  230 DO 240 J=1,JMAX
      A(J)=0.
      SIGMAA(J)=0.
      B(J)=0.
  240 SIGMAB(J)=0.
      DO 250 I=1,NPTS
  250 YFIT(I)=0.
  260 CALL MATINV(ALPHA,NTERMS,DET)
      IF (DET) 280,270,280
  270 CHISQR=0.
      GO TO 560
C
C Calculate coefficients, fit and Chi-square
C
  280 DO 300 J=1,NTERMS
      DO 290 K=1,NTERMS
  290 A(J)=A(J)+BETA(K)*ALPHA(J,K)
      DO 300 I=1,NPTS
```

```
  300 YFIT(I)=YFIT(I)+A(J)*P(I,J)
  310 CHISQ=0.
      DO 320 I=1,NPTS
  320 CHISQ=CHISQ+(Y(I)-YFIT(I))**2
      FREE=NPTS-NCOEFF
      CHISQR=CHISQ/FREE
C
C Test for end of fit
C
  330 IF (NTERMS-JMAX) 340,460,460
  340 IF (NCOEFF-2) 350,360,400
  350 IF (NEVEN ) 380,380,370
  360 IF (NEVEN) 370,380,370
  370 NTERMS=NTERMS+2
      GO TO 390
  380 NTERMS=NTERMS+1
  390 NCOEFF=NCOEFF+1
      CHISQ1=CHISQ
      GO TO 120
  400 FVALUE=(CHISQ1-CHISQ)/CHISQR
      IF (FTEST(NTERMS)-FVALUE)  360,410,410
  410 IF (NEVEN) 420,430,420
  420 NTERMS=NTERMS-2
      GO TO 440
  430 NTERMS=NTERMS-1
  440 NCOEFF=NCOEFF-1
      JMAX=NTERMS
  450 GO TO 120
C
C Calculate remainder of output
C
  460 IF (MODE) 470,480,470
  470 VARNCE=1.
      GO TO 490
  480 VARNCE=CHISQR
  490 DO 500 J=1,NTERMS
  500 SIGMAA(J)=DSQRT(VARNCE*ALPHA(J,J))
  510 IF (A(1)) 520,560,520
  520 DO 550 J=2,NTERMS
      IF (A(J)) 530,550,530
  530 B(J)=A(J)/A(1)
  540 SIGMAB(J)=B(J)*DSQRT((SIGMAA(J)/A(J))**2+(SIGMAA(1)/A(1))
     1          **2 -2.*VARNCE*ALPHA(J,1)/(A(J)*A(1)))
  550 CONTINUE
      B(1)=1.
```

```
  560 RETURN
      END
C ***************************************************
C
C Matrix inversion subroutine
C
C ***************************************************
      SUBROUTINE MATINV(ARRAY, NORDER, DET)
      IMPLICIT DOUBLE PRECISION (A-H,O-Z)
      DIMENSION ARRAY(7,7), IK(7), JK(7)
   10 DET = 1.
   20 DO 250 K=1, NORDER
C
C Find largest element ARRAY(I,J) in rest of matrix
C
      AMAX = 0.
   30 DO 60 I=K, NORDER
      DO 60 J=K, NORDER
   40 IF (DABS(AMAX) - DABS(ARRAY(I,J))) 50,50,60
   50 AMAX = ARRAY(I,J)
      IK(K) = I
      JK(K) = J
   60 CONTINUE
C
C Interchange rows and columns to put AMAX in ARRAY(K,K)
C
   70 IF (AMAX) 90,80,90
   80 DET = 0.
      GO TO 330
   90 I=IK(K)
      IF (I-K)  30,120,100
  100 DO 110 J=1, NORDER
      SAVE = ARRAY(K,J)
      ARRAY(K,J) = ARRAY(I,J)
  110 ARRAY(I,J) = -1.*SAVE
  120 J = JK(K)
      IF (J-K)  30,150,130
  130 DO 140 I=1, NORDER
      SAVE = ARRAY(I,K)
      ARRAY(I,K) = ARRAY(I,J)
  140 ARRAY(I,J) = -1. * SAVE
C
C Accumulate elements of inverse matrix
C
  150 DO 170 I=1, NORDER
```

```
      IF (I-K) 160,170,160
  160 ARRAY(I,K) = -1.* ARRAY(I,K) / AMAX
  170 CONTINUE
  180 DO 210 I=1, NORDER
      DO 210 J=1, NORDER
      IF (I-K) 190,210,190
  190 IF (J-K) 200,210,200
  200 ARRAY(I,J) = ARRAY(I,J) + ARRAY(I,K)*ARRAY(K,J)
  210 CONTINUE
  220 DO 240 J=1, NORDER
      IF (J-K) 230,240,230
  230 ARRAY(K,J) = ARRAY(K,J) / AMAX
  240 CONTINUE
      ARRAY(K,K) = 1. / AMAX
  250 DET = DET * AMAX
C
C Restore orderins of matrix
C
  260 DO 320 L=1, NORDER
      K=NORDER-L+1
      J=IK(K)
      IF (J-K) 290,290,270
  270 DO 280 I=1, NORDER
      SAVE = ARRAY(I,K)
      ARRAY(I,K) = -1.*ARRAY(I,J)
  280 ARRAY(I,J) = SAVE
  290 I=JK(K)
      IF (I-K) 320,320,300
  300 DO 310 J=1, NORDER
      SAVE = ARRAY(K,J)
      ARRAY(K,J) = -1.*ARRAY(I,J)
  310 ARRAY(I,J) = SAVE
  320 CONTINUE
  330 RETURN
      END
```

```
 10 ! ------------------------
 20 !
 30 ! TRNG+R
 40 ! Mike Hempstead
 50 ! September 1982
 60 !
 70 !    This program Hilbert
    transforms is into ir and
 80 ! then calculates the
    relative root-mean-square
    for the ir[0],ir[T] pair.
 90 !
100 ! ------------------------
110 CLEAR
120 ! Set in radian mode
130 RAD
140 ! Establish link for CHAIN
    command
150 OPTION BASE 1
160 COM N1,N2,T,T1,D(400,2)
170 ! Assign storage to r & ir
180 DIM R(400,2),U(400)
190 ! Prompt for tha datafile
200 DISP "Have you chained from
    another   program (Y/N)";
210 INPUT Q$
220 IF Q$="Y" THEN 290
230 DISP "What is the data filed
    under";
240 INPUT F$
250 ASSIGN# 1 TO F$
260 READ# 1 ; N1,N2,T,T1,D(,)
270 ASSIGN# 1 TO *
280 ! Calculate constant for ir
290 K=2/(PI*T)
300 ! Point dropping routine
310 DISP "How many points from t
    he begin- ning of the genera
    tion data are to be dropped"
    ;
320 INPUT N
330 G=N1-N
340 DISP "How many points from t
    he begin- ning of the recapt
    ure data are  to be dropped"
    ;
350 INPUT P
360 ! Prompt for output file
370 DISP "What is the output fil
    e to be named";
380 INPUT O$
390 CREATE O$,26
400 ASSIGN# 1 TO O$
410 ! Calculate the r array
420 FOR J=1 TO N1+N2
430 U(J)=D(J,1)-T1
440 NEXT J
450 ! Perform transform
460 CLEAR @ DISP "Transform is b
    eing calculated."
```

```
470 FOR M=N1+1+P TO N1+N2
480 ! Initialize sums
490 S1,S2=0
500 FOR J=1 TO G-1
510 L=J+N
520 A1=-U(L)
530 A2=-U(L+1)
540 IF J=1 THEN A1=T1
550 IF J=G-1 THEN A2=0
560 T2=U(M)
570 X=D(L+1,2)-D(L,2)
580 Y=X*T2+D(L,2)*U(L+1)-D(L+1,2
    )*U(L)
590 Z=(SQR(A2)-SQR(A1))/SQR(T2)-
    ATN(SQR(A2/T2))+ATN(SQR(A1/T
    2))
600 S1=S1+X*(A1^1.5-A2^1.5)
610 S2=S2+Y*Z
620 NEXT J
630 R(M,1)=D(M,1)
640 R(M,2)=K*(S1/(3*SQR(T2))+S2)
650 NEXT M
660 ! Fill remaining recapture
    array with zeroes
670 FOR J=1 TO N1+P
680 R(J,1),R(J,2)=0
690 NEXT J
700 ! Calculate root-mean-square
    @ array pointer
710 P1=N1+P+1
720 F=0
730 FOR J=P1 TO N1+N2
740 F=F+((D(J,2)-R(J,2))/D(J,2))
    ^2
750 NEXT J
760 F=SQR(F/(N2-P))
770 PRINT "relative"
780 PRINT USING 790 ; F
790 IMAGE "root-mean-square = ",
    D.3DE,"µA",2/
800 PRINT# 1 ; F,P1,R(,)
810 ASSIGN# 1 TO *
820 ! Output a representative
    sample
830 PRINT "  #     ir[T]µA
    ir[D]µA"
840 FOR J=N1+P+1 TO N1+N2 STEP 1
    0
850 PRINT USING 860 ; J,R(J,2),D
    (J,2)
860 IMAGE DDD,2(1X,MD.5DE)
870 NEXT J
880 CLEAR
890 END
```

```
 10 ! DSCHEM
 20 !
 30 ! DOUBLE STEP EXPERIMENT
 40 !
 50 OPTION BASE 1
 60 OUTPUT 709 ;"S01AC1VT4VR2AF1
    AL1"
 70 CLEAR
 80 DIM X$[5210],V$[5210],Z$[521
    0]
 90 COM N1,N2,T,T1,D(400,2)
100 !
110 DISP ""
120 DISP "SET PAR TO AN INITIAL
    POTENTIAL OF -1.000V AND DEP
    RESS THE       INITIAL KEY "
130 DISP ""
140 DISP ""
150 DISP "How many points in gen
    eration   and how many in re
    capture (max  total points 4
    00)";
160 INPUT N1,N2
170 DISP "Time between readings
    (minimum  140mS)?   Current
    range? (T,R)"
180 INPUT T,R
190 ! Divide R by 10 since the
      output of the PAR is 10V
      full scale
200 R=R/10
210 DISP "Generation potential (
    mV)";
220 INPUT V1@ V1=V1+1000
230 DISP "Recapture potential (m
    V)";
240 INPUT V2@ V2=V2+1000
250 DISP "What is the initial po
    tential   ie before the firs
    t step (mV)";
260 INPUT V@ V=V+1000
270 B$="A02,1,"&VAL$(V)
280 OUTPUT 709 ;B$
290 DISP "Please wait.  I'm work
    ing!"
300 !
310 IOBUFFER V$ @ IOBUFFER Z$
320 X$=""
330 FOR J=1 TO N1+N2
340 IF J<=N1 THEN V=V1 ELSE V=V2
350 B$="A02,1,"&VAL$(V)
360 B=10-LEN(B$)
370 IF B=0 THEN 410
380 FOR K=1 TO B
390 B$=B$&" "
400 NEXT K
410 X$=X$&B$
420 NEXT J
430 OUTPUT V$ USING "#,K" ; X$
440 P1=10
```

```
450 X=LEN(X$)
460 BEEP 100,100 @ BEEP 100,100
470 CLEAR
480 DISP "Switch from dummy cell
    to        external cell."
490 DISP "Hit endline when you w
    ant the   experiment to star
    t."
500 INPUT D$
510 ON TIMER# 1,T GOTO 540
520 CONTROL V$,1 ; P1
530 GOTO 530
540 TRANSFER V$ TO 709 FHS @ TRI
    GGER 709
550 TRANSFER 709 TO Z$ FHS ; EOI
560 IF P1>=X THEN 600
570 CONTROL V$,0 ; P1+1
580 P1=P1+10
590 GOTO 520
600 OFF TIMER# 1 @ CLEAR
610 DISP "Switch the cell off si
    nce the   potential will rev
    ert to -1V."
620 DISP "Hit endline when ready
    ." @ INPUT D$
630 CLEAR 709 @ OUTPUT 709 ;"TD"
     @ LOCAL 709
640 ENTER Z$ USING "#,#K" , X$
650 !
660 ! Unpacking routine
670 !
680 B=1
690 FOR J=1 TO N1+N2
700 K=B
710 IF K=LEN(X$)+1 OR X$[K,K]="↑
    " THEN 740
720 K=K+1
730 GOTO 710
740 E=K-1
750 D(J,2)=VAL(X$[B,E])*R
760 D(J,1)=((J-1)*T+20)/1000
770 B=E+2
780 DISP "I(";D(J,1);"ms)=";D(J,
    2);"μA"
790 NEXT J
800 DISP "Do you want to file th
    e data?   If so enter Y,file
    name.  If not enter N."
810 INPUT Q$,F$@ IF Q$="Y" AND F
    $="" THEN 800
820 IF Q$#"Y" AND Q$#"N" THEN 80
    0
830 IF Q$="N" THEN 890
840 CREATE F$,26
850 ASSIGN# 1 TO F$
860 T=T/1000 @ T1=N1*T
870 PRINT# 1 ; N1,N2,T,T1,D(,)
880 ASSIGN# 1 TO *
890 DISP "Do you want to Hilbert
     transformthe generation dat
    a";
```

```
900 INPUT Q1$@ IF Q1$#"Y" AND Q1
    $#"N" THEN 890
910 IF Q1$="N" THEN 930
920 CHAIN "TRNG+R"
930 CLEAR @ DISP "Finished"
940 END
```

```
 10 ! RSCHEN
 20 !
 30 ! RAMP&STEP EXPERIMENT
 40 ! This program assumes that
      you have a negative going
      ramp and that you step
 50 ! back to the initial
      potential
 60 !
 70 !
 80 OPTION BASE 1
 90 OUTPUT 709 ;"S01AC1VT4VR3A02
    ,1,0AF1AL1001,0"
100 CLEAR
110 DIM X$[5210],V$[4010],Z$[521
    0]
120 ! X$=data string
130 ! V$=buffer of data to send
          to the D/A
140 ! Z$=buffer of data from
          voltmeter
150 !
160 COM N1,N2,T,T1,D(400,2)
170 ! N1=# of generation points
180 ! N2=# in recapture
190 ! T =Time between readings
        in ms changed to s
200 ! T1=Time of step or
        recapture
210 ! D(,)=Array of data points
220 !
230 ! R =Current range (uA)
240 !   =R/10
250 !
260 DISP "Note that the number o
    f points  in the generation
    phase times"
270 DISP "the time between readi
    ngs shouldbe less than the t
    ime for the   ramp."
280 DISP " "
290 DISP "How many points in gen
    eration   and how many in re
    capture (max  total points 4
    00)";
300 INPUT N1,N2
310 DISP "Time between readings
    (>140ms)? Current range (uA)
    ? (T,R)"
320 INPUT T,R
330 ! Divide R by 10 since
      output of PAR is 10V full
      scale
340 R=R/10
350 V1=0
360 DISP "What is the difference
     between  the initial and fi
    nal potentialsin +mV";
370 INPUT V2
380 DISP "Please wait.  I'm work
    ing!"
```

```
390 !
400 IOBUFFER V$ @ IOBUFFER Z$
410 !
420 ! Create buffer of data for
      the D/A
430 X$=""
440 FOR J=1 TO N1+N2
450 IF J<=N1 THEN V=V1 ELSE V=V2
460 B$="A02,1,"&VAL$(V)
470 B=10-LEN(B$)
480 IF B=0 THEN 520
490 FOR K=1 TO B
500 B$=B$&" "
510 NEXT K
520 X$=X$&B$
530 NEXT J
540 OUTPUT V$ USING "#,K" ; X$
550 !
560 P1=10
570 X=LEN(X$)
580 BEEP 100,100 @ BEEP 100,100
    @ DISP "Hit endline to start
     experiment"
590 INPUT D$
600 OUTPUT 709 ;"OC1,0" @ ON TIM
    ER# 1,T GOTO 630
610 CONTROL V$,1 ; P1
620 GOTO 620
630 TRANSFER V$ TO 709 FHS @ TRI
    GGER 709
640 TRANSFER 709 TO Z$ FHS ; EOI
650 IF P1>=X THEN 690
660 CONTROL V$,0 ; P1+1
670 P1=P1+10
680 GOTO 610
690 OFF TIMER# 1 @ CLEAR
700 DISP "Switch the cell off  H
    it endlinewhen you are ready
    "
710 INPUT D$
720 CLEAR 709 @ OUTPUT 709 ;"TO"
     @ LOCAL 709
730 ENTER Z$ USING "#,#K" ; X$
740 !
750 ! Unpacking routine
760 !
770 B=1
780 FOR J=1 TO N1+N2
790 K=B
800 IF K=LEN(X$)+1 OR X$[K,K]="↑
    " THEN 830
810 K=K+1
820 GOTO 800
830 E=K-1
840 D(J,2)=VAL(X$[B,E])*R
850 D(J,1)=((J-1)*T+20)/1000
860 B=E+2
870 DISP "I(";D(J,1);"s)=";D(J,2
    );"uA"
880 NEXT J
```

```
890 DISP "Do you want to file th
    e data?   If so enter Y,file
    name.  If not enter N."
900 INPUT Q$,F$@ IF Q$="Y" AND F
    $="" THEN 890
910 IF Q$#"Y" AND Q$#"N" THEN 89
    0
930 IF Q$="N" THEN 980
930 CREATE F$,26
940 ASSIGN# 1 TO F$
950 T=T/1000 @ T1=N1*T
960 PRINT# 1 ; N1,N2,T,T1,D(,)
970 ASSIGN# 1 TO *
980 DISP "Do you want to Hilbert
     transformthe generation dat
    a";
990 INPUT Q1$@ IF Q1$#"Y" AND Q1
    $#"N" THEN 980
1000 IF Q1$="N" THEN 1020
1010 CHAIN "TRNG+R"
1020 END
```

APPENDIX D

It was necessary to calibrate the timing of the interfaced instruments before experimentation could begin. There were two times of particular interest:

i) the shortest interval between data points that could be controlled reproducibly by the program

and ii) the inherent offset between the imposition of the potential waveform and the sampling of the first data point.

The rate of data sampling was limited by the time required to perform a loop within the program. External to this loop there was a BASIC command

ON TIMER#1, T (D.1)

which controlled the rate of sampling. The time parameter, T, was varied until it was shorter than the time required to perform the data sampling commands. This threshold was detected quite easily by the onset of a variety of errors in program execution. The time parameter was then increased gradually until these errors desisted. This yielded a sampling time of 140 ms.

The inherent offset was determined by another calibration technique. This method used the TRIGGER command which increments the sampling channel on the HP3497A and then signals the voltmeter to take a reading. It was assumed that the voltmeter integration period began immediately after the channel was closed. The

HP3497A was manually set to output zero volts and then, under program control, the voltage was changed to some positive value. The new voltage was used to trigger a Tektronix 5103N Oscilloscope System so that the duration of the channel-closed-pulse could be monitored. The time that was measured was approximately 11½ ms. The time for the integration period was calculated from information in the HP3497A manual and was determined to be 16 ms. Therefore, if the calibration is taken to the middle of the integration period, then the offset is about 20 ms (for measurements of 5½ digit accuracy).

The program "RSCHEM" was executed for a ramp of 98.6 mv/s and a step of 5 mV as a means of testing the calibration. The step was applied near the beginning of the ramp and the output was displayed on the oscilloscope. The time between the imposition of the step and the current value obtained by the HP3497A was 20 ms to 21 ms for 5½ digit accuracy. The offset was therefore assigned the value 20 ms.

APPENDIX E

Part I

The evaluation of

$$h_{2(\rho-1)}(g) = (1+g)^{\rho-1}(1-g)^{\frac{1}{2}} \tag{EI.1}$$

and

$$f_{2(\rho-1)}(r) = -\frac{2^{\rho-\frac{1}{2}}\Gamma(\rho)}{(r-1)\pi^{\frac{1}{2}}\Gamma(\rho+3/2)}\,{}_2F_1\left[1,3/2;\rho+3/2;-\frac{2}{r-1}\right] \tag{EI.2}$$

will be provided for $\rho\varepsilon\{1/2,1,3/2,2,5/2\}$. The evaluation of equation (EI.1) is straightforward and the results are summarized in Table EI.2. The evaluation of equation (EI.2), however, is more difficult. Equation (EI.2) may be rewritten as

$$f_{2(\rho-1)}(r) = K_{2(\rho-1)}(r)\ X\ {}_2F_1\left[1,3/2;\rho+3/2;-\frac{2}{r-1}\right] \tag{EI.3}$$

in which the functionality of $K_{2(\rho-1)}(r)$ may be determined from elementary properties of the gamma function. The $K_{2(\rho-1)}(r)$ functions are summarized in Table EI.1. The evaluation of the Gauss hypergeometric functions is somewhat more laborious and therefore will be presented in more detail.

ρ	1/2	1	3/2	2	5/2
$-K_{2(\rho-1)}(r)$	$\frac{1}{r-1}$	$\frac{4(2)^{\frac{1}{2}}}{3\pi(r-1)}$	$\frac{1}{2(r-1)}$	$\frac{16(2)^{\frac{1}{2}}}{15\pi(r-1)}$	$\frac{1}{2(r-1)}$

Table EI.1 Functionality of $K_{2(\rho-1)}(r)$.

$\rho=\frac{1}{2}$

The function ${}_2F_1\left(1,\frac{3}{2};2;-\frac{2}{r-1}\right)$ may be determined by a simple relationship[1] which yields

$$ {}_2F_1\left(1,\tfrac{3}{2};2;-\frac{2}{r-1}\right) = \frac{2(r-1)}{(r^2-1)^{\frac{1}{2}}+r+1} \qquad \text{(EI.4)} $$

$\rho=1$

The evaluation of ${}_2F_1\left(1,\frac{3}{2};\frac{5}{2};-\frac{2}{r-1}\right)$ is a little more difficult. It requires the use of the recurrence formula[2]

$$ \tfrac{3}{2}(r+1){}_2F_1\left(1,\tfrac{3}{2};\tfrac{3}{2};-\frac{2}{r-1}\right) - \tfrac{3}{2}(r-1){}_2F_1\left(1,\tfrac{1}{2};\tfrac{3}{2};-\frac{2}{r-1}\right) - {}_2F_1\left(1,\tfrac{3}{2};\tfrac{5}{2};-\frac{2}{r-1}\right) = 0 \qquad \text{(EI.5)} $$

and a knowledge of the functions ${}_2F_1\left(1,\frac{3}{2};\frac{3}{2};-\frac{2}{r-1}\right)$ and ${}_2F_1\left(1,\frac{1}{2};\frac{3}{2};-\frac{2}{r-1}\right)$. The first of these functions may be shown[3] to be

$$ {}_2F_1\left(1,\tfrac{3}{2};\tfrac{3}{2};-\frac{2}{r-1}\right) = \left(\frac{r-1}{r+1}\right) \qquad \text{(EI.6)} $$

and the second is given[4] by

$$ {}_2F_1\left(1,\tfrac{1}{2};\tfrac{3}{2};-\frac{2}{r-1}\right) = \left(\frac{r-1}{2}\right)^{\frac{1}{2}} \arctan\left(\frac{2}{r-1}\right)^{\frac{1}{2}} \qquad \text{(EI.7)} $$

Therefore it can be shown that

$$ {}_2F_1\left(1,\tfrac{3}{2};\tfrac{5}{2};-\frac{2}{r-1}\right) = \frac{3(r-1)}{2}\left\{1 - \left(\frac{r-1}{2}\right)^{\frac{1}{2}} \arctan\left(\frac{2}{r-1}\right)^{\frac{1}{2}}\right\} \qquad \text{(EI.8)} $$

which can be verified for r=3 by the expression[5]

$$ {}_2F_1(1,\tfrac{3}{2};\tfrac{5}{2};-1) = \tfrac{3}{4}[\psi(\tfrac{5}{4}) - \psi(\tfrac{3}{4})] \qquad \text{(EI.9)} $$

where ψ is the digamma function.

$\rho=3/2$

The function ${}_2F_1\left(1,3/2;3;-\frac{2}{r-1}\right)$ is also desribed by a simple relationship[6] which establishes that

$$ {}_2F_1\left(1,3/2;3;-\frac{2}{r-1}\right) = 2(r-1)\{r - (r^2-1)^{1/2}\} \qquad \text{(EI.10)} $$

This expression may be verified for r=-1 by the relationship[7]

$$ {}_2F_1(a,b;c;1) = \frac{\Gamma(c)\Gamma(c-a-b)}{\Gamma(c-a)\Gamma(c-b)} \qquad \text{(EI.11)} $$

$\rho=2$

The determination of ${}_2F_1\left(1,3/2;7/2;-\frac{2}{r-1}\right)$ requires another recurrence formula[8] which can be expressed as

$$ -5/4(r+1){}_2F_1\left(1,3/2;3/2;-\frac{2}{r-1}\right) + 5/4(r+1){}_2F_1\left(1,3/2;5/2;-\frac{2}{r-1}\right) - {}_2F_1\left(1,3/2;7/2;-\frac{2}{r-1}\right) = 0 \qquad \text{(EI.12)} $$

It then follows from previously determined functions that

$$ {}_2F_1\left(1,3/2;7/2;-\frac{2}{r-1}\right) = \frac{5(r-1)}{4}\left\{\frac{3(r+1)}{2}\left[1 - \left(\frac{r-1}{2}\right)^{1/2}\arctan\left(\frac{2}{r-1}\right)^{1/2}\right] - 1\right\} \qquad \text{(EI.13)} $$

$\rho=5/2$

The general recurrence formula[8] for equation (EI.12) may also be manipulated into the form

$$ -(r+1){}_2F_1\left(1,3/2;2;-\frac{2}{r-1}\right) + 3/2(2r+3){}_2F_1\left(1,3/2;3;-\frac{2}{r-1}\right) - {}_2F_1\left(1,3/2;4;-\frac{2}{r-1}\right) = 0 \qquad \text{(EI.14)} $$

It may then be shown that

$$ {}_2F_1\left[1, 3/2; 4; -\frac{2}{r-1}\right] = (r-1)\{2(r+1)[r - (r^2-1)^{1/2}] - 1\} \qquad \text{(EI.15)} $$

which can be verified for r=-1 by equation (EI.11)

The functions $f_{2(\rho-1)}(r)$ may now be determined from equation (EI.3). These functions, along with the corresponding $h_{2(\rho-1)}(g)$ functions, are summarized in Table EI.2.

ρ	$h_{2(\rho-1)}(g)$	$f_{2(\rho-1)}(r)$
1/2	$\left(\frac{1-g}{1+g}\right)^{1/2}$	$-\left\{1 - \left(\frac{r-1}{r+1}\right)^{1/2}\right\}$
1	$(1-g)^{1/2}$	$-\frac{(2)^{3/2}}{\pi}\left\{1 - \left(\frac{r-1}{2}\right)^{1/2}\arctan\left(\frac{2}{r-1}\right)^{1/2}\right\}$
3/2	$(1-g^2)^{1/2}$	$-\{r - (r^2-1)^{1/2}\}$
2	$(1+g)(1-g)^{1/2}$	$-\frac{(2)^{3/2}(r+1)}{\pi}\left\{1 - \left(\frac{r-1}{2}\right)^{1/2}\arctan\left(\frac{2}{r-1}\right)^{1/2}\right\} + \frac{4(2)^{1/2}}{3\pi}$
5/2	$(1+g)(1-g^2)^{1/2}$	$-\{(r+1)[r - (r^2-1)^{1/2}] - 1/2\}$

Table EI.2 Functional forms of the fitting functions described by equations (EI.1) and (EI.2).

Part II

The functional forms of $P_n^{(\frac{1}{2},0)}(g)$ and $Q_n^{(\frac{1}{2},0)}(r)$ were established for $0 \leq n \leq 6$. The determination of $P_n^{(\frac{1}{2},0)}(g)$ was aided by an appropriate table[9] and is summarized in Table EII.1. All of these functions were tested with the orthogonality relationship

$$\int_{-1}^{1} (1-g)^{\frac{1}{2}} P_0^{(\frac{1}{2},0)}(g) P_n^{(\frac{1}{2},0)}(g)\, dg = 0 \quad , n \neq 0 \qquad \text{(EII.1)}$$

to check their validity. The determination of the $Q_n^{(\frac{1}{2},0)}(r)$ functions could not be performed as simply. It relied heavily on relationships that are given in chapter 2.

n	$P_n^{(\frac{1}{2},0)}(g)$
0	1
1	$(\frac{1}{4})(5g+1)$
2	$(\frac{1}{32})(63g^2+14g-17)$
3	$(\frac{1}{128})(429g^3+99g^2-225g-23)$
4	$(\frac{1}{2048})(12155g^4+2860g^3-9438g^2-1364g+827)$
5	$(\frac{1}{8192})(88179g^5+20995g^4-90610g^3-15210g^2+17615g+1207)$
6	$(\frac{1}{65536})(1300075g^6+312018g^5-1661835g^4-303620g^3+512805g^2+54930g-22181)$

Table EII.1 Functionality of $P_n^{(\frac{1}{2},0)}(g)$ for $0 \leq n \leq 6$.

n=0

The function $Q_0^{(\frac{1}{2},0)}(r)$ may be obtained from equation (2.34). This relationship establishes that

$$Q_0^{(\frac{1}{2},0)}(r) = \frac{(2)^{3/2}}{3}(r-1)^{-3/2}\ {}_2F_1\left(1,\tfrac{3}{2};\tfrac{5}{2};-\frac{2}{r-1}\right) \qquad \text{(EII.2)}$$

This expression may be simplified by substitution from equation (EI.8) to yield

$$Q_0^{(\frac{1}{2},0)}(r) = \left(\frac{2}{r-1}\right)^{\frac{1}{2}} - \arctan\left(\frac{2}{r-1}\right)^{\frac{1}{2}} \qquad \text{(EII.3)}$$

n=1

It may be shown with the aid of equation (2.35) that

$$Q_1^{(\frac{1}{2},0)}(r) = P_1^{(\frac{1}{2},0)}(r)Q_0^{(\frac{1}{2},0)}(r) - \frac{5}{6}\left(\frac{2}{r-1}\right)^{\frac{1}{2}} \qquad \text{(EII.4)}$$

where $P_1^{(\frac{1}{2},0)}(r)$ may be obtained from Table EII.1 and $Q_0^{(\frac{1}{2},0)}(r)$ is given immediately above.

$2 \leq n \leq 6$

Equation (2.36) dictates that

$$Q_n^{(\frac{1}{2},0)}(r) = P_n^{(\frac{1}{2},0)}(r)Q_0^{(\frac{1}{2},0)}(r) - q_n^{(\frac{1}{2},0)}(r) \qquad \text{(EII.5)}$$

which upon application to equations (EII.3) and (EII.4) yields

$$q_0^{(\frac{1}{2},0)}(r) = 0 \qquad \text{(EII.6)}$$

and

$$q_1^{(\frac{1}{2},0)}(r) = \frac{5}{6}\left(\frac{2}{r-1}\right)^{\frac{1}{2}} \qquad \text{(EII.7)}$$

It follows from the recurrence formula (2.29) that

$$n(2n+1)(4n-3)q_n^{(\frac{1}{2},0)}(r)$$
$$= \tfrac{1}{4}(4n-1)\{(4n+1)(4n-3)r + 1\}q_{n-1}^{(\frac{1}{2},0)}(r)$$
$$- (n-1)(2n-1)(4n+1)q_{n-2}^{(\frac{1}{2},0)}(r) \quad , \; n=2,3,4,\cdots \qquad \text{(EII.8)}$$

which enables higher order $q_n^{(\frac{1}{2},0)}(r)$ functions to be calculated. Hence the remaining $Q_n^{(\frac{1}{2},0)}(r)$ functions are given by

$$Q_2^{(\frac{1}{2},0)}(r) = P_2^{(\frac{1}{2},0)}(r)Q_0^{(\frac{1}{2},0)}(r) - \left(\frac{7}{240}\right)(45r+1)\left(\frac{2}{r-1}\right)^{\frac{1}{2}} \qquad \text{(EII.9)}$$

$$Q_3^{(\frac{1}{2},0)}(r) = P_3^{(\frac{1}{2},0)}(r)Q_0^{(\frac{1}{2},0)}(r) - \left(\frac{1}{2240}\right)(5005r^2+154r-1283)\left(\frac{2}{r-1}\right)^{\frac{1}{2}} \qquad \text{(EII.10)}$$

$$Q_4^{(\frac{1}{2},0)}(r) = P_4^{(\frac{1}{2},0)}(r)Q_0^{(\frac{1}{2},0)}(r) - \left(\frac{11}{322560}\right)(116025r^3+4095r^2-59085r-787)\left(\frac{2}{r-1}\right)^{\frac{1}{2}} \qquad \text{(EII.11)}$$

$$Q_5^{(\frac{1}{2},0)}(r) = P_5^{(\frac{1}{2},0)}(r)Q_0^{(\frac{1}{2},0)}(r) - \left(\frac{1}{935}\right)\left\{\left(\frac{19}{4}\right)(357r+1)q_4^{(\frac{1}{2},0)}(r) - 756q_3^{(\frac{1}{2},0)}(r)\right\} \qquad \text{(EII.12)}$$

$$Q_6^{(\frac{1}{2},0)}(r) = P_6^{(\frac{1}{2},0)}(r)Q_0^{(\frac{1}{2},0)}(r) - \left(\frac{1}{1638}\right)\left\{\left(\frac{23}{4}\right)(525r+1)q_5^{(\frac{1}{2},0)}(r) - 1375q_4^{(\frac{1}{2},0)}(r)\right\} \qquad \text{(EII.13)}$$

where the expressions for $q_5^{(\frac{1}{2},0)}(r)$ and $q_6^{(\frac{1}{2},0)}(r)$ were left in the form of the recurrence formula because the coefficients for the embedded polynomial became too large to be handled conveniently.

APPENDIX F

This appendix lists fits for a number of datafiles which are described in chapter 8. The coefficients of the fits and their standard deviations are provided. The quality of the fit may be judged by the magnitude of the reduced chi-square or by comparing the approximation given by the fit to the raw data that is listed.

FITS 1103
This file lists the fit for S-1T03
The corresponding fitting function data is given in GUS

Coefficients	S.D. Aj
A(-1)= 9.990499215E-01	7.68354877E-02
A(0)= 1.050347316E+00	6.64593378E-01
A(1)= 9.875488028E-01	1.508223668E+00
A(2)= 1.010528856E+00	1.299426348E+00
A(3)= 9.969940192E-01	3.742644948E-01

The value of Chi square is 8.24634419E-12

Data generated by fit

r	ir	fit
1.10	-3.618933908E+00	-3.618932334E+00
1.20	-3.044602505E+00	-3.044597752E+00
1.30	-2.676217170E+00	-2.676186966E+00
1.40	-2.406649338E+00	-2.406649396E+00
1.50	-2.197187160E+00	-2.196187416E+00
1.60	-2.025139760E+00	-2.025155706E+00
1.70	-1.882307676E+00	-1.882303986E+00
1.80	-1.760561606E+00	-1.760558116E+00
1.90	-1.655174906E+00	-1.655171686E+00
2.00	-1.562807106E+00	-1.562803996E+00
2.10	-1.481013136E+00	-1.481015436E+00
2.20	-1.407974106E+00	-1.407971326E+00
2.30	-1.342261206E+00	-1.342258486E+00
2.40	-1.282769106E+00	-1.282766486E+00
2.50	-1.228610406E+00	-1.228607936E+00
2.60	-1.179065706E+00	-1.179063326E+00
2.70	-1.133544106E+00	-1.133541866E+00
2.80	-1.091055306E+00	-1.091053096E+00
2.90	-1.052088006E+00	-1.052085836E+00
3.00	-1.016594406E+00	-1.016592336E+00
3.10	-9.829781906E-01	-9.829762006E-01
3.20	-9.515849506E-01	-9.515830226E-01
3.30	-9.221948306E-01	-9.221929616E-01
3.40	-8.946168406E-01	-8.946150266E-01
3.50	-8.686840806E-01	-8.686823186E-01
3.60	-8.442500006E-01	-8.442482876E-01
3.70	-8.211853406E-01	-8.211836736E-01
3.80	-7.993755906E-01	-7.993739676E-01
3.90	-7.787189506E-01	-7.787173686E-01
4.00	-7.591244806E-01	-7.591229386E-01
4.10	-7.405108106E-01	-7.405093056E-01
4.20	-7.228047306E-01	-7.228032616E-01
4.30	-7.059403406E-01	-7.059389056E-01
4.40	-6.898580006E-01	-6.898565976E-01
4.50	-6.745037206E-01	-6.745023486E-01
4.60	-6.598284206E-01	-6.598270776E-01
4.70	-6.457873706E-01	-6.457860566E-01
4.80	-6.323397706E-01	-6.323384836E-01
4.90	-6.194482706E-01	-6.194470076E-01
5.00	-6.070786206E-01	-6.070773896E-01

FIT:4S-1T03
This file lists the fit for 4S-1T03
The corresponding Gauss hypergeometric function data is given in GUS

Coefficents	S.D. AJ
A(-1)= -1.36751137E+01	7.15075974E+00
A(0)= 1.27593246E+02	6.18537069E+01
A(1)= -2.85560303E+02	1.40375067E+02
A(2)= 2.45408813E+02	1.20015022E+02
A(3)= -6.97824402E+01	3.48356340E+01

The value of Chi-square is 7.12765646E-08

Data generated by fit

r	ir	fit
1.10	-3.61900000E+00	-3.61946474E+00
1.20	-3.04500000E+00	-3.04531683E+00
1.30	-2.67600000E+00	-2.67661538E+00
1.40	-2.40700000E+00	-2.40690052E+00
1.50	-2.19600000E+00	-2.19636504E+00
1.60	-2.02500000E+00	-2.02531912E+00
1.70	-1.88200000E+00	-1.88248202E+00
1.80	-1.76100000E+00	-1.76076201E+00
1.90	-1.65500000E+00	-1.65540333E+00
2.00	-1.56300000E+00	-1.56306065E+00
2.10	-1.48100000E+00	-1.48129226E+00
2.20	-1.40800000E+00	-1.40826289E+00
2.30	-1.34200000E+00	-1.34255947E+00
2.40	-1.28300000E+00	-1.28307206E+00
2.50	-1.22900000E+00	-1.22891386E+00
2.60	-1.17900000E+00	-1.17936601E+00
2.70	-1.13400000E+00	-1.13383835E+00
2.80	-1.09200000E+00	-1.09184098E+00
2.90	-1.05300000E+00	-1.05296319E+00
3.00	-1.01700000E+00	-1.01685768E+00
3.10	-9.83000000E-01	-9.83228406E-01
3.20	-9.51600000E-01	-9.51821257E-01
3.30	-9.22200000E-01	-9.22416675E-01
3.40	-8.94600000E-01	-8.94823851E-01
3.50	-8.68700000E-01	-8.68876066E-01
3.60	-8.44200000E-01	-8.44426916E-01
3.70	-8.21200000E-01	-8.21347256E-01
3.80	-7.99400000E-01	-7.99522672E-01
3.90	-7.78700000E-01	-7.78851404E-01
4.00	-7.59100000E-01	-7.59242613E-01
4.10	-7.40500000E-01	-7.40614925E-01
4.20	-7.22800000E-01	-7.22895215E-01
4.30	-7.05900000E-01	-7.06017565E-01
4.40	-6.89900000E-01	-6.89922391E-01
4.50	-6.74500000E-01	-6.74555682E-01
4.60	-6.59800000E-01	-6.59868360E-01
4.70	-6.45800000E-01	-6.45815719E-01
4.80	-6.32300000E-01	-6.32356942E-01
4.90	-6.19400000E-01	-6.19454683E-01
5.00	-6.07100000E-01	-6.07074704E-01

This file lists the fit for Q0706
The corresponding fitting function data is given in JACOBI7

Coefficents		S.D. AJ
A(0)=	1.00006890E+00	2.18183234E-04
A(1)=	9.97609768E-01	6.80553540E-03
A(2)=	1.02600181E+00	4.96717092E-03
A(3)=	8.71525764E-01	3.34669250E-01
A(4)=	1.31707859E+00	8.25648609E-01
A(5)=	6.18991852E-01	1.01121393E+00
A(6)=	1.17741394E+00	4.84209905E-01

The value of Chi-square is 7.19243975E-12

Data generated by fit

r	ir	fit
1.10	5.96055700E+00	5.96054262E+00
1.20	3.12769600E+00	3.12769143E+00
1.30	2.09382250E+00	2.09382020E+00
1.40	1.55718990E+00	1.55718877E+00
1.50	1.22918130E+00	1.22918089E+00
1.60	1.00847530E+00	1.00847562E+00
1.70	8.50218530E-01	8.50217356E-01
1.80	7.31471120E-01	7.31470352E-01
1.90	6.39283720E-01	6.39283450E-01
2.00	5.65790710E-01	5.65790621E-01
2.10	5.05939600E-01	5.05939668E-01
2.20	4.56338350E-01	4.56338549E-01
2.30	4.14626120E-01	4.14626281E-01
2.40	3.79109440E-01	3.79109627E-01
2.50	3.48543410E-01	3.48543478E-01
2.60	3.21991740E-01	3.21991820E-01
2.70	2.98738120E-01	2.98738190E-01
2.80	2.78225000E-01	2.78224994E-01
2.90	2.60012090E-01	2.60011977E-01
3.00	2.43747170E-01	2.43747128E-01
3.10	2.29145770E-01	2.29145705E-01
3.20	2.15975220E-01	2.15975049E-01
3.30	2.04043450E-01	2.04043234E-01
3.40	1.93190690E-01	1.93190617E-01
3.50	1.83283630E-01	1.83283394E-01
3.60	1.74208640E-01	1.74208578E-01
3.70	1.65870250E-01	1.65870171E-01
3.80	1.58186140E-01	1.58186092E-01
3.90	1.51085910E-01	1.51085795E-01
4.00	1.44508360E-01	1.44508299E-01
4.10	1.38400730E-01	1.38400657E-01
4.20	1.32716770E-01	1.32716698E-01
4.30	1.27416010E-01	1.27415965E-01
4.40	1.22462810E-01	1.22462872E-01
4.50	1.17826040E-01	1.17826032E-01
4.60	1.13477470E-01	1.13477604E-01
4.70	1.09392760E-01	1.09392867E-01
4.80	1.05549750E-01	1.05549784E-01
4.90	1.01928410E-01	1.01928630E-01
5.00	9.85115770E-02	9.85117296E-02

FIT400T06

This file lists the fit for 400T06

The corresponding fitting function data is given in J. GRI7

Coefficents		S.D. nJ
A(0)=	1.01482713E+00	5.42047941E-03
A(1)=	4.98494446E-01	1.69074703E-01
A(2)=	6.48452216E+00	1.73090322E+00
A(3)=	-2.67190151E+01	8.31469803E+00
A(4)=	7.18052950E+01	2.05121486E+01
A(5)=	-8.75539408E+01	2.51222984E+01
A(6)=	4.40299950E+01	1.20791315E+01

The value of Chi-square is 4.43307053E-09

Data generated by fit

r	ir	fit
1.10	5.96100000E+00	5.96098657E+00
1.20	3.12800000E+00	3.12800462E+00
1.30	2.09400000E+00	2.09396312E+00
1.40	1.55700000E+00	1.55703273E+00
1.50	1.22900000E+00	1.22893304E+00
1.60	1.00800000E+00	1.00825477E+00
1.70	8.50200000E-01	8.50061109E-01
1.80	7.31500000E-01	7.31377626E-01
1.90	6.39300000E-01	6.39239741E-01
2.00	5.65800000E-01	5.65779506E-01
2.10	5.05900000E-01	5.05947187E-01
2.20	4.56300000E-01	4.56354272E-01
2.30	4.14600000E-01	4.14643075E-01
2.40	3.79100000E-01	3.79123100E-01
2.50	3.48500000E-01	3.48551058E-01
2.60	3.22000000E-01	3.21992524E-01
2.70	2.98700000E-01	2.98731929E-01
2.80	2.78200000E-01	2.78212288E-01
2.90	2.60000000E-01	2.59993703E-01
3.00	2.43700000E-01	2.43724350E-01
3.10	2.29100000E-01	2.29119552E-01
3.20	2.16000000E-01	2.15946640E-01
3.30	2.04000000E-01	2.04013631E-01
3.40	1.93200000E-01	1.93160794E-01
3.50	1.83300000E-01	1.83254223E-01
3.60	1.74200000E-01	1.74180828E-01
3.70	1.65900000E-01	1.65844503E-01
3.80	1.58200000E-01	1.58163070E-01
3.90	1.51100000E-01	1.51065886E-01
4.00	1.44500000E-01	1.44491884E-01
4.10	1.38400000E-01	1.38388046E-01
4.20	1.32700000E-01	1.32708129E-01
4.30	1.27400000E-01	1.27411615E-01
4.40	1.22500000E-01	1.22462868E-01
4.50	1.17800000E-01	1.17830455E-01
4.60	1.13500000E-01	1.13486495E-01
4.70	1.09400000E-01	1.09406235E-01
4.80	1.05500000E-01	1.05567608E-01
4.90	1.01900000E-01	1.01950867E-01
5.00	9.85100000E-02	9.85383169E-02

FIT:GAL-R
This file lists the fit for GALVAN-R
The corresponding fitting function data is given in JACOBI7

Coefficents		S.D. Aj
A(0)=	9.99999976E-01	4.97326953E-08
A(1)=	1.18685421E-07	9.10137377E-07
A(2)=	1.71805732E-06	4.81965043E-06
A(3)=	-8.66898336E-06	9.85917322E-06
A(4)=	9.78354365E-06	6.86092664E-06
A(5)=	.00000000E+00	.00000000E+00
A(6)=	.00000000E+00	.00000000E+00

The value of Chi-square is 1.53178009E-17

Data generated by fit

r	ir	fit
1.10	3.12132770E+00	3.12132770E+00
1.20	1.89775870E+00	1.89775870E+00
1.30	1.38070150E+00	1.38070150E+00
1.40	1.08580600E+00	1.08580600E+00
1.50	8.92851280E-01	8.92851284E-01
1.60	7.56038550E-01	7.56038545E-01
1.70	6.53738230E-01	6.53738235E-01
1.80	5.74285150E-01	5.74285145E-01
1.90	5.10788410E-01	5.10788414E-01
2.00	4.58896950E-01	4.58896944E-01
2.10	4.15719600E-01	4.15719603E-01
2.20	3.79256160E-01	3.79256163E-01
2.30	3.48076650E-01	3.48076652E-01
2.40	3.21130650E-01	3.21130642E-01
2.50	2.97628600E-01	2.97628591E-01
2.60	2.76965320E-01	2.76965321E-01
2.70	2.58669030E-01	2.58669031E-01
2.80	2.42366440E-01	2.42366441E-01
2.90	2.27758270E-01	2.27758270E-01
3.00	2.14601830E-01	2.14601840E-01
3.10	2.02698240E-01	2.02698240E-01
3.20	1.91882950E-01	1.91882960E-01
3.30	1.82018730E-01	1.82018730E-01
3.40	1.72990150E-01	1.72990150E-01
3.50	1.64699530E-01	1.64699530E-01
3.60	1.57063600E-01	1.57063600E-01
3.70	1.50010980E-01	1.50010979E-01
3.80	1.43480130E-01	1.43480129E-01
3.90	1.37417740E-01	1.37417739E-01
4.00	1.31777380E-01	1.31777379E-01
4.10	1.26518460E-01	1.26518459E-01
4.20	1.21605340E-01	1.21605339E-01
4.30	1.17006590E-01	1.17006589E-01
4.40	1.12694400E-01	1.12694399E-01
4.50	1.08644100E-01	1.08644099E-01
4.60	1.04833680E-01	1.04833679E-01
4.70	1.01243500E-01	1.01243499E-01
4.80	9.78559620E-02	9.78559601E-02
4.90	9.46552350E-02	9.46552341E-02
5.00	9.16270720E-02	9.16270721E-02

FIT:GAL-4R

This file lists the fit for GALVAN-4R

The corresponding fitting function data is given in JACOBI7

Coefficents	S.D. Adj
A(0)= 9.99787320E-01	2.02224189E-03
A(1)= -1.73666924E-02	6.30774371E-02
A(2)= 4.44348454E-01	6.45755614E-01
A(3)= -3.39992332E+00	3.10188874E+00
A(4)= 1.12815952E+01	7.65256421E+00
A(5)= -1.68968477E+01	9.37248544E+00
A(6)= 9.34476089E+00	4.50641427E+00

The value of Chi-square is 6.17014613E-10

Data generated by fit

r	ir	fit
1.10	3.12100000E+00	3.12099379E+00
1.20	1.89800000E+00	1.89799562E+00
1.30	1.38100000E+00	1.38101462E+00
1.40	1.08600000E+00	1.08596607E+00
1.50	8.92900000E-01	8.92902124E-01
1.60	7.56000000E-01	7.56037239E-01
1.70	6.53700000E-01	6.53719575E-01
1.80	5.74300000E-01	5.74266253E-01
1.90	5.10800000E-01	5.10776196E-01
2.00	4.58900000E-01	4.58893095E-01
2.10	4.15700000E-01	4.15723446E-01
2.20	3.79300000E-01	3.79266115E-01
2.30	3.48100000E-01	3.48090950E-01
2.40	3.21100000E-01	3.21147663E-01
2.50	2.97600000E-01	2.97646973E-01
2.60	2.77000000E-01	2.76983984E-01
2.70	2.58700000E-01	2.58687158E-01
2.80	2.42400000E-01	2.42393439E-01
2.90	2.27800000E-01	2.27773727E-01
3.00	2.14600000E-01	2.14615489E-01
3.10	2.02700000E-01	2.02709924E-01
3.20	1.91900000E-01	1.91892609E-01
3.30	1.82000000E-01	1.82026334E-01
3.40	1.73000000E-01	1.72995746E-01
3.50	1.64700000E-01	1.64703186E-01
3.60	1.57100000E-01	1.57065406E-01
3.70	1.50000000E-01	1.50011040E-01
3.80	1.43500000E-01	1.43478556E-01
3.90	1.37400000E-01	1.37414646E-01
4.00	1.31800000E-01	1.31772682E-01
4.10	1.26500000E-01	1.26512672E-01
4.20	1.21600000E-01	1.21598371E-01
4.30	1.17000000E-01	1.16998545E-01
4.40	1.12700000E-01	1.12685380E-01
4.50	1.08600000E-01	1.08634198E-01
4.60	1.04800000E-01	1.04822984E-01
4.70	1.01200000E-01	1.01232093E-01
4.80	9.78600000E-02	9.78439186E-02
4.90	9.46600000E-02	9.46426282E-02
5.00	9.16300000E-02	9.16139671E-02

```
COM:GAL-CG
 This file lists the comparison for GALVAN-G

 Coefficents
 A(0)= 9.99999976E-01
 A(1)= 1.18685421E-07
 A(2)= 1.71805732E-06
 A(3)= -8.66898336E-06
 A(4)= 9.78634365E-06
 A(5)=  .00000000E+00
 A(6)=  .00000000E+00


 Comparison of fit
   S              is                fit
 -.90      1.00000000E+00      1.00000605E+00
 -.80      1.00000000E+00      9.99997534E-01
 -.70      1.00000000E+00      9.99993366E-01
 -.60      1.00000000E+00      9.99992251E-01
 -.50      1.00000000E+00      9.99993231E-01
 -.40      1.00000000E+00      9.99995479E-01
 -.30      1.00000000E+00      9.99998734E-01
 -.20      1.00000000E+00      1.00000096E+00
 -.10      1.00000000E+00      1.00000315E+00
  .00      1.00000000E+00      1.00000460E+00
  .10      1.00000000E+00      1.00000507E+00
  .20      1.00000000E+00      1.00000450E+00
  .30      1.00000000E+00      1.00000319E+00
  .40      1.00000000E+00      1.00000131E+00
  .50      1.00000000E+00      9.99999015E-01
  .60      1.00000000E+00      9.99997148E-01
  .70      1.00000000E+00      9.99996279E-01
  .80      1.00000000E+00      9.99997321E-01
  .90      1.00000000E+00      1.00000073E+00
 1.00      1.00000000E+00      1.00000849E+00


 The value of Chisquare is  5.15026135E-11
```

```
COM GAL-40
 This file lists the comparison for GALVAN-40

 Coefficients
 A(0) =  9.29787320E-01
 A(1) = -1.73666924E-02
 A(2) =  4.44345454E-01
 A(3) = -3.39992332E+00
 A(4) =  1.12815952E+01
 A(5) = -1.68768477E+01
 A(6) =  9.54176089E+00


 Comparison of Fit
  x              is                 fit
 -.90       1.00000000E+00      8.76361902E-02
 -.80       1.00000000E+00     -1.28665679E+01
 -.70       1.00000000E+00     -1.10194194E+01
 -.60       1.00000000E+00     -3.80981274E+00
 -.50       1.00000000E+00      3.25629708E+00
 -.40       1.00000000E+00      7.57531353E+00
 -.30       1.00000000E+00      8.54666851E+00
 -.20       1.00000000E+00      6.80733462E+00
 -.10       1.00000000E+00      3.59990911E+00
  .00       1.00000000E+00      2.73568940E-01
  .10       1.00000000E+00     -2.08000128E+00
  .20       1.00000000E+00     -2.85921199E+00
  .30       1.00000000E+00     -2.05019594E+00
  .40       1.00000000E+00     -1.91568112E-01
  .50       1.00000000E+00      1.79439024E+00
  .60       1.00000000E+00      2.90401522E+00
  .70       1.00000000E+00      2.48801912E+00
  .80       1.00000000E+00      8.20718513E-01
  .90       1.00000000E+00     -1.97264254E-01
 1.00       1.00000000E+00      3.79717167E+00


 The value of Chisquare is  4.29137330E+01
```

TABLE I[1]

This table lists some properties of Hilbert transformation as well as examples of Hilbert transform pairs.

$G(g)$	$R(r) = H\{G(g)\} = \frac{1}{\pi}\int_{-\infty}^{\infty}\frac{G(g)}{g-r}\,dg$
$R(g)$	$-G(r)$
$cG(a\pm bg)$, $b>0$	$cR(a\pm br)$
$G_o(-g) = -G_o(g)$ i.e. G_o an odd function of g	$\frac{2}{\pi}\int_0^{\infty}\frac{gG(g)}{g^2-r^2}\,dg$, an even function of r
$G_e(-g) = G_e(g)$ i.e. G_e an even function of g	$\frac{2r}{\pi}\int_0^{\infty}\frac{G(g)}{g^2-r^2}\,dg$, an odd function of r
$\sin(ag)$, $a>0$	$\cos(ar)$
$\frac{g}{g^2+a^2}$, $a>0$	$\frac{a}{r^2+a^2}$
0 , $-\infty<g<a$ 1 , $a<g<b$ 0 , $b<g<\infty$	$\frac{1}{\pi}\,\ell n\left\lvert\frac{b-r}{a-r}\right\rvert$
0 , $-\infty<g<-a$ $(a^2-g^2)^{\frac{1}{2}}$, $-a<g<a$ 0 , $a<g<\infty$	$-r-(r^2-a^2)^{\frac{1}{2}}$, $-\infty<r<-a$ $-r$, $-a<r<a$ $-r+(r^2-a^2)^{\frac{1}{2}}$, $a<r<\infty$

(cont.)

TABLE I (cont.)

$G(g)$	$R(r) = H\{G(g)\} = \frac{1}{\pi}\int_{-\infty}^{\infty}\frac{G(g)}{g-r}\,dg$
0 , $-\infty<g<-a$	$-1+\left(\frac{-r+a}{-r-a}\right)^{\frac{1}{2}}$, $-\infty<r<-a$
$\left(\frac{a-g}{a+g}\right)^{\frac{1}{2}}$, $-a<g<a$	-1 , $-a<r<a$
0 , $a<g<\infty$	$-1+\left(\frac{r-a}{r+a}\right)^{\frac{1}{2}}$, $a<r<\infty$
0 , $-\infty<g<a$	$\frac{\Gamma(\rho)\Gamma(\sigma)(b-a)^{\rho+\sigma-1}}{(b-r)\pi\Gamma(\rho+\sigma)}$ $\times {}_2F_1\left(1,\sigma;\rho+\sigma;\frac{b-a}{b-r}\right)$ $-\infty<r<a$ or $b<r<\infty$
$(g-a)^{\rho-1}(b-g)^{\sigma-1}$, $a<g<b$	$(r-a)^{\rho-1}(b-r)^{\sigma-1}\operatorname{ctn}(\sigma\pi)$ $-\frac{\Gamma(\rho)\Gamma(\sigma-1)}{\pi\Gamma(\rho+\sigma-1)}(b-a)^{\rho+\sigma-2}$ $\times {}_2F_1\left(1,2-\rho-\sigma;2-\sigma;\frac{b-r}{b-a}\right)$ $a<r<b$
0 , $b<g<\infty$ $\rho>0$, $\beta>0$	
0 , $-\infty<g<-1$	$-(2/\pi)(r-1)^{\alpha}(r+1)^{\beta}Q_n^{(\alpha,\beta)}(r)$ $-\infty<r<-1$ or $1<r<\infty$
$(1-g)^{\alpha}(1+g)^{\beta}P_n^{(\alpha,\beta)}(g)$, $-1<g<1$	$-(2/\pi)(1-r)^{\alpha}(1+r)^{\beta}Q_n^{(\alpha,\beta)}(r)$ $-1<r<1$
0 , $1<g<\infty$	

TABLE II

This table summarizes the state of knowledge of the three regions of the generation and recapture functions.

	value of g or r		
	between $-\infty$ and -1	between -1 and 1	between 1 and ∞
G(g)	known to be zero	unknown and sought as a means of reconstructing the generation current $i_g(t)$	known to be zero
R(r)	unknown	unknown	known from the measured values of the recapture current $i_r(t)$

LIST OF SYMBOLS

A	electrode area (m^2)
A	auxillary electrode
A_n	a coefficient in a series of fitting functions
A/D	analog-to-digital converter
$A(s)$	arbitrary constant independent of x
a	a constant proportional to the slope of a linear fit between consecutive data points (A)
a	a location to the right of any singularity of f(s)
a_j	a coefficient in a series approximation
a_j	activity of species j
a_n	a coefficient in a series describing $i_g(t)$
$(a)_n$	Pochhammer's symbol
$B(s)$	arbitrary constant independent of x
$B_1(s)$, $B_2(s)$	arbitrary constants independent of x
b	a constant proportional to the intercept of a linear fit between consecutive data points (As)
b	a dimensionless parameter
b_k	a coefficient for a fit to orthogonal polynomials
C_i	integral capacitance of the double layer (Fm^{-2})
C_j	concentration of species j (mol m^{-3})
C_j^s	concentration of species j at the electrode surface (mol m^{-3})
C_j^*	bulk concentration of species j (mol m^{-3})

$C_j(x,t)$	concentration of species j at a distance x and time t (mol m^{-3})
c	location of a singularity in F(x)
D	operator denoting differentiation
D	diffusion coefficient ($m^2 s^{-1}$)
D_j	diffusion coefficient of species j ($m^2 s^{-1}$)
$\frac{d^{\frac{1}{2}}}{dt^{\frac{1}{2}}}$	semidifferentiation operator ($s^{-\frac{1}{2}}$)
$\frac{d^{-\frac{1}{2}}}{dt^{-\frac{1}{2}}}$	semiintegration operator with lower limit zero ($s^{\frac{1}{2}}$)
$\frac{d^{-\frac{1}{2}}}{[d(t-T)]^{-\frac{1}{2}}}$	semiintegration operator with lower limit T ($s^{\frac{1}{2}}$)
$\frac{dE}{dt}$	ramp rate (Vs^{-1})
d_{Hg}	density of mercury (gm^{-3})
$\vec{E}_p$	peak potential for forward scan of a cyclic voltammogram (V)
$\overleftarrow{E}_p$	peak potential for backward scan of a cyclic voltammogram (V)
E°	standard potential (V)
$E^{\circ\prime}$	formal potential (V)
E_1	initial potential for experimental cyclic voltammograms (V)
E_2	final potential for experimental cyclic voltammograms (V)
E_{ac}	ac component of potential (V)
E_d	depositing potential (V)

E_{dc}	dc component of potential (V)
E_g	generation potential (V)
E_h	half-wave potential (V)
E_i	initial potential (V)
E_n	null potential (V)
E_p	peak potential (V)
E_r	reversal potential (V)
E_r	recapture potential (V)
E_rC_i	mechanism in which a reversible electron transfer is followed by an irreversible homogeneous chemical reaction
E_z	potential of zero charge (V)
e	an electron
erf(x)	error function
erfc(x)	complementary error function
F	Faraday's costant (96,485 $Cmol^{-1}$)
$\overline{F}(s)$	Laplace transform of F(t)
${}_2F_1(a,b;c;x)$	Gauss' hypergeometric function
FFT	fast Fourier transform
FT-IR	Fourier transform infrared
FT-NMR	Fourier transform nuclear magnetic resonance
f	frequency (s^{-1})
$f_?(t)$	a function which varies unpredictably with time (A)
$f_n(r)$	fitting functions for $R_3(r)$ (A)

$f(s)$	Laplace transform of $F(t)$
G	image of the function F
$G(g)$	generation function in terms of g (A)
$G(\theta)$	generation function in terms of θ (A)
$G_2(g)$	generation function in the domain $-1<g<1$ (A)
GC/MS	gas chromatography / mass spectrometry
$G_k(x)$	a polynomial in an orthogonal series
g	undimensionalized time variable in the generation domain
$g(s)$	Laplace transform of $G(t)$
H	operator denoting Hilbert transformation
HMDE	hanging mercury drop electrode
$H(f)$	a function of frequency defined by Fourier transformation
$h(t)$	a function of time defined by inverse Fourier transformation
$h_n(g)$	fitting functions for $G_2(g)$
I	operator denoting integration
I	magnitude of a constant current (A)
I_{ac}	magnitude of ac component of a current (A)
IR	infrared
$\vec{i}$	current for the forward going ramp (A)
$\overleftarrow{i}$	current for the backward going ramp (A)
$\vec{i}_p$	peak current for the forward going ramp (A)
$\overleftarrow{i}_p$	peak current for the backward going ramp (A)

i_D	current at a disc electrode (A)
i_R	current at a ring electrode (A)
i_c	capacitative current (A)
i_f	faradaic current (A)
i_g	generation current (A)
i_j	current at a specific data point (A)
i_{pa}	anodic peak current (A)
i_{pc}	cathodic peak current (A)
i_r	recapture current (A)
i_r	reversal current (A)
$i_r[D]$	recapture current as described by experimental data (A)
$i_r[T]$	recapture current as described by the Hilbert transform of the generation current (A)
J	number of data points
J_j	flux of species j (mol $s^{-1}m^{-2}$)
$J_j(x,t)$	flux of species j at a distance x and time t (mol $s^{-1}m^{-2}$)
j	a loop counter
K_0	dc level (V)
K_n	amplitude of a potential with frequency nω (V)
K(t,x)	kernel of an integral transform of F(t) which will yield a function f(x)
k	a homogeneous rate constant (s^{-1})
k	a heterogeneous rate constant (ms^{-1})

k	abbreviation for $nAFC_o^* D_o^{\frac{1}{2}}$ $(As^{\frac{1}{2}})$
k	abbreviation for $nAFC^* (2D/\pi T)^{\frac{1}{2}}$ (A)
k_c	constant associated with capacitative current at a dropping mercury electrode $(As^{1/3})$
k_f	constant associated with faradaic current at a dropping mercury electrode $(As^{-1/6})$
k_s	standard heterogeneous charge-transfer rate constant (ms^{-1})
L	operator denoting Laplace transformation
L^{-1}	operator denoting inverse Laplace Transformation
LCEC	liquid chromatography / electrochemistry
m	a loop counter
m	rate of mercury flow in a dropping mercury electrode (gs^{-1})
$m(t)$	faradaic semiintegral $(s^{-\frac{1}{2}})$
$m_r(t)$	"recapture semiintegral" $(s^{-\frac{1}{2}})$
N	order of fit
N	collection efficiency
NMR	nuclear magnetic resonance
n	number of electrons transferred in an oxidation or reduction process
n	degree of a polynomial
n	a loop counter
n_g	number of electrons consumed in the generation of a Y
n_r	number of electrons consumed in the recapture of a Y

O	oxidized form of R
$P_n(x)$	Legendre polynomial of degree n
$P_n^{(\alpha,\beta)}(x)$	Jacobi polynomial of degree n
p	a factor which is common to all exponents in a power series
Q(t)	charge passed as a function of time (C)
Q_g	charge passed during the generation phase (C)
$Q_n(x)$	Legendre's function of the second kind
$Q_n^{(\alpha,\beta)}(x)$	Jacobi's function of the second kind
Q_r	charge passed during the reversal phase (C)
q	order of differentiation
$q_n^{(\alpha,\beta)}(x)$	a function which aids in the evaluation of $Q_n^{(\alpha,\beta)}(x)$
R	the reduced form of O
R	universal gas constant (8.3143 $Jmol^{-1}k^{-1}$)
R	reference electrode
R(r)	recapture funtion in terms of r (A)
$R_1(r)$	recapture function in the domain r<-1 (A)
$R_2(r)$	recapture function in the domain -1<r<1 (A)
$R_3(r)$	recapture function in the domain r>1 (A)
$R(\phi)$	recapture function in terms of ϕ (A)
RRDE	rotating ring-disc electrode

r	undimensionalized time variable in the recapture domain
r_o	radius of a mercury drop (m)
s	dummy variable of Laplace Transformation with respect to t (s^{-1})
s^2	reduced chi-square (A^2)
$\mathcal{T}$	operator denoting transformation
$\mathcal{T}^{-1}$	operator denoting inverse transformation
T	thermodynamic temperature (K)
T	duration of the generation phase (s)
t_1	a time prior to the transition time (s)
t_g	a time in the generation phase (s)
t_r	a time in the reversal phase (s)
UV	ultraviolet
u	dummy variable of integration (s)
W	working electrode
X	species which is the precursor to Y
$\|x\|$	absolute value of x
Y	species produced in the generation phase
y	a dimensionless parameter
y'	derivative of y with respect to x
y''	second derivative of y with respect to x
y^s	a dimensionless parameter
y_j^s	a dimensionless parameter

Z	species produced in the recapture phase
α	a parameter used in the description of Jacobi functions
α	transfer coefficient
β	a parameter used in the description of Jacobi functions
β	a dimensionless parameter
$\Gamma(x)$	gamma function
γ	time variable in the generation domain (s)
γ_j	γ at the data point j
γ_j	activity coefficient of species j
Δj	difference between the fit and the data at γ_j (A)
Δt	interval between data points (s)
ε	a small positive number
$\zeta(p)$	zeta function
θ	time variable in the generation domain (radians, degrees)
λ	duration of the forward scan of a cyclic voltammogram (s)
$\lambda(p)$	lamda function
ν	ramp rate (Vs^{-1})
ς	time variable in the recapture domain (s)
σ	dummy variable for Laplace transformation with respect to t-T (s^{-1})
τ	dummy variable of integration
τ	transition time

τ_2	second transition time (s)
ϕ	phase angle of ac current with respect to E_{ac}
ϕ	time variable in the recapture domain (radians, degrees)
$\chi(x)$	chi function
$\psi(x)$	digamma function
ω	rotational frequency (s^{-1})
0_j^s	a dimensionless parameter
$\int\!\!\!\!\!\!-$	Cauchy Principal Value of an integral

REFERENCES

Chapter 1

(1) A.G. Marshall, "Fourier, Hadamard, and Hilbert Transforms in Chemistry", Plenum, New York, 1982, p. vii.

(2) J.W. Cooley and J.W. Tukey, Math. Comput. 19, 297 (1965).

(3) A.G. Marshall, op. cit., p. viii.

(4) R.R. Ernst, J. Magn. Resonance (1), 1, 7 (1969).

Chapter 2

(1) R.V. Churchill, "Operational Mathematics", 3rd. ed., McGraw-Hill, New York, 1972, chap. 1.

(2) Lord Rayleigh, Phil. Mag. (5), 34, 407 (1892).

(3) A.A. Michelson, ibid., 34, 280 (1892).

(4) P.R. Griffiths, "Transform Techniques in Chemistry", Plenum, New York, 1978, p. 2.

(5) E.A. Guillemin, "The Mathematics of Circuit Analysis", M.I.T. Press, Cambridge, Mass., 1962.

(6) P.R. Griffiths, op. cit., p. 5.

(7) A.J. Bard and L.R. Faulkner, "Electrochemical Methods: Fundamentals and Applications", Wiley, 1980, p. 672.

(8) ibid., p. 672.

(9) P.R. Griffiths, op. cit., p. vii.

(10) F.E. Nixon, "Handbook of Laplace Transformation: Fundamentals, Applications, Tables, and Examples", 2nd. ed., Prentice-Hall, Englewood Cliffs, N.J., 1965, p. 21.

(11) H.S. Carslaw and J.C. Jaeger, "Conduction of Heat in Solids", 2nd. ed., Prentice-Hall, Englewood Cliffs, N.J., 1965, p. 297.

(12) M. Abramowitz and I.A. Stegun, Eds., "Handbook of Mathematical Functions", National Bureau of Standards, Washington, D.C., 1964, chap. 29.

(13) G.E. Roberts and H. Kaufman, "Table of Laplace Transforms", Saunders, Philadelphia, 1966.

(14) A. Erdélyi, Ed., "Tables of Integral Transforms", McGraw-Hill, New York, 1954, vol. 1, pp. 125-301.

(15) F. Oberhettinger and L. Badii, "Tables of Laplace Transforms", Springer-Verlag, Berlin, 1973.

(16) D.D. MacDonald, "Transient Techniques in Electrochemistry", Plenum, New York, 1977, p. 62.

(17) E.C. Titchmarsh, "Introduction to the Theory of Fourier Integrals", 2nd. ed., Oxford University Press, New York, 1948, p. 120.

(18) A. Erdélyi, op. cit., vol. 2, p. 423.

(19) A. Papoulis, "Systems and Transforms with Applications in Optics", McGraw-Hill, New York, 1968, p. 435.

(20) E.A. Guillemin, "The Mathematics of Circuit Analysis", M.I.T. Press, Cambridge, Massachusetts, 1962, p. 338.

(21) J. Irving and N. Mullineux, "Mathematics in Physics and Engineering", Academic Press, New York, 1964, p. 633.

(22) R.R. Ernst, J. Magn. Resonance (1), 1, 7 (1969).

(23) P.R. Bevington, "Data Reduction and Error Analysis For The Physical Sciences", McGraw-Hill, New York, 1969, p. 144.

(24) L.A. Pipes, "Applied Mathematics for Engineers and Physicists", 3rd. ed., McGraw-Hill, New York, 1970, p. 333.

(25) P.R. Bevington, op. cit., p. 149.

(26) J. Irving and N. Mullineux, op. cit., p. 84, p. 96.

(27) M. Abramowitz and I.A. Stegun, op. cit., eq.8.6.19.

(28) W. Magnus, et. al., "Formulas and Theorems for the Special Functions of Mathematical Physics", Springer-Verlag, New York, 1966, p. 229, p. 333.

(29) M. Abramowitz and I.A. Stegun, op. cit., eq.15.1.1, eq.6.1.22.

(30) G. Szegö, "Orthogonal Polynomials", American Mathematical Society, New York, 1959, p. 71.

(31) G.M. Murphy, "Ordinary Differential Equations and Their Solutions", D. Van Nostrand, Toronto, 1960, p. 352.

(32) M. Abramowitz and I.A. Stegun, op. cit., eq.6.1.21.

(33) ibid, eq.6.1.15, eq.6.1.8.

(34) G. Szegö, op. cit., p. 77.

Chapter 3

(1) A.J. Bard and L.R. Faulkner, "Electrochemical Methods: Fundamentals and Applications", Wiley, 1980, chaps. 1-2.

(2) D.D. MacDonald, "Transient Techniques in Electrochemistry", Plenum, New York, 1977, p. 1.

(3) J. Koryta, J. Dvořák, and V. Boháčková, "Electrochemistry", Plenum, New York, 1977, p. 1.

(4) J.J. Lingane, "Electroanalytical Chemistry", 2nd. ed., Wiley, New York, p. 284.

Chapter 4

(1) J.G. Holbrook, "Laplace Transforms for Electronic Engineers", 2nd. ed., Pergamon, New York, 1966, pp. 66-70.

(2) D.D. MacDonald, "Transient Techniques in Electrochemistry", Plenum, New York, 1977, p. 51.

(3) ibid., pp. 57-61.

(4) ibid., p. 62.

(5) A.J. Bard and L.R. Faulkner, "Electrochemical Methods: Fundamentals and Applications", Wiley, 1980, p. 362.

(6) A.A. Pilla, J. Electrochem. Soc., 117, 467 (1970).

(7) A.J. Bard and L.R. Faulkner, op. cit., pp. 316-362, pp. 671-672.

(8) P.R. Griffiths, "Transform Techniques in Chemistry", Plenum, 1978, pp. 355-377.

(9) A.G. Marshall, "Fourier, Hadamard, and Hilbert Transforms in Chemistry", Plenum, New York, 1982, pp. 453-522.

(10) P.R. Griffiths, op. cit., p. 367.

(11) S.C. Creason, J.W. Hayes, and D.E. Smith, J. Electroanal. Chem., 47, 2158 (1971).

(12) A.J. Bard and L.R. Faulkner, op. cit., pp. 577-645.

(13) A.G. Marshall, op. cit., pp. 527-546.

(14) P. Rossi, C.W. McCurdy, and R.L. McCreery, J. Am. Chem. Soc., 103, 2524 (1981).

(15) A.J. Bard, Ed., "Electroanalytical Chemistry", Marcel Dekker, New York, 1974, vol. 7.

(16) R.L. McCreery, R. Pruiksma, and R. Fagan, Anal. Chem., 51, 2253 (1979).

(17) R. Pruiksma and R.L. McCreery, ibid., 51, 2253 (1979).

(18) A.J. Bard and L.R. Faulkner, op. cit., p. 236.

(19) Fu-Chin Soong and J.T. Maloy (Seton Hall University, South Orange, N.J.), "Riemann-Liouville Transform Polarography: Theoretical Development and Experimental Verification for Trace Analysis", in press.

(20) K.B. Oldham and J. Spanier, "The Fractional Calculus", Academic Press, New York, 1974.

(21) ibid, pp. 136-148.

(22) A.J. Bard and L.R. Faulkner, op. cit., chap. 5.

Chapter 5

(1) A.J. Bard and L.R. Faulkner, "Electrochemical Methods: Fundamentals and Applications", Wiley, 1980, p. 140.

(2) ibid, p. 430.

(3) F.G. Cottrell, Z. Phys. Chem., 42, 385 (1903).

(4) T. Kambara, Bull. Chem. Soc. Jap., 27, 523 (1954).

(5) C. Amatore and J.M. Savéant, J. Electroanal. Chem., 107, 353 (1980).

(6) W.J. Albery and S. Bruckenstein, Trans. Faraday Soc., 62, 1946 (1966).

(7) W.J. Albery, M.L. Hitchman, and J. Ulstrup, ibid., 64, 2831 (1968).

(8) W.J. Albery and M.L. Hitchman, "Ring-Disc Electrodes", Clarendon Press, Oxford, 1971.

(9) A.J. Bard and L.R. Faulkner, op. cit., p. 468.

(10) ibid, p. 200.

(11) ibid., p. 33.

(12) ibid, p. 253.

(13) ibid., p. 265.

(14) ibid., p. 442.

(15) ibid., p. 227.

(16) J. Albery, "Electrode Kinetics", Oxford Chemistry Series, Clarendon Press, Oxford, 1975, p. 156.

(17) J.E.B. Randles, Trans. Faraday Soc., 44, 327 (1948).

(18) A. Sevcik, Collect. Czech. Chem. Commun., 13, 349 (1948).

(19) W.H. Reinmuth, Anal. Chem., 34, 1446 (1962).

(20) K.B. Oldham, J. Electroanal. Chem., 105, 373 (1979).

(21) J. Myland and K.B. Oldham, "An Analytical Expression For The Current-Voltage Relationship During Reversible Cyclic Voltammetry", J. Electroanal. Chem., in press.

(22) M. Abramowitz and I.A. Stegun, Eds., "Handbook of Mathematical Functions", National Bureau of Standards, Washington, D.C., 1964, eq.23.2.20.

(23) E. Barendrecht, J. Electroanal. Chem., 2, 53 (1967).

(24) A.J. Bard and L.R. Faulkner, op. cit., p. 416.

(25) ibid., p. 413.

Chapter 6

(1) K.B. Oldham, Anal. Chem., 40, 1799 (1968).

Chapter 7

(1) K. Yamashita and H. Imai, Bull. Chem. Soc. Jap., 41, 1339 (1968).

(2) J. Myland and K.B. Oldham, "An Analytical Expression For The Current-Voltage Relationship During Reversible Cyclic Voltammetry", J. Electroanal. Chem., in press.

Chapter 9

(1) W. Jacobs, Current Separations, 4 (3), 45, 1982.

(2) R.E. Shoup, C.S. Bruntlett, W.A. Jacobs, and P.T. Kissenger, (Bioanal. Systems Inc. USA), Am. Lab. (Fairfield Conn.) 13 (10), 144, 1981.

(3) P.T. Kissenger, Anal. Chem., 49, 447A (1977).

Table I

(1) A. Erdélyi, Ed., "Tables of Integral Transforms", McGraw-Hill, New York, 1954, vol. 2, pp. 239-263.

Appendix A

(1) D.D. MacDonald, "Transient Techniques in Electrochemistry", Plenum, New York, 1977.

(2) R.V. Churchill, "Operational Mathematics", McGraw-Hill, New York, 1958, pp. 45-48.

(3) G.M. Murphy, "Ordinary Differential Equations and Their Solutions", Van Nostrand, Princeton, 1960.

(4) M. Abramowitz and I.A. Stegun, Eds., "Handbook of Mathematical Functions", National Bureau of Standards, Washington D.C., 1964, eq.29.3.114.

Appendix B

(1) K.B. Oldham and J. Spanier, J. Electroanal. Chem., 26, 331 (1970).

(2) K.B. Oldham and J. Spanier, "The Fractional Calculus", Academic Press, New York, 1974.

Appendix C

(1) M. Abramowitz and I.A. Stegun, Eds., "Handbook of Mathematical Functions", National Bureau of Standards, Washington D.C., 1964, eq.15.1.14.

(2) ibid., eq.15.2.20.

(3) ibid., eq.15.1.8.

(4) ibid., eq.15.1.5.

(5) ibid., eq.15.1.23.

(6) ibid., eq.15.1.13.

(7) ibid., eq.15.1.20.

(8) ibid., eq.15.2.12.

(9) ibid., table 22.1.